COLD SINGLE ATOMS FOR CAVITY QED EXPERIMENTS

A Thesis
Presented to
The Academic Faculty

by

Soo Y. Kim

In Partial Fulfillment
of the Requirements for the Degree
Doctor of Philosophy in the
School of Physics

Georgia Institute of Technology
December 2008

COLD SINGLE ATOMS FOR CAVITY QED EXPERIMENTS

Approved by:

Professor Michael Chapman, Advisor
School of Physics
Georgia Institute of Technology

Professor T. A. Brian Kennedy
School of Physics
Georgia Institute of Technology

Professor Alexander Kuzmich
School of Physics
Georgia Institute of Technology

Professor Chandra Raman
School of Physics
Georgia Institute of Technology

Professor David Citrin
School of Electrical and Computer
Engineering
Georgia Institute of Technology

Date Approved: 14 November 2008

"The only way of finding the limits of the possible is by going beyond them into the impossible."

-Arthur C. Clarke

ACKNOWLEDGEMENTS

I would like to thank all those who have been integral parts of my life throughout the past 5-6 years of my graduate career at the Georgia Institute of Technology. First, I would like to thank my advisor, Professor Michael Chapman. He has given me the privilege of having the opportunity of spending my days studying the fascinating world of atoms and light. His patient guidance and encouragement have been indispensable in my work on the cavity QED experiment. Though the journey was arduous, in the end it was rewarding and Mike's words would always ring true, "I know you'll make it work."

Of course, none of this work would have been possible without every one of my dear friends and colleagues. Dr. Jacob Sauer was the first to take me under his wing and get me started in the lab my first year. Though he graduated soon after, he still remains as a close friend, mentor, and personal photographer. I have also enjoyed my collaborations with fellow labmates, Dr. Kevin Fortier and Chung-Yu Shih. Their support has been indispensible. I must also acknowledge the help of my other colleagues in Chapman Labs: Dr. Peyman Ahmadi, Dr. Ghazal Behin-Aein, Michael Gibbons, Eva Bookjans, Mingshien Chang, Chris Hamley, Adam Steele, Layne Churchill, and Michael DePalatis. Each person has been a critical part of my graduate career and contributed to the lively dynamics of our lab group. Also, I cannot forget my wonderful study group: Kristan Marshall, Lina Merchan, and Jorge Millan. Their constant motivation, discipline, and unforgettable friendships have helped me immensely during my years at Georgia Tech.

My family and friends, especially my fabulous share group: Sarah Lee, Kyong Hwangbo, Peggy Lee, Su Nam, and Kyungmee Kim have been a wall of support

TABLE OF CONTENTS

LIST OF TABLES

LIST OF FIGURES

SUMMARY

A neutral atom interacting with a single mode of a high finesse cavity provides an opportunity to study uncharted quantum mechanical systems and to explore the field of quantum computing and networking. Ranging from being a deterministic single photon source to a coherent storage unit for quantum information, a strong coupling cavity QED system has proven to be a powerful tool. In this thesis, single atoms are deterministically delivered over long distances and probed in an optical cavity. Once in the cavity, a single atom is stored and continuously observed for over 15 seconds. Progress towards using atoms in the cavity to produce entangled photon pairs is presented. Dual 1D optical lattices are implemented to create a foundation for advancements in two qubit quantum operations and entanglements.

CHAPTER I

INTRODUCTION

Although known to many for his unique fashion trademarks, Albert Einstein is more appreciated for his great contributions in the field of science. Thinking far beyond his time and the available technology, Einstein laid the theoretical foundation for the invention of the laser in his 1917 paper *Zur Quantentheorie der Strahlung* [1]. In 1958, Charles Townes and Arthur Schawlow introduced the idea for the "optical maser" [2]. Later coined by Gordon Gould as the "LASER", an acronym for "Light Amplification by Stimulated Emission of Radiation", it was finally demonstrated on May 16, 1960 by Theodore Maiman at Hughes Research Laboratories.

Today, lasers have become an indispensable tool in fields ranging from medicine to research to entertainment. In the field of physics, one application is laser cooling. Proposed simultaneously in 1975 by Hans Dehmelt and David Wineland [3], and Theodore Hänsch and Arthur Schawlow [4], laser cooling and trapping of atoms was accomplished and awarded the Nobel Prize in 1997 to three recipients: Steven Chu, William Phillips, and Claude Cohen-Tannoudji. By the end of the millenium, cold atom traps have become standard in AMO laboratories worldwide.

Cold atoms have opened a new door for probing beyond the classical world into the realm of quantum mechanics, even creating a new form of matter called a Bose-Einstein condensate. Direct investigations of interactions between a single atom and single photon have also been made possible, especially in the field of cavity quantum electrodynamics, or cavity QED and have led to prospects in quantum information and computing.

1

1.1 Cavity QED

In 1946, Edward Purcell predicted that the spontaneous emission rate of a nuclear magnetic moment would increase when coupled into a resonator circuit [5]. Although he was describing this effect on NMR systems, it can also be applied to atoms in a cavity. After the technological advancements of high finesse cavity mirrors, the first manifestation of vacuum Rabi splitting with thermal atoms in a strong coupling optical cavity was presented in 1992 by Thompson et al.[6]. Since then, single atoms have been trapped and continuously observed in a cavity for up to a minute [7], sub-micron positioning has been demonstrated [8, 9, 10], and entanglement between atom and cavity photon has been achieved [11]. These are just a few examples of the continual progress being made by numerous research groups around the world to fully understand and utilize cavity QED systems.

A cavity QED system is a fundamental quantum system consisting of individual atoms localized in a high-finesse optical micro-cavity. Nonlinear dynamics [12, 13], quantum chaos [14], and quantum random walks [15] are just a few examples of the vast areas that cavity QED can explore. However, the most popular application of this system is towards the progress of quantum information processing [16, 17].

The preparation and coherent manipulation of multi-atom entangled quantum states is one of the essential key ingredients in the implementation of large scale quantum communication and quantum computation. Probabilistic generation of atom-photon entanglement using free-space coupling of individual atoms [18, 19], observation of entanglement between remote atomic ensembles [20, 21, 22], and entangling two separated ions [23, 24, 25] are the hallmarks of recent experimental achievements towards realizing this goal. A major obstacle in current experimental implementation is the low entanglement probability and the lack of control on individual qubits that can be independently manipulated. Fortunately, a cavity QED system in the strong coupling regime readily provides both of these requirements. The

intrinsic entanglement of atoms within the cavity mode and the cavity field provides a means to reversibly transfer quantum information between matter and light, and the eventual leakage of a photon from the well-defined mode of the cavity provides a means for high-fidelity, long-distance quantum communication which can fuel the growth of quantum information.

1.2 Quantum Computing and Information

Following the invention of the transistor by William Shockley, John Bardeen, and Walter H. Brattain in 1947 and the development of the integrated circuit by Jack Kilby in 1958, the era of computing began to grow. The number of components on integrated chips nearly doubles every 18 months, as originally pointed out by Gordon Moore [26]. However, "Moore's Law" will reach a natural limit when the transistors reach the size of individual atoms, making quantum effects no longer ignorable. Quantum computing offers a possible solution to overcome this problem.

1.2.1 Leading up to the Quantum Computer

Richard Feynman first envisioned a nonclassical simulator that would be able to process quantum mechanical systems [27]. Soonafter, David Deutsch developed the theory of a universal quantum computer [28]. One of the most significant contributions was made in 1994 by Peter Shor at Bell Labs with his famous eponymous algorithm [29]. He was able to reveal the power of a quantum computer by proving that it can factor large numbers (much like the system used in RSA encryption) exponentially faster than a classical computer, stirring immediate interest in the data encryption and national security communities. A few years later, Lov Grover proposed an algorithm for a quantum computer to search an unordered database [30] in only the fraction of the time $(O(\sqrt{N}))$ a classical computer would take $(O(N))$. As more algorithms continued to surface, developing the quantum computer became more desirable.

In 1995, Peter Zoller and Ignacio Cirac proposed utilizing trapped ions to create a quantum computer [31]. Subsequentially, trapped neutral atoms, quantum dots, nuclear magnetic resonance and superconductors have all been proposed to be the perfect candidate to become the first quantum computer. In this thesis, we concentrate on trapping neutral atoms for quantum computing.

1.2.2 Quantum Computing Basics

Modern classical information technology is built upon the binary digit (bit), which can take one of two possible values: 0 or 1. In quantum information, the corresponding basic unit is called a quantum bit, or a qubit. Likewise, the qubit has two possible values, $|0\rangle$ or $|1\rangle$. But the rules of quantum mechanics allow the qubit to also be in a superposition of the two states,

$$|\psi\rangle = \alpha |0\rangle + \beta |1\rangle \ , \tag{1.1}$$

where α and β are the complex amplitudes and obey the condition $|\alpha|^2 + |\beta|^2 = 1$.

When two qubits (A and B) are entangled, they are no longer independent of each other and must be described together. A simple two particle quantum state exhibiting entanglement is the Bell state

$$\Phi = \frac{1}{\sqrt{2}} \left(|0\rangle_A \otimes |0\rangle_B + |1\rangle_A \otimes |1\rangle_B \right) \ . \tag{1.2}$$

If the first qubit is measured, information about the second qubit is immediately known, i.e., if qubit A is measured to be in state $|0\rangle$, the state of the qubit B will be $|0\rangle$. Likewise, if qubit A is measured to be in state $|1\rangle$, qubit B will be in state $|1\rangle$.

The strength in quantum computing lies in the exponential scaling associated with entangled systems. For N entangled qubits, the possible combinations is 2^N where the state is written as

$$|\Psi\rangle_N = \sum_{i=1}^{2^N} c_i |x_1 x_2 ... x_N\rangle \ , \tag{1.3}$$

and c_i is the complex coefficient. This means that a quantum computer of 500 qubits can store more information and perform more calculations than there are atoms in the universe, something that could not be possible with a classical computer.

Similarly to classical computers, the quantum computer utilizes logic gates to perform calculations by operating on the qubits. A gate operator can simultaneously address all states at the same time, increasing the speed of which calculations are computed. Matrix notation is typically used to represent the gate operator and vectors are used to represent the states of the qubit. The most simple one qubit gates are

$$X = \begin{bmatrix} 0 & 1 \\ 1 & 0 \end{bmatrix} \tag{1.4}$$

$$Y = \begin{bmatrix} 0 & -i \\ i & 0 \end{bmatrix} \tag{1.5}$$

$$Z = \begin{bmatrix} 1 & 0 \\ 0 & -1 \end{bmatrix}, \tag{1.6}$$

where the two states of a qubit are represented as

$$|0\rangle = \begin{bmatrix} 1 \\ 0 \end{bmatrix} \quad |1\rangle = \begin{bmatrix} 0 \\ 1 \end{bmatrix}. \tag{1.7}$$

X is often referred to as a bit flip because it converts $|0\rangle$ to $|1\rangle$. Z is referred to as the phase flip, which leaves $|0\rangle$ unchanged and flips the sign of $|1\rangle$. In quantum physics, operators X, Y, and Z are more commonly known as the Pauli matrices: σ_x, σ_y, and σ_z.

In addition to these gates, there are two more important basic gates, the Hadamard and controlled-not (CNOT) gates. The Hadamard gate is also a one qubit gate and is represented as the normalized matrix

$$H = \frac{1}{\sqrt{2}} \begin{bmatrix} 1 & 1 \\ 1 & -1 \end{bmatrix}. \tag{1.8}$$

The CNOT gate is a two qubit gate and is represented as

$$C = \begin{bmatrix} 1 & 0 & 0 & 0 \\ 0 & 1 & 0 & 0 \\ 0 & 0 & 0 & 1 \\ 0 & 0 & 1 & 0 \end{bmatrix}. \tag{1.9}$$

The CNOT gate requires two qubits, a control qubit and a target qubit. If the control qubit is set to be $|0\rangle$, the target qubit is left alone. But if the control qubit is set to be $|1\rangle$, the target qubit is flipped.

Any unitary operation can be essentially be performed using the Hadamard and CNOT gates [32]. The first quantum gate was demonstrated with a trapped single atom in 1995 [33]. However, it took twelve years for physicists to implement the first quantum computer to factor the number 15 [34], proving that there still is much work to be done.

Unfortunately, quantum computers do have a drawback. Decoherence, or the loss of information, inevitably occurs as the system interacts with the environment. This governs that gate operations must be completed in much shorter times than it takes for the system to decohere. An estimate of decoherence times and operation times is shown in Table 1, taken from Ref. [32]. While it is possible to complete many operations before the system decoheres, it is still an obstacle that must continuously be addressed.

Table 1: An estimate of decoherence times and operation times for different systems for quantum computing.

System	Decoherence Times (s)	Operation Times (s)
Nuclear spin	$10^{-2} - 10^{8}$	$10^{-3} - 10^{-6}$
Electron spin	10^{-3}	10^{-7}
Ion Trap	10^{-1}	10^{-14}
Quantum dot	10^{-6}	10^{-9}
Optical cavity	10^{-5}	10^{-14}
Microwave cavity	10	10^{-4}

6

1.2.3 Quantum Computing Necessities

David DiVincenzo developed a list of five requirements that are needed to create a quantum computer [35]. As will be explained, neutral atoms in cavity QED satisfy all five requirements, proving to be a good candidate to build the basis for a quantum computer.

- A scalable physical system with well characterized qubits.

For a neutral atom in cavity QED, this is easily satisfied due to the quantized energy structure of an atom and the cavity excitation levels. The state of the system can be measured and accurately known.

- The ability to initialize the state of the qubits to a simple fiducial state, such as $|000...\rangle$.

Through optical pumping, neutral atoms can be initialized to a hyperfine ground state. Due to the long lifetime of the ground state, decoherence effects are negligible.

- Long relevant decoherence times, much longer than the gate operation time.

Being in the strong coupling regime demands that the coupling rate between the cavity photon and atom trumps the loss rates. As long as the decoherence time is more than $10^4 - 10^5$ times greater than the operation time, error correction is also possible.

- A universal set of quantum gates.

Entanglement schemes have been proposed and demonstrated for neutral atoms in cavity QED with high fidelities. Laser pulses are used to execute gate operations, making them highly controllable.

- A qubit-specific measurement capability.

Cavity QED is well-established as an efficient single atom detector. By placing single atoms in separate sites in an optical trap, they can be shuttled through the cavity and addressed independently.

DiVincenzo adds two more requirements to ensure quantum communication is possible.

- The ability to interconvert stationary and flying qubits.

Strong coupling in a cavity increases the rate in which information is transferred between a stationary qubit (atom) and a flying qubit (photon). The eventual leakage of the photon through the cavity mirrors allows the flying qubit to leave the system in a well-defined mode.

- The ability faithfully to transmit flying qubits between specified locations.

Fiber optics allow photons to be carried from one site to another with great efficiency and low loss in information.

All these requirements show that a trapped neutral atom in an optical cavity system is an excellent candidate to build the quantum computer.

1.3 Organization of This Thesis

I began working in the labs of Dr. Michael Chapman when I arrived at Georgia Tech in the fall of 2003. I dabbled in the cavity QED experiment with Dr. Jacob Sauer. He soon graduated the next September, and I continued the experiment with Dr. Kevin Fortier. Together, we saw the project evolve through various cavity and laser systems. Through hard work and perseverance, deterministic delivery to an optical cavity was achieved in January 2007 and published in Physical Review Letters [9]. After Dr. Kevin Fortier's departure that February, I took on the experiment alone. After attempts in molecular formation and entanglements of single photon pairs in

the cavity, dual lattices were introduced. Chung-Yu Shih began to work with me in 2008 and has successfully taken on the experiment.

This thesis starts with two chapters on the theoretical background of the basics of this experiment: trapping atoms and cavity quantum electrodynamics. The next chapter describes the different components of the experimental apparatus for this project. The latter three chapters explain the development of the deterministic delivery procedure, steps taken towards producing entangled single photon pairs, and the implementation of dual lattices in the cavity. Finally, the thesis concludes with a look at future goals and the promising direction of the cavity QED research.

CHAPTER II

ATOM TRAPPING

For our experiments, we must first trap the atoms. Subject of a Nobel Prize in 1997, cooling and trapping atoms has rapidly become standard in AMO laboratories around the world. There have been various applications and studies of trapped atoms.

In this chapter, the theory of trapping that provides the fundamental backbone of the experiments is outlined. The first half focuses on the initial trapping of atoms from the background into a controlled system. In this section, the topics of laser cooling and magnetic field gradients are addressed. The latter half describes the second type of trapping utilized in our experiments, optical dipole traps. These trapping techniques allows us to manipulate multiple and single atoms.

2.1   *Rubidium Atoms*

Atoms in the first column of the periodic table, known as the alkali metals, are most commonly used for trapping and laser cooling. The alkali metals have a single valence electron as can be seen in Fig. 1 [36], that provide convenient closed optical transitions. The electron core consists of closed shells, which do not add to the angular momentum of the electron. All the alkali metals have been previously trapped.

The wavelengths of the transitions used for trapping and cooling in alkali metals are within the visible to near-IR spectrum, shown in Table 2. Current laser technology can easily achieve these wavelengths, making it convenient to obtain the necessary optical equipment for the atoms. Except for francium, these atoms are relatively stable in a non-oxidizing environment and can be stored in vacuum sealed ampules or as a chromate compound with a reducing agent in getters. Heating the ampules or getters a few hundred degrees centrigrade produce sufficient atom vapor pressures
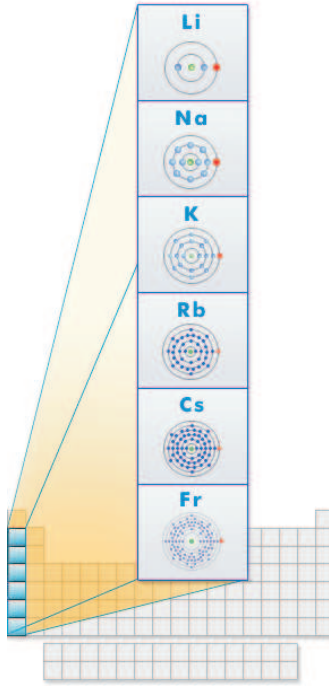
Figure 1: Alkali metals form the leftmost column on the periodic table. We use rubidium atoms for our experiments. Figure from *Interactives: The Periodic Table* [36].

in a vacuum chamber for capturing atoms in a magneto-optical trap.

Rubidium is the 37th atom on the periodic table, naturally occurring in two isotopic forms, ^{85}Rb (72%) and ^{87}Rb (28%). While ^{85}Rb is more abundant, it has a low and negative s-wave scattering length at low temperatures, hindering evaporative cooling for Bose-Einstein condensation (although it is possible using Feshbach resonances [37]).

Table 2: Alkali metals with corresponding wavelengths and linewidths for the trapping transitions.

Alkali Metal	Wavelength (nm)	Linewidth (MHz)
Lithium (Li)	670.96	5.92
Sodium (Na)	589.16	10.01
Potassium (K)	766.60	6.09
Rubidium (Rb)	780.24	6.07
Francium (Fr)	718.22	7.57

For ^{87}Rb, the transition from the $5^2S_{1/2}$ and the $5^2P_{3/2}$ hyperfine states is 780.241 nm shown in Fig. 2 [38]. Standard commercial compact disc player laser diodes run at 785 nm, providing a ready supply of inexpensive laser diodes at relatively high powers. With temperature control and feedback tunability, these laser diodes can be coerced to be resonant with the transition for ^{87}Rb. Unfortunately, current media technology is advancing to DVD (650-660 nm) and Bluray (405 nm) formats, causing compact disc player laser diode productions to decline and reducing availability for the Rb trapping community.
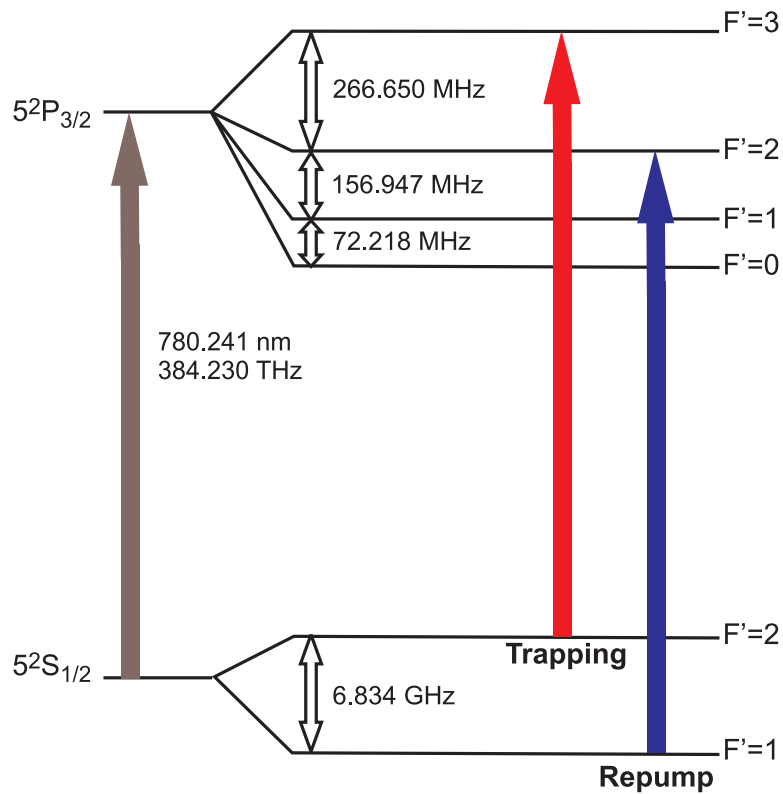
Figure 2: The hyperfine levels for ^{87}Rb.

2.2 *Magneto-Optical Trap*

At room temperature, atoms move at $\sim$ km/s speeds. Using the technique of laser cooling, the atoms can be slowed down to speeds around a centimeter per second, corresponding to temperatures in the microKelvin level. For monatomic ideal gases,

the kinetic energy of an atom can be related to the temperature by the relation,

$$K.E = \frac{1}{2}mv_{rms}^2 = \frac{3}{2}k_B T\,.$$

(2.1)

Combined with a magnetic field gradient, atoms can be trapped in a magneto-optical trap.

2.2.1   Laser cooling

From the perspective of atom-light interactions with the valence electrons, the alkali metals can be approximated as single electron systems due to the lone electron in the outmost shell. The valence electron only interacts with photons at the same energy, or frequency, of the ground to the excited state transition within a narrow linewidth of a few MHz.

A moving atom experiences a Doppler shift of

$$\omega_{doppler} = -\mathbf{k} \cdot \mathbf{v}$$

(2.2)

where $\mathbf{k}$ is the light wave propagation vector and $\mathbf{v}$ is the velocity of the atom. For an atom traveling in the same direction of the light wave propagation, it experiences a negative shift in frequency. Opposing directions of the atom and light induces a positive shift. These frequency shifts are the principle mechanisms behind laser cooling. The frequency of the light is negatively adjusted such that the light is shifted into resonance only when an atom is traveling towards the light. When the atom absorbs a photon, it undergoes a momentum kick of $\hbar\mathbf{k}$ and is slowed down. Once the atom is cooled and slowed, doppler effects subside, and the light is no longer on resonant with the atom. By counterpropagating two cooling beams in all three orthogonal directions, an atom constantly experiences cooling effects in this "optical molasses" configuration.

The steady state solution of the optical Bloch equations for a 2-level system gives

the total scattering rate due to the cooling lights at wavelength λ [39],

$$\gamma_{scatter} = \frac{s_0\gamma/2}{1 + s_0 + [2(\delta + \omega_D)/\gamma]^2} \tag{2.3}$$

where γ is the spontaneous decay rate of the atom, δ is the effective detuning of the laser light, $\omega_D = \mp\mathbf{k} \cdot \mathbf{v}$ is the doppler shift, $s_0 = I/I_0$ is the saturation parameter, I is the intensity of the light, and $I_0 = \frac{\pi\hbar\gamma c}{3\lambda^3}$ is the saturation intensity. By multiplying the scattering rate with the momentum kick due to a photon, the force on the atom due to absorption and spontaneous emission is

$$F_{sp} = \hbar k \frac{s_0\gamma/2}{1 + s_0 + [2(\delta + \omega_D/\gamma]^2} \,. \tag{2.4}$$

In 1D, the net force on the atom due to two counterpropagating beams becomes

$$F_{sp} = \frac{\hbar k s_0 \gamma}{2} \left[\frac{1}{1 + s_0 + [2(\delta + kv)/\gamma]^2} - \frac{1}{1 + s_0 + [2(\delta - kv)/\gamma]^2} \right] \tag{2.5}$$

assuming that the two beams do not interfere and act on the atom independently. In the approximation that $|kv| \ll \gamma, |\delta|$ and using the binomial series expansion, the force simplifies to

$$F_{cool} = -4\hbar k^2 s_0 \frac{2\delta/\gamma}{1 + s_0 + (2\delta/\gamma)^2} \mathbf{v} \tag{2.6}$$

for three pairs of orthogonal counterpropagating beams. The result is a velocity dependent damping force and therefore cools the atoms.

Unfortunately, adverse heating occurs from the atom spontaneously decaying from the excited state to the ground state. A balance of the cooling and heating limits the minimum temperature of the atoms to the Doppler limit

$$T_D = \frac{\hbar\gamma}{2k_B} \,. \tag{2.7}$$

Upon early studies of cold atoms in 1988 [40], atom temperatures were measured to be colder than the Doppler limit. It was found that this was a result of sub-Doppler cooling.

14

A year later, Dalibard and Cohen-Tannoudji [41], and Chu et al. [42] independently explained the effect of sub-Doppler cooling. Two counterpropagating beams of opposite polarization produce a polarization gradient. For two counterpropagating beams with orthogonal linear polarizations, a lin⊥lin gradient is formed. The resulting polarization of the light field cycles from linear to circular, creating "potential hills". Moving atoms experience a "Sisyphus cooling" effect as they expend their kinetic energy to climb a potential hill until they reach the point of circular polarization light and are optically pumped down, where they have to start climbing another hill. The process is repeated until the atoms have no more energy to climb another potential hill.

Circularly polarized light provides a different mechanism for cooling. For two counterpropagating fields with orthogonal circular polarizations (σ^+, σ_-), Sisyphus effects are not possible. For this $\sigma^+ - \sigma^-$ gradient, the polarization is always linear but the direction is rotating an angle of 2π over one optical wavelength. The rotating polarization axis selectively pumps moving atoms into one ground Zeeman sublevel more than the other sublevels. Unbalanced radiation pressure from the population differences acts as a damping force, more effective than typical Doppler cooling, and lowers the temperature of an atom to near the recoil temperature

$$T_r = \hbar^2 k^2/(2k_B M) \tag{2.8}$$

where M is the mass of the atom.

Laser cooling provides only a technique for slowing atoms. To trap atoms, a position-dependent force is needed. This is accomplished by introducing a magnetic field gradient in combination with laser cooling.

2.2.2 Magnetic Field Gradient

For simplicity, consider an atom with a ground state with zero angular momentum and an excited state with total angular momentum of $F = 1$. In the presence of an

external magnetic field, the degeneracy of the m_f levels is lifted due to the Zeeman shift. Each level is shifted by

$$\Delta = m_f \mu B \,, \tag{2.9}$$

where μ is the magnetic dipole moment of the electron and B is the applied magnetic field. Equation 2.9 shows that the energy shift is proportionately dependent on the m_f quantum number and the magnetic field. In a magnetic field gradient created by coils in an anti-Helmholtz configuration, the m_f levels split, as shown in Fig. 3.
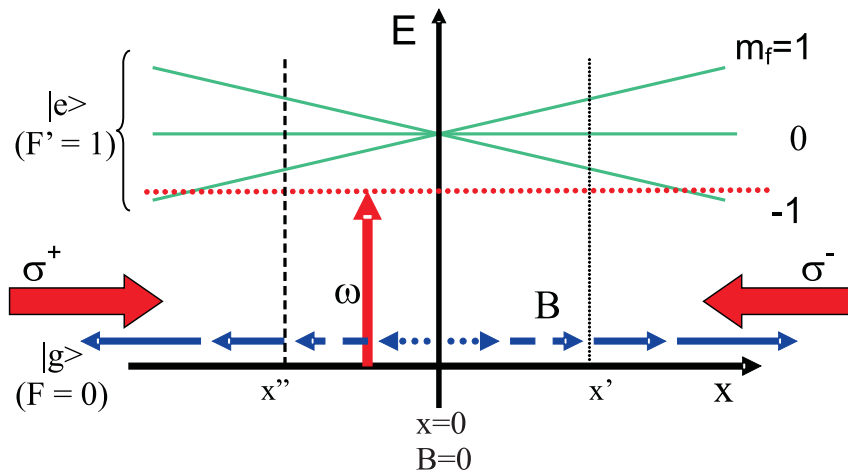
Figure 3: The excited energy level of an atom splits with respect to the B-field. At point x', frequency of the laser light is closer to resonance with $m_f = -1$ state, which is pumped by σ^- polarized light and pushed toward the center of the gradient where the magnetic field is zero. Likewise, at point x'', the laser light is closer to resonance with the $m_f = +1$ state, which is pumped by σ^+ polarized light and also pushed towards the center of the trap.

If the frequency of the cooling light is detuned as shown in the figure, atoms only scatters photons when they are away from the gradient center. Since the selection rules allow only certain states to interact with specific polarizations, having two counter-propagating beams with opposite circular polarizations result in the atoms experiencing a force pushing them to where the magnetic field is zero. It should be noted that it is critical that the polarizations are orientated correctly with respect to the magnetic field gradient. For a higher field gradient, the trapping region (area

between x' and x" in Fig. 3) becomes smaller and fewer atoms can be trapped. For our experiments, very large gradients are used to trap single atoms, and low gradients are used to trap many atoms.

2.3 Optical Dipole Traps

In 1986, the first optical trap was demonstrated by trapping small particles with a focused laser beam [43]. Within a year, optical traps were used to trap bacteria [44] and neutral atoms [42]. In atomic physics, these traps have expanded to methods to create all-optical Bose-Einstein condensates [45] and better atomic clocks [46, 47]. In our experiment, we use optical traps to capture, store, and transport single atoms to a high-finesse optical cavity. The following sections review the operation of an optical dipole trap, following closely to the review article by Grimm [48].

2.3.1 Optical Trapping

In the presence of an electric field $\mathbf{E}(\mathbf{r}, t) = \hat{e}\tilde{E}(\mathbf{r})e^{i\omega t} + c.c$ oscillating at a frequency ω, an electric dipole is induced in a neutral atom

$$\mathbf{p}(\mathbf{r}, t) = \hat{e}\tilde{p}(\mathbf{r})e^{i\omega t} + c.c.\,, \tag{2.10}$$

where $\hat{e}$ is the polarization unit vector, $\tilde{E}$ is the electric field amplitude, and $\tilde{p}$ is the dipole moment amplitude. The interaction potential of the induced dipole is given by

$$U_{dip} = -\frac{1}{2}\langle \vec{p} \cdot \vec{E} \rangle = -\frac{1}{2\epsilon_0 c}Re(\alpha)I\,, \tag{2.11}$$

where $I = 2\epsilon_0 c^2|\tilde{E}|^2$ is the intensity of the light and α is the complex polarizability. This equation demonstrates that the atom prefers to be at the point of greatest intensity to be at its lowest energy configuration. The force exerted on the dipole by the field is found by taking the negative gradient of the potential

$$F_{dip}(\mathbf{r}) = -\nabla U_{dip}(\mathbf{r}) = \frac{1}{2\epsilon_0 c}Re(\alpha)\nabla I(\mathbf{r})\,. \tag{2.12}$$

17

An atom in the trap will absorb energy from the driving field at a rate

$$P_{abs} = \langle \dot{\mathbf{p}} \cdot \mathbf{E} \rangle = \frac{\omega}{\epsilon_0 c} Im(\alpha) I \,, \tag{2.13}$$

and re-emit it as dipole radiation. The corresponding photon scatter rate is found by dividing the power absorbed by the energy of one emitted photon $\hbar\omega$,

$$\Gamma_{sc}(\mathbf{r}) = \frac{P_{abs}}{\hbar\omega} = \frac{1}{\hbar\epsilon_0 c} Im(\alpha) I(\mathbf{r}) \,. \tag{2.14}$$

As will be seen, both the dipole potential and the scattering rate are dependent on the frequency of the electric field because of the frequency dependency of the polarizability.

To find the polarizability, we model the system as a Lorentz oscillator, where an electron with mass m_e and charge e is bound to a massive nucleus by a spring with a resonant frequency ω_0. When the atom is driven by an electric field $E(t)$, the equation of motion is [49]

$$\ddot{x} + \Gamma_\omega \dot{x} + \omega_0^2 x = -\frac{eE(t)}{m_e} \,, \tag{2.15}$$

where

$$\Gamma_\omega = \frac{e^2 \omega^2}{6\pi\epsilon_0 m_e c^3} \tag{2.16}$$

is the damping rate due to radiation. By integrating the equation of motion and using the relation

$$\tilde{p} = \alpha \tilde{E} \,, \tag{2.17}$$

the polarizability can be found to be

$$\alpha = \frac{e^2}{m_e} \frac{1}{\omega_0^2 - \omega^2 - i\omega\Gamma_\omega} \,. \tag{2.18}$$

If we define an on-resonance damping rate (spontaneous decay rate) $\gamma = (\omega_0/\omega)^2 \Gamma_\omega$, the polarizability can be written as

$$\alpha = 6\pi\epsilon_0 c^3 \frac{\gamma/\omega_0^2}{\omega_0^2 - \omega^2 - i(\omega^3/\omega_0^2)\gamma} \,. \tag{2.19}$$

18

Finally, substituting the polarizability into the dipole potential and scattering rate, we find that

$$U_{dip}(\mathbf{r}) = -\frac{3\pi c^2}{2\omega_0^3}\left(\frac{\gamma}{\omega_0 - \omega} + \frac{\gamma}{\omega_0 + \omega}\right)I(\mathbf{r}),\tag{2.20}$$

$$\Gamma_{sc}(\mathbf{r}) = \frac{3\pi c^2}{2\hbar\omega_0^3}\left(\frac{\omega}{\omega_0}\right)^3\left(\frac{\gamma}{\omega_0 - \omega} + \frac{\gamma}{\omega_0 + \omega}\right)^2.\tag{2.21}$$

For most experiments, the trap frequency is not on resonance with the atom, but the difference $\Delta = \omega - \omega_0$ is still small compared to the atomic frequency, $|\Delta| \ll \omega_0$. This approximates the dipole potential and the scatter rate to be expressed as

$$U_{dip}(\mathbf{r}) = -\frac{3\pi c^2}{2\omega_0^3}\frac{\gamma}{\Delta}I(\mathbf{r})\tag{2.22}$$

$$\Gamma_{sc}(\mathbf{r}) = \frac{3\pi c^2}{2\hbar\omega_0^3}\left(\frac{\omega}{\omega_0}\right)^3\left(\frac{\gamma}{\Delta}\right)^2.\tag{2.23}$$

It can be clearly seen that as the trapping field is further detuned from the atomic potential, the potential becomes shallower. But when the trapping field is near resonant with the atom, the scattering rate increases which can cause heating and decoherence. Fortunately, the scatter rate is inversely proportionate to the second order of the detuning while the trap depth is inversely proportionate to the first order of the detuning, allowing for frequencies where the trap is relatively deep but with few scattering events.

2.3.2 Optical Lattice

The simplest form of an optical trap is a single focused Gaussian beam with a potential of [50]

$$U(\mathbf{r}) = U_0\frac{\omega_0}{\omega(z)}exp\left(-\frac{\rho^2}{\omega^2(z)}\right)exp\left(-ikz - ik\frac{\rho^2}{2R(z)} + i\zeta(z)\right),\tag{2.24}$$

where $\zeta(z) = tan^{-1}(z/z_r)$ is the Guoy parameter and $R(z) = z\sqrt{1 + (z_r/z)^2}$ is the radius of curvature. ω_0 is the beam waist which leads the beam width at position z to be

$$\omega = \omega_0\sqrt{1 + \left(\frac{z}{z_r}\right)^2}\tag{2.25}$$

19

and the Rayleigh range z_r to be

$$z_r = \frac{\pi \omega_0^2}{\lambda} \,.$$ (2.26)

For tighter confinement along the trap axis (z-axis), another beam is introduced to form a 1D optical lattice. Counterpropagating two beams of the same frequency and polarization creates an interference pattern with a "well" spacing of $\lambda/2$. The resultant dipole potential, neglecting the Guoy phase shift and wavefront curvature of the beams, is

$$U(\mathbf{r}) = U_0 \frac{\omega_0^2}{\omega^2(z)} e^{-2\rho^2/\omega^2(z)} \cos^2(kz)$$ (2.27)

The combination of the two beams provides a maximum intensity of

$$I_{max} = \frac{4P}{\pi \omega_0^2} \,,$$ (2.28)

where P is the total power of the two beams. This leads to a maximum trap depth of

$$U_{max} = \frac{\hbar \gamma}{2} \frac{I_{max}}{I_0} \frac{\gamma}{\Delta} \,.$$ (2.29)

2.3.3 Conveyor Lattice

When the frequencies of the two lattice beams are the same, they produce a standing wave. However when a frequency shift $\Delta\nu$ is induced, the standing wave becomes a traveling wave with a frequency-dependent velocity. The frequency difference is introduced into the phase of the dipole potential as [51]

$$U(\mathbf{r}) = U_0 \frac{\omega_0^2}{\omega^2(z)} e^{-2\rho^2/\omega^2(z)} \cos^2(\pi \Delta\nu t - kz) \,.$$ (2.30)

If the traveling wave is modeled as a standing wave moving at a velocity v, the phase must be constant in this frame of reference, which gives the condition

$$\frac{d}{dt} (\pi \Delta\nu t - kz) = 0 \,.$$ (2.31)

20

Combining this with the definition of $k = 2\pi/\lambda$, the velocity of the traveling wave is found to be

$$v = \frac{\lambda \Delta \nu}{2} \, . \tag{2.32}$$

For our experiments, we shift the frequency of one lattice beam by 5 kHz, which translates to a velocity of 2.66 mm/s.

CHAPTER III

CAVITY QED

As one could imagine, simply observing single photons interacting with single atoms with a detector is a difficult endeavor. While it can be done, the detection efficiencies tend to be very low. An atom in free space emits photons in all directions, reducing the efficiency of coupling the signal into the detector. By placing the atom in a strong coupling cavity system, the photon is favored to be emitted along the cavity axis, increasing the probability of detecting the photon through the cavity transmission.

This chapter presents the background theory for an atom-cavity system. The first section introduces three important cavity parameters: the atom-cavity coupling rate g_0, the atomic linewidth γ, and the cavity linewidth κ. The requirements for an atom-cavity system to be in the strong coupling regime is also described in this section by various characteristics. The next section builds the theory of cavity QED from the Jaynes-Cummings Hamiltonian for a driven cavity and the presence of a single atom. In the final section, the theory addresses the case where the atom in the cavity is driven, not the cavity, and the effect of adding additional atoms into the cavity mode (not driven).

3.1 Cavity QED Parameters

An atom-cavity system is largely characterized by three parameters, g_0, κ, and γ. g_0 describes the interaction rate between the atom and the cavity mode photon. κ is the linewidth of the cavity and describes the rate of losses from the cavity mode due to the cavity mirrors. γ is the decay rate of the atomic system in the cavity. A schematic of the atom-cavity system and the relevant parameters is illustrated in Figure 4.
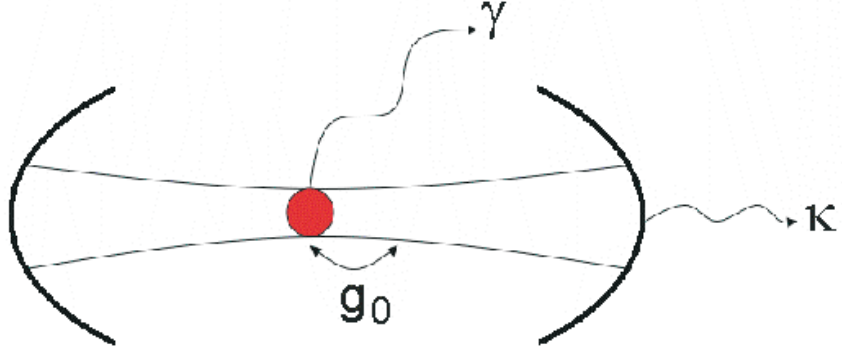
Figure 4: Schematic of the atom-cavity system.

3.1.1 Atom-Cavity Interaction

The position dependent atom-cavity interaction rate $g(\vec{r})$ is defined by the interaction of the dipole moment of the atom $\mathbf{d}$ and the electric field of the cavity mode $\mathbf{E}(\vec{r})$

$$g(\vec{r}) = \frac{\mathbf{d} \cdot \mathbf{E}(\vec{r})}{\hbar} \,. \tag{3.1}$$

Since the interaction term is based on the spatial structure of the cavity mode, it can be expressed as

$$g(\vec{r}) = g_0 \psi(\vec{r}) \tag{3.2}$$

where g_0 is the maximum coupling rate. The spatial function of the cavity mode $\psi(\vec{r})$ is chosen so that it corresponds to the cavity mode volume (V_m) as

$$V_m = \int d^3 x |\psi(\vec{r})|^2 \,. \tag{3.3}$$

For a TEM$_{00}$ mode, the spatial function is given as

$$\psi(\vec{r}) = e^{-(x^2+y^2)/w_c^2} \cos(kz) \tag{3.4}$$

which indicates a Gaussian profile with a waist of w_c in the transverse plane of the cavity mode and a standing wave along the cavity mode axis (z-direction). The

23

electric field amplitude inside a resonator due to a single photon is [52]

$$E = \sqrt{\frac{\hbar \omega_c}{2\epsilon_0 V_m}} \tag{3.5}$$

where ω_c is the frequency of the cavity. Using this and Eqns. 3.1 and 3.2, the maximum coupling rate can be expressed as

$$g_0 = d\sqrt{\frac{\omega_c}{2\hbar\epsilon_0 V_m}} \; . \tag{3.6}$$

3.1.2 Linewidth of Cavity

Current coating technologies allows mirrors to have extremely high reflectivities, with corresponding low transmission losses in the parts per million (ppm) range. The finesse of the cavity $\mathcal{F}$ is

$$\mathcal{F} = \frac{2\pi}{losses} \; , \tag{3.7}$$

where the losses are due to absorptions and the transmission of the cavity. Cavities finesses can range up 10^6, where losses through the cavity mirrors are very low. In our experiments, we want photons to interact with atoms in the cavity many times before they leave the system, so cavities with high finesses, in the 10^5 range, are used.

As the probe through the cavity is detuned, the cavity transmission profile is Lorentzian where the half-width half-maximum (HWHM) is denoted as κ. This cavity linewidth is inversely proportionate to the finesse

$$\kappa = \frac{\nu_F}{2\mathcal{F}} \; , \tag{3.8}$$

where ν_F is the free spectral range and is defined as

$$\nu_F = \frac{c}{2L} \; , \tag{3.9}$$

where L is the length of the spacing between the cavity mirrors and c is the speed of light.

We measure κ directly by coupling a probe beam into the cavity mode and detecting the transmission of the probe on the other side of the cavity. By scanning the

frequency of the probe beam and directly recording the changing transmission, the linewidth can be measured experimentally. Using this and the length of the cavity, the losses can be found from

$$losses = \frac{4\pi\kappa L}{c}\,. \tag{3.10}$$

3.1.3 Linewidth of Atom Decay

The linewidth of an atomic transition in free space is related to the lifetime of the upper excited state $\gamma = \tau^{-1}$. In our experiments, we use ^{87}Rb and concentrate mainly on the D2 transition from the $5^2S_{1/2} \rightarrow 5^2P_{3/2}$ hyperfine states. The lifetime for this transition τ is 26.2 ns, which gives a linewidth of $\gamma = \tau^{-1} = 2\pi \times 6.1$ MHz [38].

In some cavity QED references, $\gamma_\perp$,the atomic decay rate into all modes except the cavity mode, is used to describe the atomic linewidth of the system. $\gamma_\perp$ is half of the atomic inversion decay rate $\gamma_\parallel$, which is also the free space atomic linewidth γ due to the small solid angle into the cavity mode [53]. For this thesis, $\gamma = \gamma_\parallel$ is used and all equations have been adjusted to account for all relevant factors of 2.

3.2 Strong Coupling Regime

To increase single atom-single photon interactions in the cavity, the system needs to be in the strong coupling regime. Specifically, the interaction rate of the atom and cavity field must be greater than the loss rates due to decay out the cavity mirrors and scatter or decoherence due to the spontaneous emission of the atom, $g_0 \gg \kappa, \gamma$. The coupling strength of a cavity is defined by the single atom cooperativity parameter

$$C = \frac{g_0^2}{\kappa\gamma}\,. \tag{3.11}$$

Strong coupling is achieved when the single atom cooperativity is much greater than 1. When it is much less than 1, it is in the weak coupling regime.

There are two additional characteristics that can describe an atom-cavity system. The saturation photon number n_0 specifies the role of the number of photons in a

cavity [16] and is expressed as

$$n_0 = \frac{1}{3}\frac{\gamma^2}{g_0^2} \qquad (3.12)$$

for a Gaussian cavity mode. The saturation photon number determines the number of photons needed in the cavity mode to yield an optical intensity sufficient to saturate the atomic transition in free space. For strong coupling, $n_0 \ll 1$.

The other characteristic is the critical atom number N_0, which specifies the role of the number of atoms in the cavity [16] and is expressed as

$$N_0 = \frac{\gamma\kappa}{g_0^2} = C^{-1}. \qquad (3.13)$$

The critical atom number determines the number of atoms needed to change the cavity response. To be in the strong coupling regime, $N_0 \ll 1$. When these conditions are satisfied, the atom-cavity system is sensitive to single photons and atoms.

3.3   Single Atom-Cavity Interactions

The atom-cavity system is described by the Jaynes-Cummings Hamiltonian, which consists of the Hamiltonians of the atom H_A, the cavity field H_C, and the interaction between the atom and cavity H_I [54],

$$H = H_A + H_C + H_I = \frac{\hbar\omega_a}{2}\hat{\sigma}_z + \hbar\omega_c\hat{a}^\dagger\hat{a} + \hbar g_0(\hat{a}\hat{\sigma}^\dagger + \hat{a}^\dagger\hat{\sigma}), \qquad (3.14)$$

where g_0 is the atom-cavity coupling strength, σ_z is the atomic inversion operator, ω_a and ω_c are the resonant frequencies of the atom and the cavity, respectively, and $\hat{a}^\dagger$ and $\hat{a}$ are the field creation and annihilation operators. For a two level atom where $|g\rangle$ and $|e\rangle$ are the ground and excited states, $\hat{\sigma}^\dagger = |e\rangle\langle g|$ and $\hat{\sigma} = |g\rangle\langle e|$ are the atomic raising and lowering operators. If the interaction term is ignored ($g_0 = 0$) and the cavity is set to be on resonance with the atom, the eigenvalues of the Hamiltonian are degenerate. When the coupling term is added ($g_0 \neq 0$), the degeneracy of the
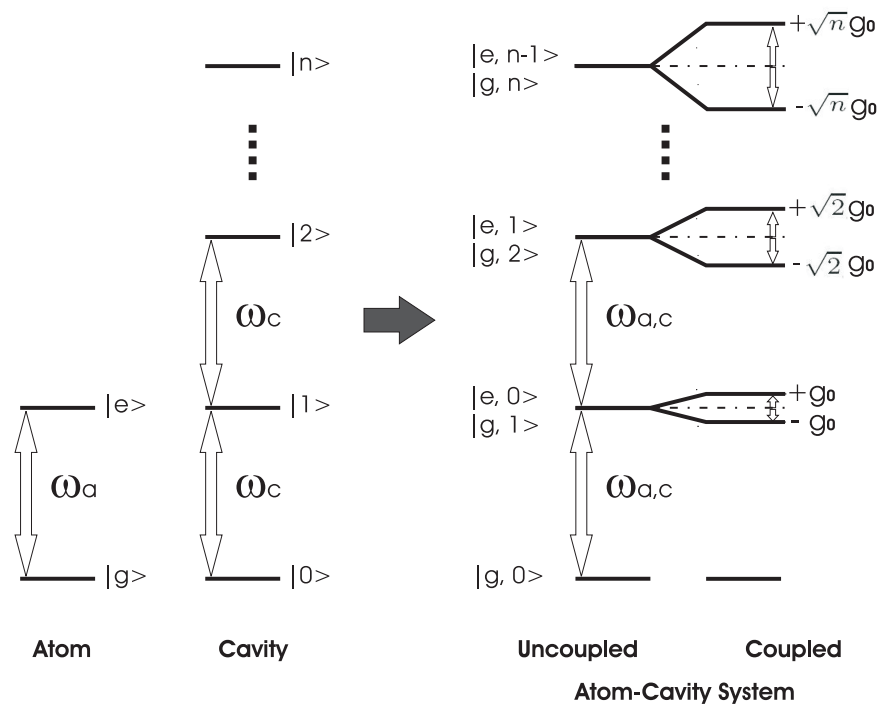
Figure 5: When an atom and cavity on resonance are coupled, the degeneracy of the eigenstates is lifted by $2\sqrt{n}g_0$. The splitting structure is called the Jaynes-Cummings ladder.

states is lifted and the resulting energy eigenstates are

$$|E_{n-}\rangle = (|e, n-1\rangle - |g, n\rangle)/\sqrt{2} \tag{3.15}$$

$$|E_{n+}\rangle = (|e, n-1\rangle + |g, n\rangle)/\sqrt{2} \tag{3.16}$$

where e and g refer to the excited and ground states of the atom and n refers to the cavity field excitation level. The corresponding energy eigenvalues for each energy eigenstate are

$$E_{n-} = n\hbar\omega - \sqrt{n}\hbar g_0 \tag{3.17}$$

$$E_{n+} = n\hbar\omega + \sqrt{n}\hbar g_0 \,. \tag{3.18}$$

Each splitting pair is separated by $2\sqrt{n}\hbar g_0$, and this splitting of states is often referred to as the Jaynes-Cummings ladder, shown in Fig. 5.

The model, however, does not sufficiently describe a realistic system. Dissipation, such as the atomic spontaneous decay rate and the leakage through mirrors of finite reflectivity, is not taken into account. These losses and possible detunings are added to the Jaynes-Cummings Hamiltonian using standard density matrix formalisms. This gives us a generic master equation in the electric dipole and rotating wave approximations [55],

$$\dot{\rho} = \mathcal{L}\rho \tag{3.19}$$

where the Liouvillian operator $\mathcal{L}$ and density matrix ρ are defined in the Lindbland equation as [56]

$$\mathcal{L}\rho = -\frac{i}{\hbar}[\hat{H}_0, \rho] + \hat{\mathcal{C}}\rho\hat{\mathcal{C}}^\dagger - \frac{1}{2}\hat{\mathcal{C}}^\dagger\hat{\mathcal{C}}\rho - \frac{1}{2}\rho\hat{\mathcal{C}}^\dagger\hat{\mathcal{C}} \,. \tag{3.20}$$

The collapse operator $\hat{\mathcal{C}}$ is used to add in dissipation due to the cavity decay rate κ and the atomic decay rate γ as [57]

$$\hat{\mathcal{C}} = \sqrt{2\kappa}a + \sqrt{\gamma}\sigma \,. \tag{3.21}$$

The cavity can also be coherently driven by an external probing field ε, which is added into the Jaynes-Cummings Hamiltonian. Accounting for detuning in the
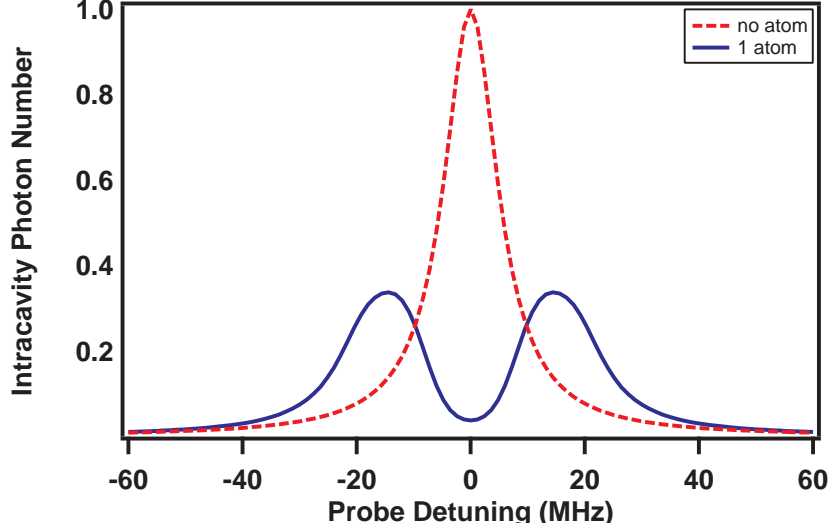
Figure 6: Vacuum Rabi splitting for a cavity with parameters $(g_0, \kappa, \gamma) = 2\pi \times (17, 6, 6)$ MHz and the driving field is such that there is one intracavity photon. The dashed red trace shows the transmission of the cavity with no atom present in the mode. When an atom is present in the solid blue trace, the transmission splits with a spacing of $2g_0$ between the two peaks.

rotating frame with respect to the probe frequency ω_p and adding a term for the driving field $H_\varepsilon = \hbar\varepsilon(\hat{a} + \hat{a}^\dagger)$, the Hamiltonian becomes

$$\hat{H}_0 = \hbar\Delta_c\hat{a}^\dagger\hat{a} + \hbar\Delta_a\hat{\sigma}_z + \hbar g(\vec{r})(\hat{a}\hat{\sigma}^\dagger + \hat{a}^\dagger\hat{\sigma}) + \hbar\varepsilon(\hat{a} + \hat{a}^\dagger)\,, \tag{3.22}$$

where Δ_c is the detuning of the cavity with respect to the probe $(\omega_c - \omega_p)$ and Δ_a is the atom-probe detuning $(\omega_a - \omega_p)$.

The master equation can be solved numerically for any given cavity parameters (g_0, κ, γ). Figure 6 shows a steady state solution for an empty cavity and for a cavity with a single atom in the center of its mode. In the presence of an atom, the Gaussian transmission profile of the empty cavity "splits" into two peaks separated by $2g_0$ and is referred to as the vacuum Rabi splitting. As can be seen, if the probe is on resonance with the cavity, the transmission level drops drastically when an atom is brought into the mode. For our experiments, this change in output is used to ensure that the atoms delivered via the conveyor lattice to the cavity mode.
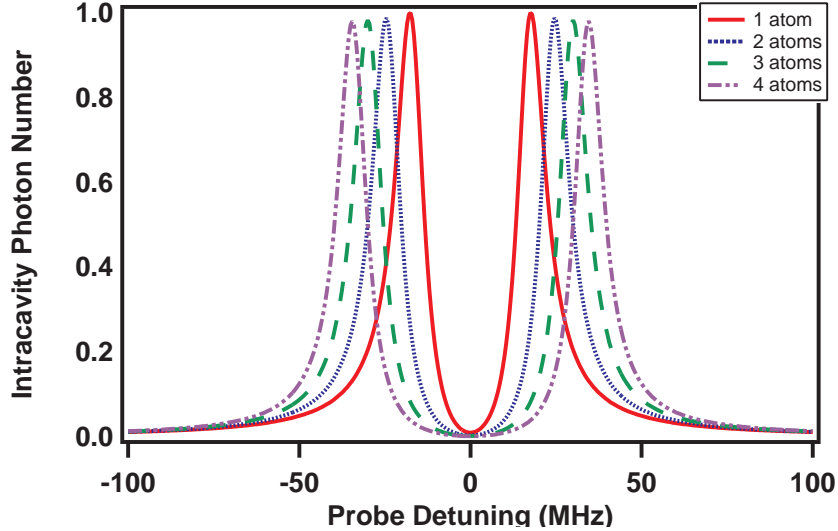
Figure 7: Cavity output signal for a driven cavity and atom system plotted vs the detuning of the driving field. The red solid line represents one atom, the blue dotted line represents 2 atoms, the green dashed line represents 3 atoms, and the purple dashed/dotted line represents 4 atoms in the cavity mode. The cavity parameters are $(g_0, \kappa, \gamma) = 2\pi \times (17, 7, 6)$ MHz and the driving field is set so that the intracavity photon number is 1.

As more atoms are added into the cavity, the transmission of the cavity changes. The Jaynes-Cummings ladder shows that the splitting goes with $\sqrt{N}g_0$, where N is the number of atoms in the cavity. Figure 7 is a plot of the cavity transmission for varying number of atoms in the mode. As can be seen, the splitting of the peaks grow as $\sqrt{N}g_0$.

3.4   Many Atoms-Cavity Interaction

By introducing more atoms in the cavity, atom-atom entanglement is possible. Using the cavity mode as a mode of information exchange, two relatively remote atoms can indirectly interact with each other via photons in the cavity but be addressed separately. Two qubit entanglements is useful in applications such as the fundamental controlled-NOT gate for quantum computing.

For atom that is driven from the side of the cavity and not down the cavity mode

axis, the Hamiltonian is expressed as

$$\hat{H}_0 = \hbar\Delta_c \hat{a}^\dagger \hat{a} + \hbar\Delta_a \hat{\sigma}_z + \hbar g(\vec{r})(\hat{a}\hat{\sigma}^\dagger + \hat{a}^\dagger \hat{\sigma}) + \hbar\varepsilon(\hat{\sigma} + \hat{\sigma}^\dagger) \,. \qquad (3.23)$$

Compared to the previous section, only the final term has changed from the probe field driving the cavity to driving the atom. Now, an additional atom is introduced into the cavity but is not driven by the field. The Hamiltonian is written as

$$\hat{H}_0 = \hbar\Delta_c \hat{a}^\dagger \hat{a} + \hbar\Delta_a \hat{\sigma}_{1z} + \hbar g(\vec{r})(\hat{a}\hat{\sigma}_1^\dagger + \hat{a}^\dagger \hat{\sigma}_1) + \hbar\Delta_a \hat{\sigma}_{2z} + \hbar g(\vec{r})(\hat{a}\hat{\sigma}_2^\dagger + \hat{a}^\dagger \hat{\sigma}_2) + \hbar\varepsilon(\hat{\sigma}_1 + \hat{\sigma}_1^\dagger) \,,$$
$$(3.24)$$

where the subscript 1 represents the first atom being driven and the subscript 2 represents the second atom added. Clearly, as more atoms are introduced to the cavity mode, they simply add to the total Hamiltonian as

$$\hat{H}_0 = \hbar\Delta_c \hat{a}^\dagger \hat{a} + \sum_{n=1}^{N} \left[\hbar\Delta_a \hat{\sigma}_{nz} + \hbar g(\vec{r})(\hat{a}\hat{\sigma}_n^\dagger + \hat{a}^\dagger \hat{\sigma}_n) \right] + \hbar\varepsilon(\hat{\sigma}_1 + \hat{\sigma}_1^\dagger) \,, \qquad (3.25)$$

for N atoms.

In Fig. 8, the cavity output signal is plotted for different number of atoms. As the number of atoms increase, the signal decreases. The splitting also increases, which is expected since it depends on N, as was seen in Fig. 5. It is interesting to see that in section A of Fig. 8, where the probe detuning is zero, the signal drops. However, at very specific detunings, such as section B of the figure, the signal increases for 2 atoms and then proceeds to drop as more atoms are introduced into the cavity.

In comparison, Figure 9 is a plot of the cavity output signal for all the atoms being driven in the system. In this case, the signal does not drop at zero probe frequency as it did in Fig. 8. The peaks merely spread out by $\sqrt{N}g_0$ as expected, but increase in power, as each atom adds more scatter into the cavity.

One would näively assume that for the case where only one atom is driven, the cavity output would increase as more atoms are delivered into the cavity. While the other atoms are not driven by the probe, they would be probed by the light scattered
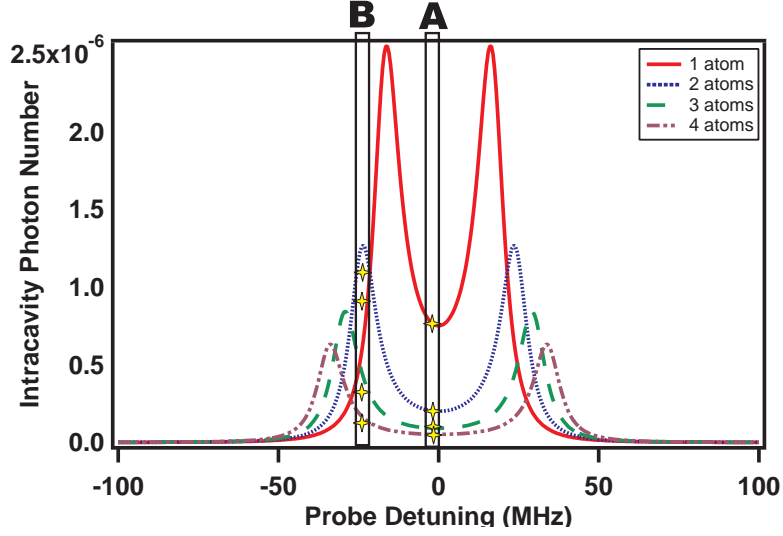
Figure 8: Cavity output signal for a cavity and driven atom system plotted vs the detuning of the driving field. The red solid line represents only the driven atom present in the cavity. The blue dotted line represents 2 atoms in the system, the green dashed line represents 3 atoms, and the purple dotted-dashed line represents 4 atoms, with only one atom driven for all cases. The cavity parameters are $(g_0, \kappa, \gamma) = 2\pi \times (17, 7, 6)$ MHz.

by the driven atom into the cavity mode. Also, as more atoms are introduced into the cavity, the coupling rate of the cavity should increase. However, we see that the power drops. In both Figs. 8 and 9, the driving field is set to be 10^{-3} times the saturation intensity.

When the atom driven system probe intensity is increased to saturation intensity, an interesting feature occurs. For more than one atom, a third peak emerges in the cavity output signal around zero detuning, shown in Fig. 10. This does not happen for the cavity driven system.

When the driving field intensity is much greater than saturation, the middle extraneous peak disappears again in Fig 11. However, unlike the driven cavity case, the splitting is still present. One would expect that to be so, because an atom is limited to a maximum scatter rate of $\gamma/2$ for a probe beam much larger than the saturation intensity ($s_0 \gg 1$), given from Eqn. 2.3. A driven cavity would continuously increase
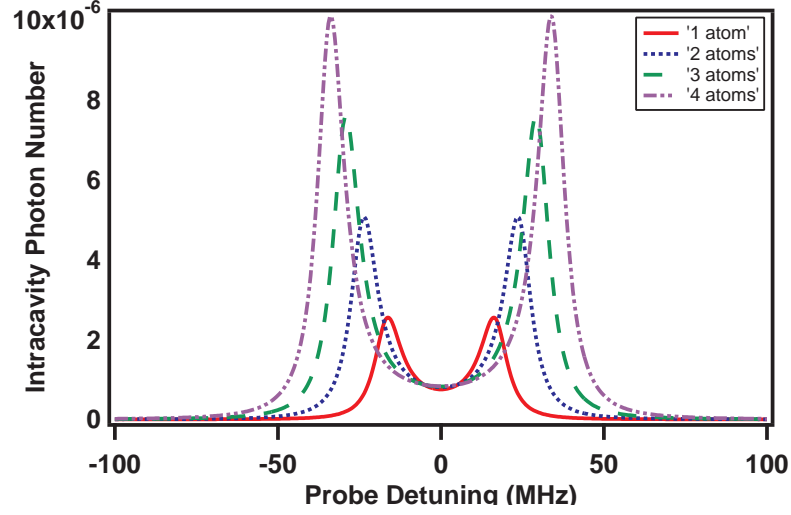
Figure 9: Cavity output signal for driven atoms plotted vs the detuning of the driving field. The red solid line represents one atom, the blue dotted line represents 2 atoms, the green dashed line represents 3 atoms, and the purple dotted-dashed line represents 4 atoms in the cavity mode. The cavity parameters are $(g_0, \kappa, \gamma) = 2\pi \times (17, 7, 6)$ MHz .
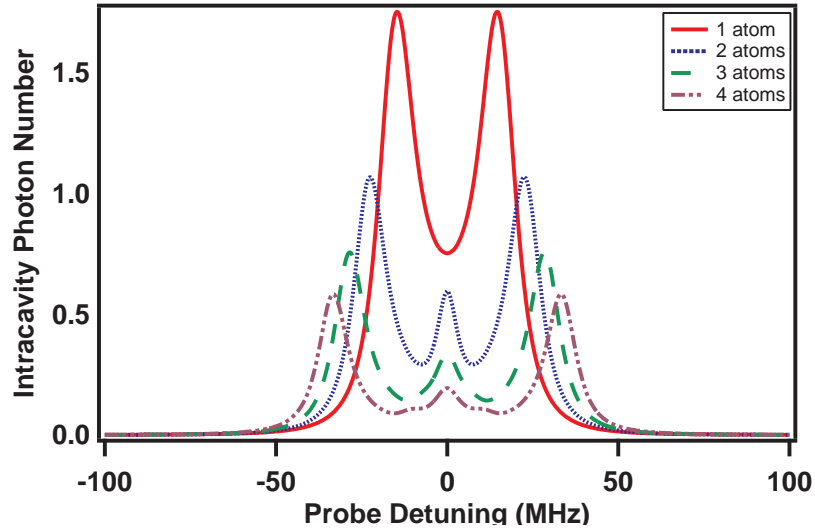
Figure 10: Cavity output signal for a cavity and driven atom system plotted vs the detuning of the driving field. The driving field is at saturation intensity. The red solid line represents only the driven atom present in the cavity. The blue dotted line represents 2 atoms, the green dashed line represents 3 atoms, and the purple dotted-dashed line represents 4 atoms in the cavity mode, where only one atom is driven in each case. The cavity parameters are $(g_0, \kappa, \gamma) = 2\pi \times (17, 7, 6)$ MHz.

33
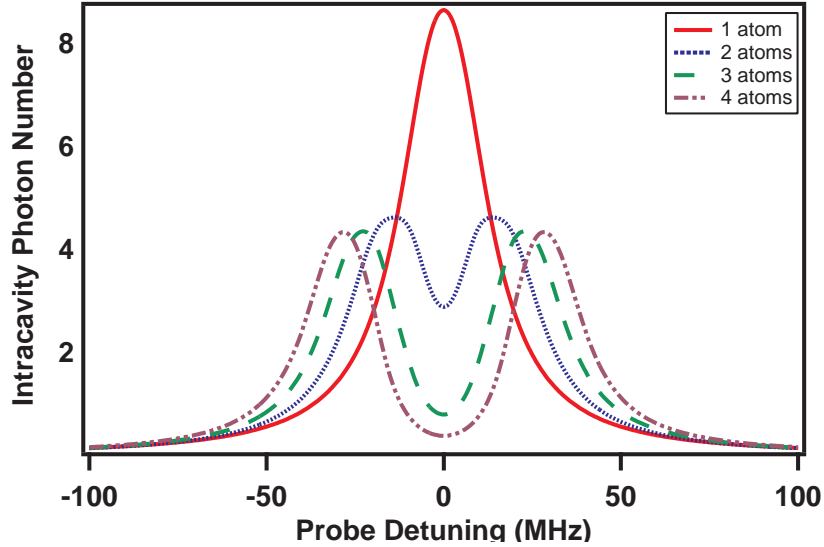
Figure 11: Cavity output signal for a cavity and driven atom system plotted vs the detuning of the driving field. The driving field is 10^3 times the saturation intensity. The red solid line represents only the driven atom present in the cavity. The blue dotted line represents 2 atoms, the green dashed line represents 3 atoms, and the purple dotted-dashed line represents 4 atoms in the cavity mode, where only one atom is driven in each case. The cavity parameters are $(g_0, \kappa, \gamma) = 2\pi \times (17, 7, 6)$ MHz.

with the field intensity and oversaturate the system, making the presences of the atoms insignificant to the whole system.

Adding detunings from the cavity or the atom with respect to the probe shifts the center point of the output signal and favors one peak over another. Figure 12 plots the cavity output for a low intensity probe field, similar to Fig. 8, but with an effective atom detuning with respect to the probe of +7 MHz in Fig. 12(a), and a cavity detuning of +7 MHz in Fig. 12(b). While they both shift the center point by the same amount (+7 MHz), the weighting of the peaks is opposite. Otherwise, the continuously dropping signal for adding atoms into the system is similar to the case of no detuning in Fig. 8.
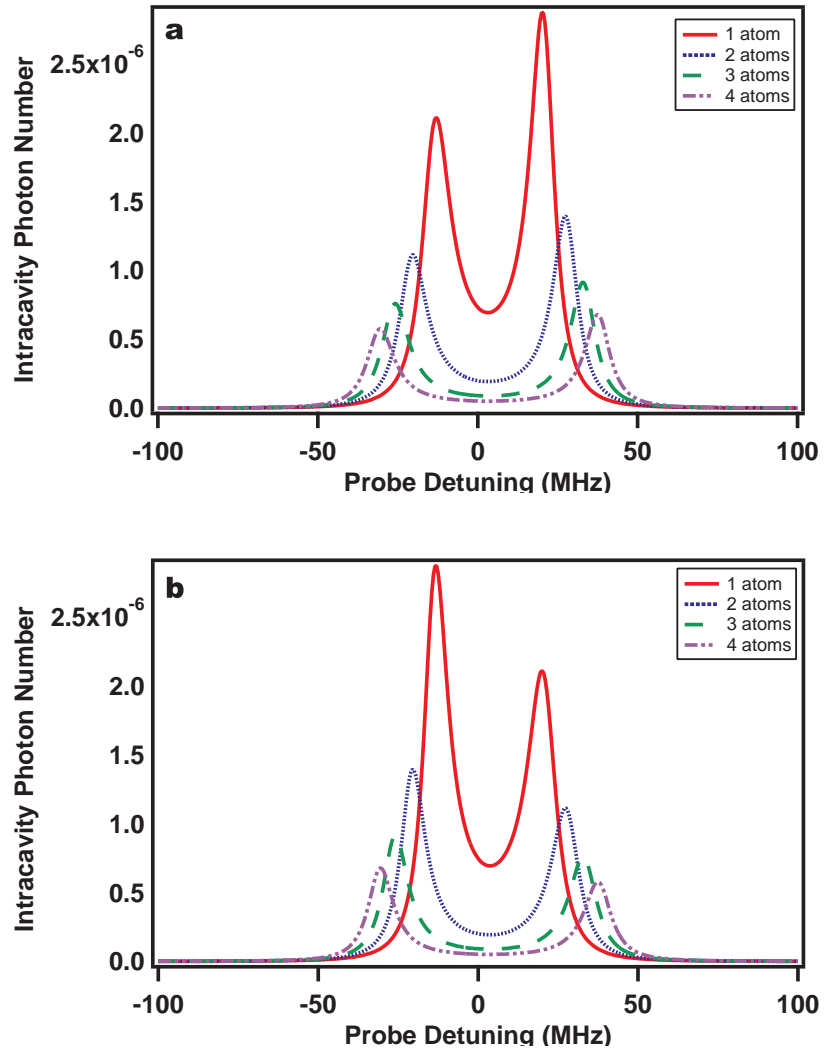
Figure 12: Same as Fig. 8, but the effective atom detuning from the probe is +7 MHz in part (a). In part (b), the cavity is detuned from the probe by +7 MHz.

CHAPTER IV

EXPERIMENTAL APPARATUS

In this section, the various components of the experimental apparatus are described. The main sections concentrate on the vacuum chamber system, the laser systems to create the MOT, the optical dipole trap, the various cavities, and the different types of detection used in our experiments.

4.1 Vacuum Chamber System
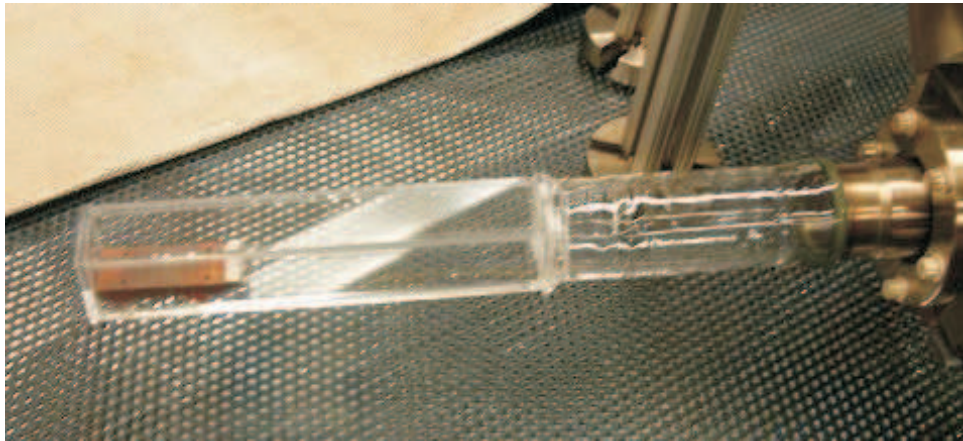
Figure 13: A picture of the quartz vacuum cell.

The experiment apparatus consists of a vacuum system made up of four main parts: a quartz cell, an ion gauge, an ion pump, and a titanium sublimation pump. The quartz cell is a rectangular 6" × 1.25" × 1.25" structure constructed by Allen Scientific Glass. It transitions to a 2.75" CF flange which is attached to a stainless steel six-way cube, shown in Fig. 13. The top and bottom sides of the cube are occupied by getters (2 Rb, 1 K) which are attached to BNC connections that lead out of the chamber. A window with an anti-reflection (AR) coating is placed on
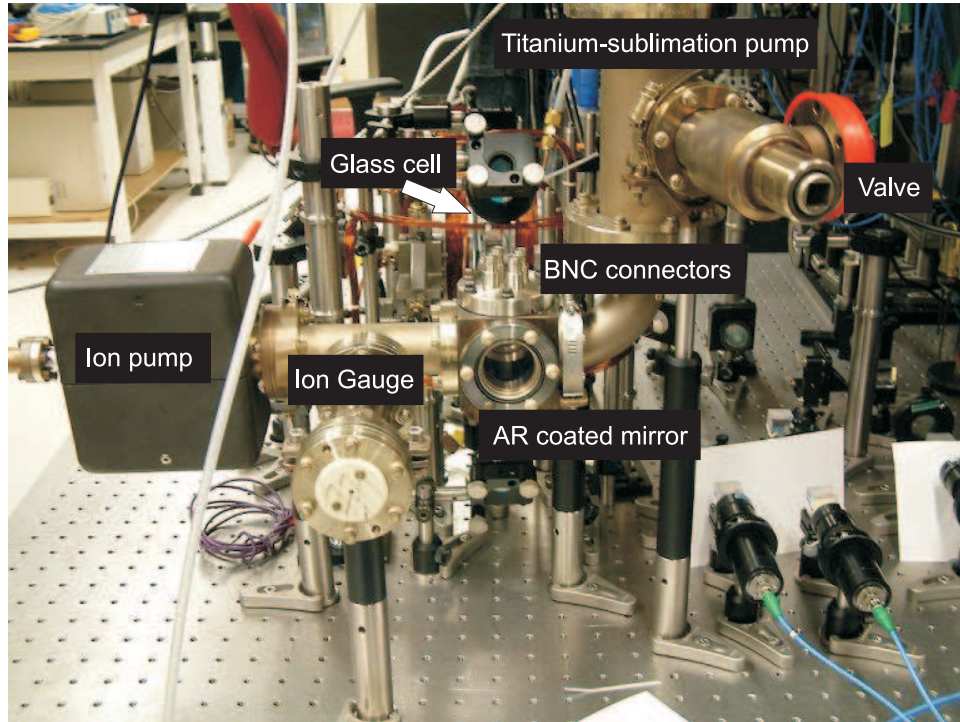
Figure 14: A picture of the vacuum chamber.

the side opposite the cell for optical access down the axis of the quartz cell. One of the remaining sides is connected to an ion gauge and ion pump, and the last side is connected to a Titanium sublimation pump. A picture of the vacuum system is shown in Fig. 14.

In order to reach ultra-high vacuum (UHV), the system is connected to a series of pumps. First, a roughing pump, connected via a valve, brings down the pressure of the chamber to 10^{-3} torr. A turbomolecular pump is also connected to the system to further reduce the pressure to $10^{-4} - 10^{-9}$ torr. While being pumped down, the system is baked above $100°$ C to drive water and other gases from the walls of the chamber to reduce outgassing. To monitor the progress of the vacuum system, a residual gas analyzer (RGA) is used. The system is connected to the system until the RGA shows that the pressures of water, nitrogen, oxygen and carbon dioxide are sufficiently reduced to partial pressures in the $10^{-12} - 20^{-14}$ range. To check for any

possible leaks in the system, the whole chamber is sprayed with helium gas and any sudden jumps in the helium gas pressure in the chamber is monitored on the RGA.

The valve is sealed off and the system is disconnected from the vacuum pumping station. The ion pump and ion gauge on the vacuum chamber is immediately turned on to maintain and monitor the pressure in the system. The titanium sublimation pump is fired 2-3 times to reduce the pressure of the system further to a desired 10^{-11} torr.

4.2   MOT Beams and Coils

In order to make a MOT, two main components are needed, the optical molasses laser beams and the magnetic field coils.

4.2.1   Optical molasses laser systems
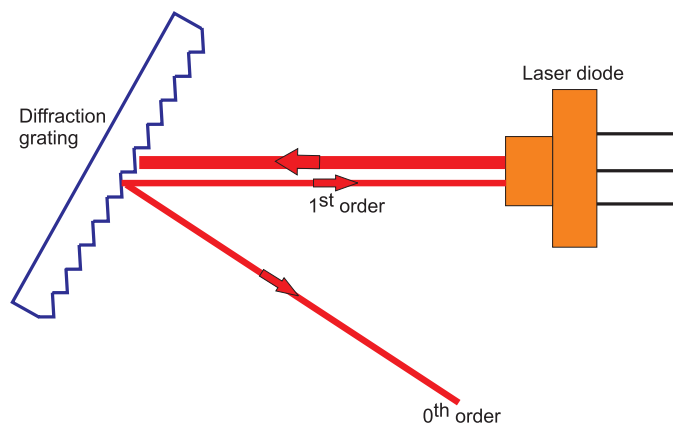
Figure 15: A diffraction grating splits the laser output into different frequencies, all at different angles of refraction. The grating is fixed so that the first order of the laser output power is fed back into the diode. Small changes in the angle of the grating adjusts the frequency that pumps the laser. The zeroth order of the output is used as the main experimental beam.

The light for laser cooling and trapping comes from a central master laser system seeding a slave laser system. The master laser diode (Sharp GH0781JA2C) is set in an external cavity diode laser (ECDL) system which consists of a diffraction grating in

38

a Littrow configuration (Fig. 15). In addition, the temperature and current applied to the diode can be adjusted to coerce the diode to operate at the desired frequency. A piezoelectric transducer (PZT) behind the grating provides fine tuning to put the output of the laser at the correct frequency with a linewidth of around 1 MHz. By taking a few mW of the light into a separate locking setup, the master laser is locked to the $F = 2 \rightarrow F' = 3$ D2 transition of ^{87}Rb via FM spectroscopy [58].

The remaining light is double-passed through a 110 MHz AOM (Isomet 1206C) before seeding a slave laser to provide the ability to adjust the frequency of the trapping light with a range of -90 MHz to +20 MHz from the lockpoint. By doublepassing the AOM with a 1:1 telescope, shown in Fig. 16, spatial movement of the light is minimized as the frequency of the modulation is shifted. This is beneficial for when light is later coupled into a fiber or the slave laser.
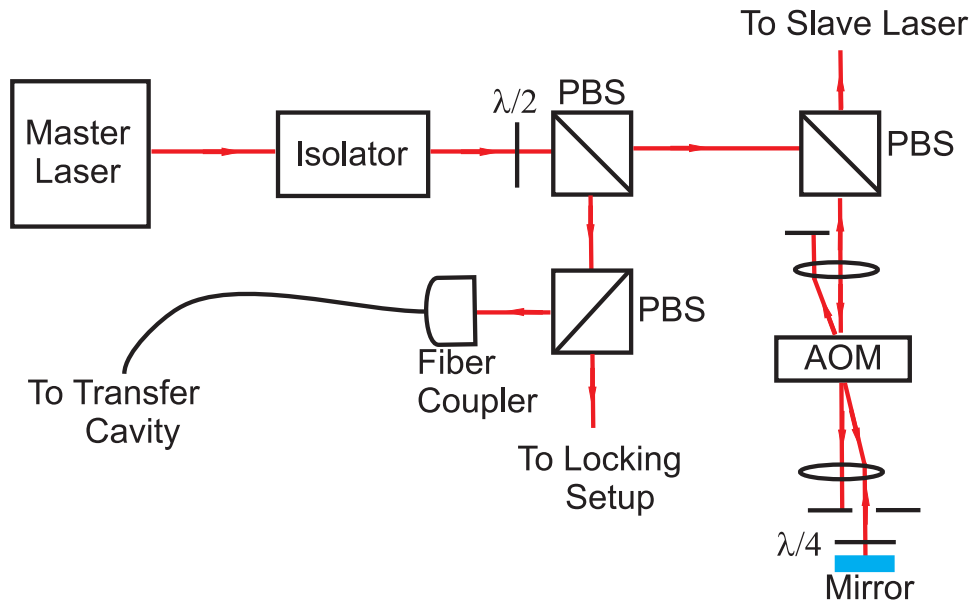
Figure 16: A schematic of the trapping master laser setup.

The slave laser is set on the correct wavelength by seeding it with the master laser. Through a rejection exit port on an optical isolator, the seeding light is set into the slave diode, shown in Fig. 17. Only a few hundred microwatts is needed

to seed the laser, so an attenuation wheel is used to adjust the light being inserted into the slave. The temperature and current are also adjusted on the slave so that it is stable at the desired wavelength. The slave does not need to be locked since it can follow the master system mode-hop free when adjusted correctly. Another AOM is used to adjust total power of the light before it is split with half-wave plates and polarizing beamsplitters. The light is then coupled into six fibers: three MOT fibers, two cooling fibers, and one probe fiber. 8-12 mW of laser power are coupled into the three MOT fibers. The remaining light is split amongst the cooling and probe fibers, and the powers are adjusted by attenuation wheels.
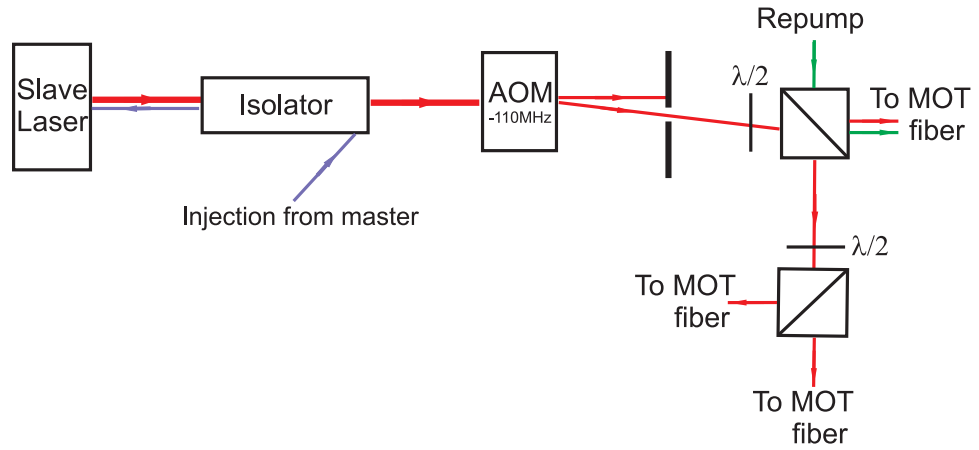
Figure 17: A schematic of the trapping slave laser setup.

The repump light is controlled by a main master laser that provides seeds for all the repump lasers in the lab. This laser is locked to the $F = 1 \to F' = 2$ D2 transition for ^{87}Rb. The AOM modulation in the locking setup shifts the frequency by -80 MHz, which allows all the slaves to have power adjustability as well by adding an 80 MHz AOM in their paths to compensate for the shift. The repump light is split into two paths, one to a fiber for the MOT and the other combines with the cooling and probe lights by a 50/50 beamsplitter.

The three MOT trapping fibers and repump fiber are brought to a separate table that has the vacuum chamber system. The numerical aperture of the fiber is 0.11,

so the beam expands to a diameter of 1" when collimated with a 125 mm lens. The beam is then apertured to a 0.5" diameter so that the light has a "top hat" profile. The beam can be further apertured to smaller diameters of a few millimeters, which is useful for alignment purposes.

As explained earlier, a MOT requires three pairs of counterpropagating beams. The three expanded MOT beams are split in two by a half-wave plate and a polarizing beamsplitter (PBS), shown in Fig. 18. This also allows us to have the ability to balance the powers of the light in each direction. Each pair is set to counterpropagate along one of the three dimensional axes. The expanded repump beam is added into one of the MOT lights by the polarizing beamsplitter used to split the light, as seen in Fig. 18. Before the lasers enter the chamber, quarter-wave plates make each beam the correct circular polarization for trapping.

4.2.2 Magnetic coils

The magnetic field gradient is created by two coils constructed by 1/4" diameter refrigerator copper tubing wrapped in Kapton tape to provide electrical insulation. There are 3 rows of 4 turns, 12 turns total. The coils are held together with plastic restraints to prevent eddy currents when the coils are quickly turned off in the experiments. The inner radius of the coils is 1.25", and due to the thickness of the tubing, the outer radius is 4.5". The coils are set in an anti-Helmholtz configuration to provide a magnetic field gradient. In order to count single atoms in a MOT, a very high gradient of ~ 300 G/cm is required. To create such gradients, the coils are positioned to be as close as possible, limited only by the vacuum quartz cell which causes the distance between the center of the coils to be 3.5". While one coil is secured, the other is placed on a 3D translation stage to provide a few mm of adjustability on the position of the center of the gradient as will be seen later. A schematic of the magnetic coils is shown in Fig. 19.
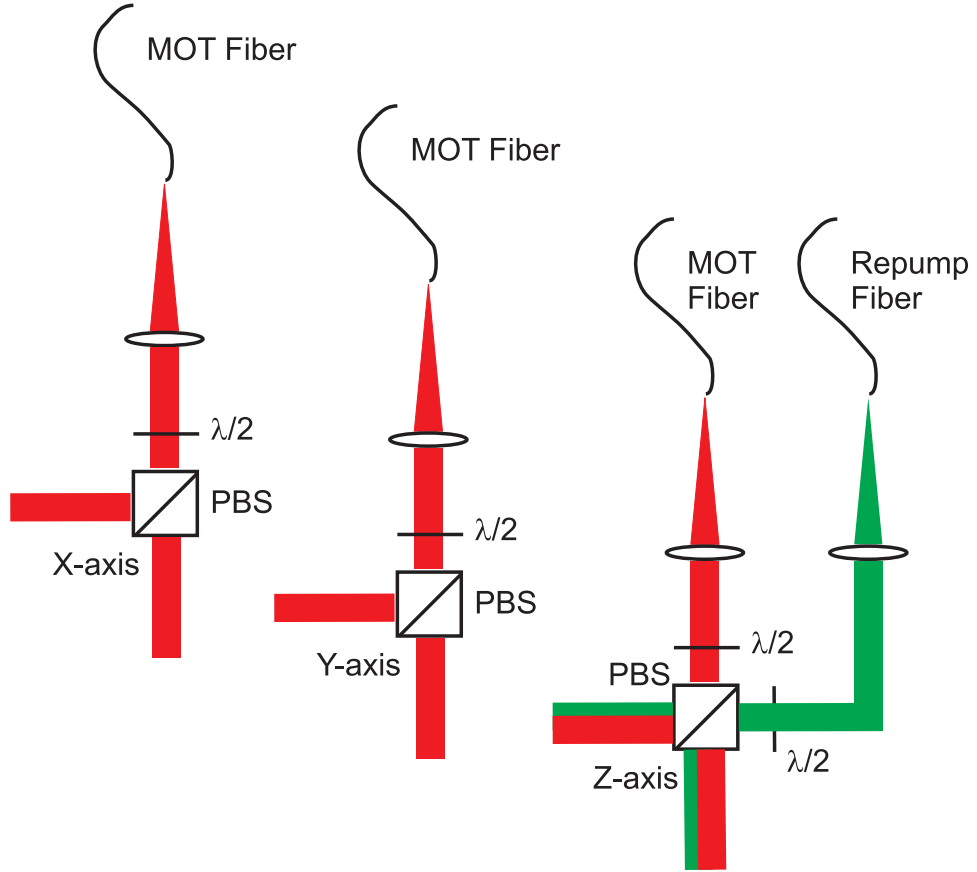
Figure 18: A schematic of the MOT beam setup.

A 15 kW Electronic Measurement Inc. power supply is used to provide current for the coils. The power supply can provide up to 500 A due to the 15 V limit on the power supply and the 30 mΩ resistance of the coils, giving a maximum gradient of 280 G/cm which is what we require to trap single atoms. When run at full power, the resistance causes the coils to get extremely hot, above 100° C, so water cooling is necessary to keep the system at a reasonable temperature of 50° C.

4.3   Optical Dipole Trap

As mentioned earlier, we also trap our atoms in an optical dipole trap. Though my first experience dealt with two seeded tapered amplifier (TA) systems at 850 nm, the bulk of my studies was spent working with a fiber laser operating at 1064 nm. The
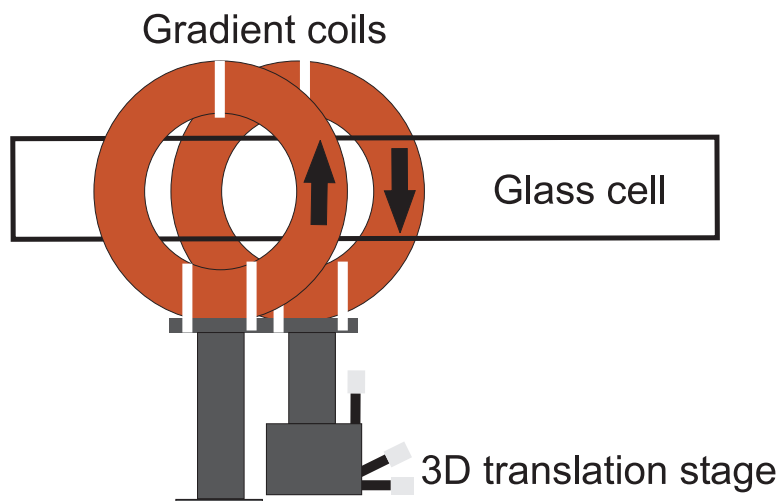
Figure 19: The coils used to create the magnetic field gradient for the MOT. One coil is mounted on a 3D translation stage. The current in the coils run in opposite directions, making them anti-Helmholtz.

fiber laser from IPG Photonics (YAR-20-LP-SF) provides a 20 W single mode beam, linearly polarized in a simple turnkey system. The laser is sufficiently stable and does not require locking or any feedback systems. To protect the laser from harmful back-reflections, two -40 dB isolators are placed immediately after the fiber collimator. The beams are then split by a half-wave plate and a PBS for controllability of the powers in the separate beams, as shown in Fig. 20.

IntraAction AOMs (AOM-40) are used to modulate and control the two beams independently. Because the beams are used to form a lattice inside the vacuum chamber, they must be phase coherent. Thus, the two rf signals that modulate the beams via the AOMs must have the same phase. This is accomplished by phase-locking the two HP signal generators (HP 8647A and HP E4430B) to each other via their 10 MHz references.

The first order beams of the AOMs are used to create the optical trap and the zeroth order beam is blocked with a beam dump. A half-waveplate is placed in one of the beams to make the polarizations of the two the same. Because we want the waist of the lattice focus to be ~ 20 μm, the beams are first magnified to beam waists
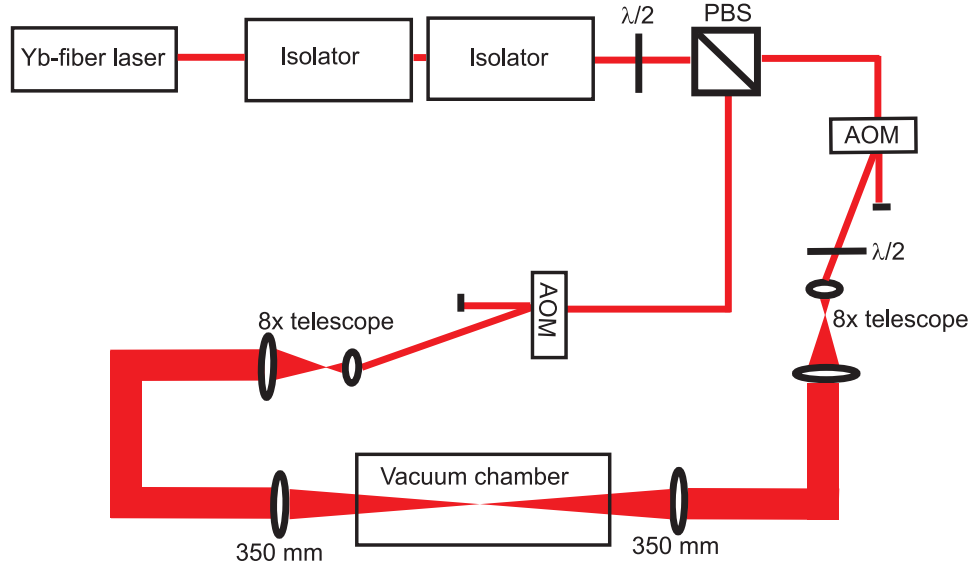
Figure 20: A schematic of the optical dipole trap laser beams.

of 4-5 mm with a 8× telescope before focused into the vacuum chamber with 350 mm achromatic lenses as seen in Fig. 20. Very carefully, the two counterpropagating beams are adjusted so that they are overlapped over a long distance (1-2 meters) to ensure that the lattice is optimized. To produce a conveyor lattice, the frequency of one of the AOMs is modulated up to 100 kHz, controlled by our LabVIEW system. This modulation provides a differential frequency between the two beams and results in a traveling wave.

4.4   Cavities

Our experimental setup requires the usage of two cavities. The science cavity is where the experiments are performed. The transfer cavity is used in the locking scheme of the laser that locks the science cavity. The next sections describe the two cavities and the different ways that they are used.

4.4.1 Science cavity system

The optical cavity is constructed so that it is in the strong coupling regime for single atoms. This requires the single-atom coupling cooperativity to be large, $C_0 >> 1$, where $C_0 = g_0^2/(\kappa\gamma)$. γ is a physical constant and cannot be changed. One can reduce κ, but there is a limit to the quality of mirrors available and the amount of signal needed in order to be able to detect and measure the system. Thus, the other option is to increase g_0. As was seen in Eqn. 3.18, this can be done by reducing the cavity mode volume but has realistic physical limitations. Typically for our experiments, the cavity has a length of a few hundred microns and the finesse of the mirrors are relatively high, ensuring that we are in the strong coupling regime.

The cavity in which the atomic experiments are carried out is constructed of two Research Electro-Optics, Inc. (REO) mirrors coned so that the mirrored face is only 1 mm in diameter and the body is 3 mm in diameter. Because a cavity mirror is curved, the coning helps to prevent the mirrors from colliding due to the short cavity length and to allow maximum optical access to the center of the cavity mode for a lattice and probes.

The cleaning of the mirrors is an arduous task, but possible with patience and care. Methods have been outlined in detail in several theses [52, 53]. Once the mirrors are cleaned, they are attached to a small rectangular piezoelectric transducer with a tiny amount of Torr-Seal so that the length of the cavity can be adjusted by applying a voltage onto the PZT. The cavity system is then mounted onto a copper block system for vibrational isolation to keep the cavity locked on a transverse electromagnetic (TEM) cavity mode.

We have experimented with various types of cavity mount systems. If we simply model the system as a simple harmonic oscillator, the resonance frequency is found to be

$$\omega = \sqrt{\frac{k}{m}} \tag{4.1}$$

where k is the spring constant and m is the mass of the system. Thus, we attach the cavity to a relatively large copper piece to lower the resonance frequency so that the cavity cannot be driven by any acoustic or vibrational disturbances from the environment. A Room Temperature Vulcanizing (RTV) silicone rubber compound is used to provide vibrational isolation of the cavity from the external system. We have found that the RTV is UHV-compatible and has superior dampening.

Over the years, many versions of the science cavity have been made and used. During my years in the lab, I have mainly dealt with two cavities. The first cavity system, nicknamed the "skiff" cavity shown in Fig. 21, was employed after an older chamber had to be replaced. The "skiff" is a one-sided cavity, providing more leakage out one mirror for improved detection while keeping the cavity in the strong coupling regime. The mirrors have a radius of curvature of 2.5 cm and specified to have transmissions of 8 ppm and 100 ppm. However, after the cavity vacuum system was set up, they were measured to be a little larger, a total transmission of 130 ppm. This increases the cavity linewidth but the system is still in the strong coupling regime. By separating these mirrors by 222 μm, the cavity parameters become $g = 17.1$ MHz, $\kappa = 7$ MHz, and $\gamma = 6$ MHz. The deterministic delivery experiment was performed on this cavity.

The second cavity is very much different than the previous cavity in that it is set vertically, seen in Fig. 22. The copper block had to be drastically reduced for the vertical cavity. While this decreases the stability of the system, it was sufficient to allow us to lock the cavity within a fraction of the linewidth. The vertical cavity does also has the disadvantage in that its optics are difficult to assemble and adjust compared to the earlier designs. However, due to the orientation of the cavity in the vacuum cell, aligning all the MOT and FORT optics are easier than in the skiff cavity.

The vertical cavity is 500 μm long, which yields cavity parameters of $g = 9.3$ MHz, $\kappa = 6.1$ MHz, and $\gamma = 6$ MHz. This allows us to still be in the strong coupling
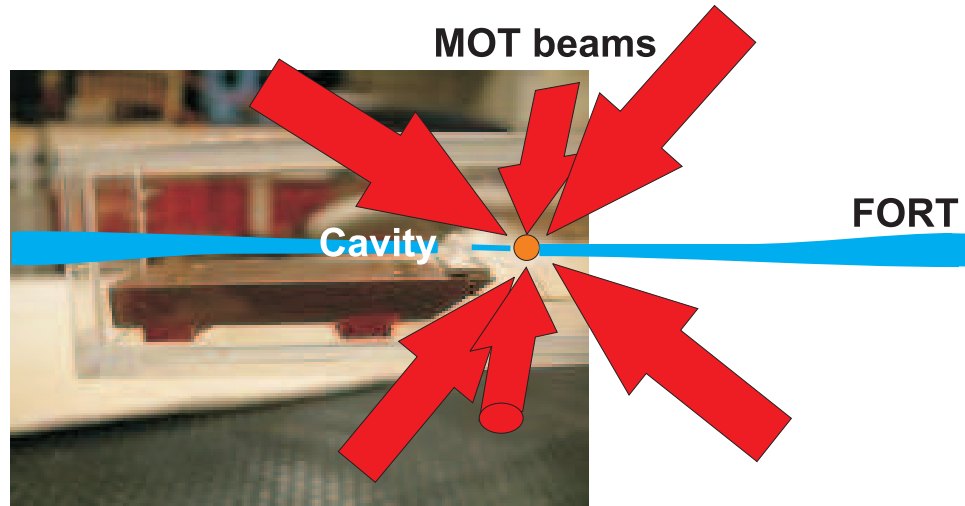
Figure 21: The "skiff" cavity and the configuration of the MOT and FORT beams. Two pairs of the MOT beams are vertical as shown. The third pair are set to perpendicular to the plane of the page.

regime while having the option of adding a second lattice.

Offresonant light (at 784 nm) is used to lock the science cavity. Along with a 780 nm probe, the two beams are expanded before they are focused into the cavity with a lens so that the beam waists focus to the same as the waist of the cavity mode. The TEM$_{00}$ mode of both the 780 nm and 784 nm light are optimized so that the other modes are suppressed. The light that transmits through the cavity is collimated with a lens before it is split for detection and locking, shown in Fig. 23. We used several techniques to separate the 784 nm locking light from the 780 nm probe/signal. A diffraction grating was used initially but suffered from low efficiencies into the first order due to polarization dependencies and the large amount of required propagation space for the two beams to be spatially resolvable. A 50/50 beamsplitter was also used to eliminate the polarization and spatial problems, but half the signal was lost in this method. Finally, a laserline filter (Semrock LL01-780-12.5) was used to separate the lights. Because it only has around a 3 nm bandwidth, the 784 nm light reflects with over 99% efficiency while the 780 nm light transmits with over 99% efficiency.
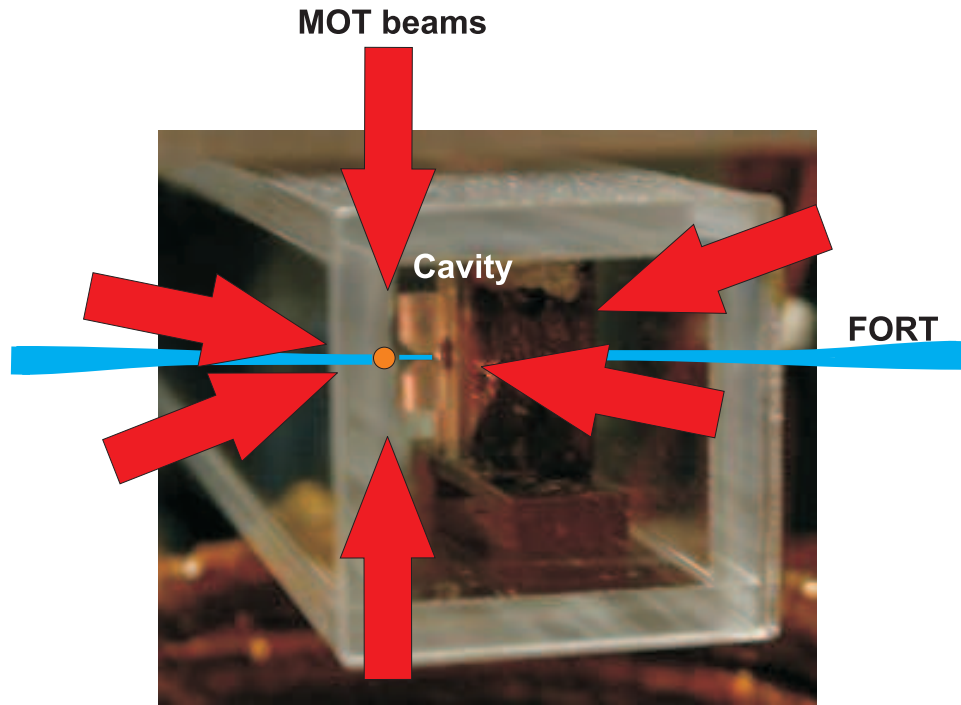
Figure 22: The "vertical" cavity and the configuration of the MOT and FORT beams. Two pairs of the MOT beams are set at angles to the cavity in the horizontal axis of the setup. The third pair runs along the vertical axis.

Additionally, it is polarization independent. The filter is set to be slightly tilted from normal incidence so that the 784 nm light does not reflect back onto its incoming path, but the angle is kept as small as possible as to not change the effectiveness and center wavelength of the optic, as seen in Fig. 23. The 784 nm light is then fiber coupled and used in a heterodyne detection system while the 780 nm signal is fiber coupled into a detection device.

4.4.2 Transfer cavity system

A 784 nm light is used to lock the science cavity. Because it is 6-7 free spectral ranges of the science cavity from the $F = 2 \rightarrow F' = 3$ D2 transition, it will not interact with atoms. However, there is no convenient atomic transition around this wavelength, so a transfer cavity system is utilized to lock the laser. The transfer cavity consists of two mirrors and a cylindrical PZT in a large invar hollow tube. Invar is used for its
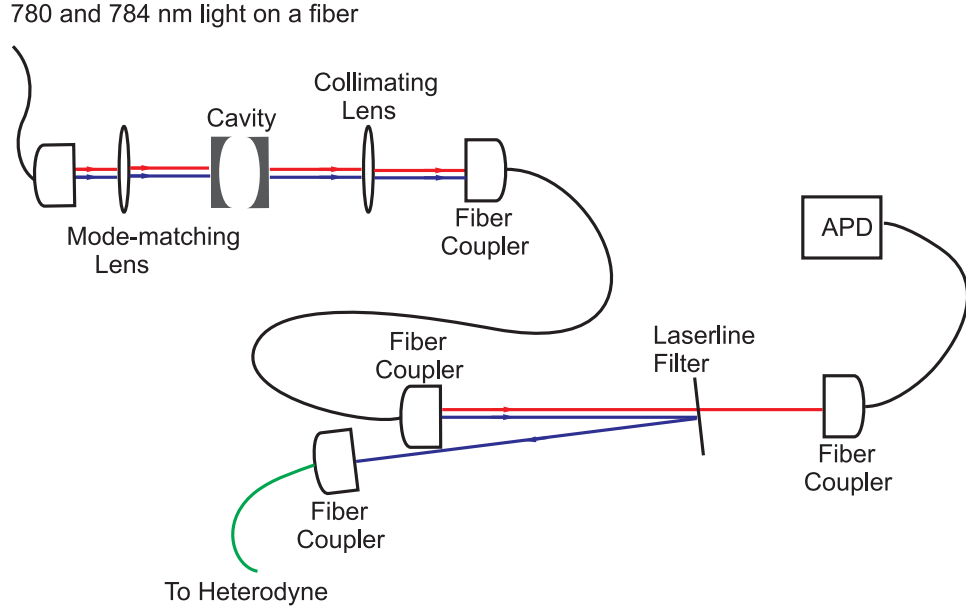
Figure 23: A schematic of the cavity output detection optics setup. The blue path represents the 784 nm light, and the red path represents the 780 nm light.

low thermal expansion coefficient ($\alpha = 1.2 \times 10^{-6}$/K at 20° C) so that the cavity is less sensitive to thermal fluctuations in the environment. The mirrors have a radius of curvature of 25 cm and are coated by VLOC to have 99% reflectivity at 780 nm. The cavity is constructed to be about 30 cm, giving a free spectral range of near 0.5 GHz and a linewidth of $\kappa = 0.8$ MHz.

In order to lock the 784 nm laser to the transfer cavity, the cavity must first be locked. 5-6 mW of the locked MOT trapping laser is used to stabilize the cavity to a TEM mode of the 780 nm light. First, the 780 nm light is double-passed through a 200 MHz AOM so that the lockpoint of the cavity can be adjusted ±20 MHz by changing the driving RF frequency of the AOM. A telescope is placed around the AOM to minimize spatial steering of the beam. The light is then coupled into a fiber that leads to the transfer cavity, shown in Fig. 24.

After the transfer cavity is locked to the MOT laser, the 784 nm laser can be
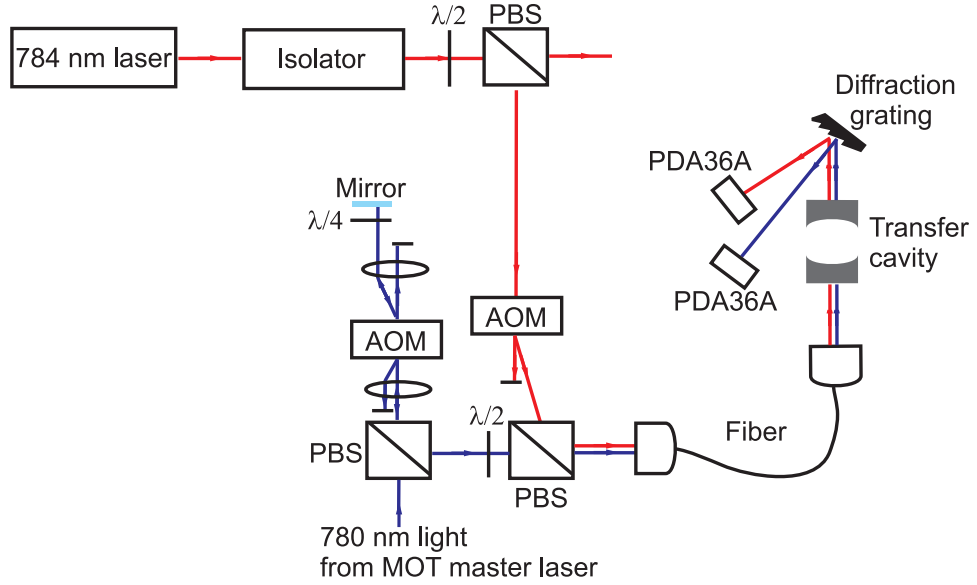
Figure 24: A schematic of the laser system for the transfer and science cavities. The orange lines represents the 780 nm path, and the red lines represent the 784 nm path.

locked. A few mW of the 784 nm light is sent through an 110 MHz AOM for modulation before it is coupled into the same fiber as the 780 nm light. A mode coupling lens is not used because the waist of the light out of the fiber is near the cavity mode waist. Also, obtaining the TEM$_{00}$ mode is not as critical in this cavity as it is in the science cavity.

The two wavelengths from the cavity output is split on a diffraction grating and detected by two Thorlabs PDA36A detectors. Since the science cavity needs to be locked to the $F = 2 \rightarrow F' = 3$ transition for ^{87}Rb, the 784 nm light is adjusted so that it is overlapped with the transition in the science cavity. Once the frequency of the 784 nm light is set, the RF frequency for the double-passed AOM on the 780 nm light is adjusted so that in the transfer cavity, the 780 nm and 784 nm lights are overlapped. First, the transfer cavity is locked to the 780 nm light using the Pound-Drever-Hall technique [59] with a bandwidth of ~ 20 kHz. Then, the 784 nm light is locked to the transfer cavity. Lastly, The science cavity is locked to the 784

nm light and should be on resonant with the correct transition wavelength.

4.5   Locking Schemes

All lasers used in the experiments are locked to either an atomic transition or a cavity. Both cavities are also stabilized, as mentioned earlier. This section explains the different locking techniques used.

4.5.1   Laser locking electronics

The frequency of the lasers are controlled by temperature, the current, and a PZT on a diffraction grating. The temperature of the laser diode is monitored by a thermocouple and maintained with a thermoelectric cooler (TEC) peltier placed on the aluminum laser diode housing. A PI (proportional-integral) feedback loop system [60] controls the current to the peltier in order to heat/cool the diode towards the set temperature.

The current is controlled by a circuit design proposed in Ref. [61]. This current controller provides a stable DC current for the laser. It also has an input for modulation to provide fast feedback on the current of the diode. The modulation is supplied by the proportional circuit from a homemade PI control lockbox. The integrator signal from the PI system controls the PZT behind the diffraction grating and corrects for long term drifts in the laser system.

4.5.2   Master laser

To provide a dispersion signal for the PI control lockbox for the current and PZT modulation, FM spectroscopy [58] is used. A few mW of the light from the master laser is split into two beams, one weak and one strong. The strong saturation pump beam counterpropagates with the weak probe beam inside a Rb vapor cell, shown in Fig. 25. The probe beam is detected by a Thorlabs photodetector (PDA36A), and when the laser PZT is scanned, the doppler free saturation spectroscopy signal can
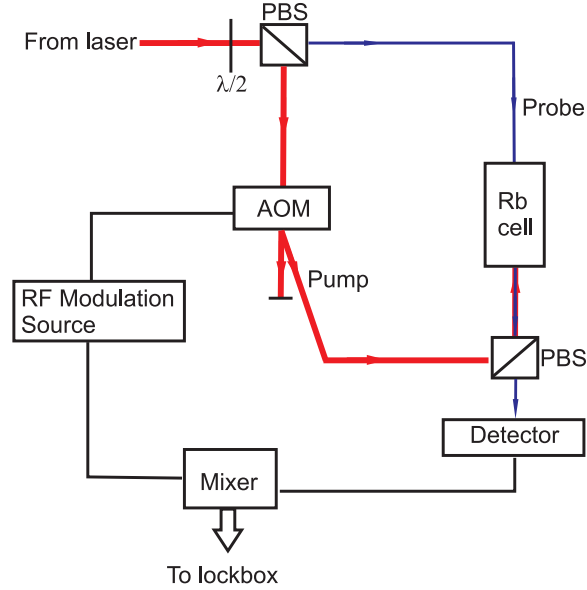
Figure 25: The locking setup for the master MOT laser.

be seen on an oscilloscope, Fig. 26. For the dispersive signal, the saturation beam is modulated by an AOM before the vapor cell. The signal from the PDA36A is demodulated in a mixer before sent to the error signal input of the PI control.

4.5.3 Slave laser

Like the master MOT laser, the slave temperature is controlled by a TEC and a PI control loop. However, there is no diffraction grating and the current is not actively controlled as it is for the master laser. Instead, the slave is injected by the master laser and coerced to follow it. To ensure that it is following the master, a few mW of the slave laser light is sent into a Rb vapor cell, Fig. 27. Because no dispersion signal is needed, no AOM is needed. To simplify the setup, the pump probe is simply retro-reflected to act as the probe beam as well. The pump is sent to a detector and viewed on an oscilloscope. To ensure that the slave is stable, the double-passed AOM in Fig. 16 is scanned and the current and temperature of the slave is adjusted until the slave follows the master with no mode hops.
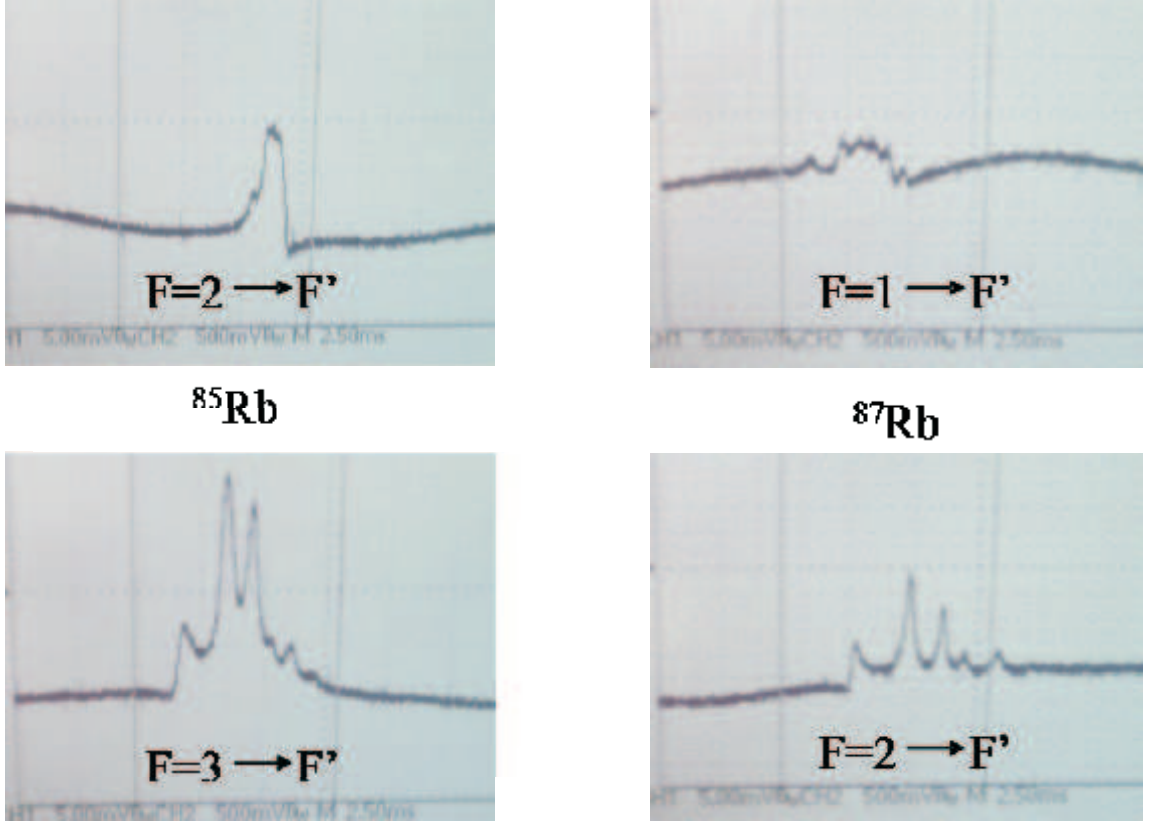
Figure 26: A saturation spectroscopy signal for ^{85}Rb and ^{87}Rb. The repumping signals are on top, and the trapping signals are on the bottom for each isotope.

4.5.4 Cavities

As mentioned earlier, each cavity is locked to a TEM mode. Resonant cavity modes are created when the light produces a standing wave between the two mirrors, or when the cavity length l is an integer multiple of light wavelength $l = n\lambda$. Using the dispersion relation for an EM wave $c = k/\omega$ and the definition of the wavevector $k = 2\pi/\lambda$, we can describe the resonant cavity frequency by the cavity length,

$$\omega = \frac{m\pi c}{l},\tag{4.2}$$

where c is the speed of light and m is the mode number. From Eqn. 4.2, we find that for a small change in the cavity frequency,

$$\Delta\omega = -\frac{m\pi c}{l^2}\Delta l = -\frac{\omega}{l}\Delta l\,.\tag{4.3}$$
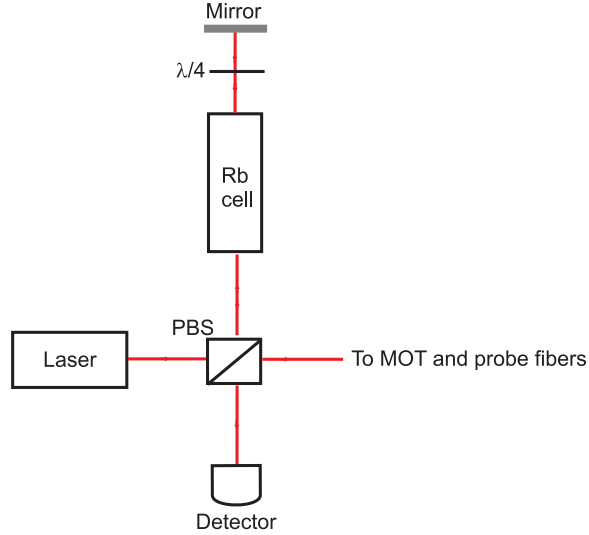
Figure 27: The saturation spectroscopy setup for the slave laser.

If the cavity frequency is changed by the cavity linewidth $\Delta\omega = \kappa = c/(2\mathcal{F}l)$ and the speed of light $2\pi c = \omega\lambda$, the corresponding change in length becomes

$$\Delta l = \frac{\lambda}{8\pi\mathcal{F}} \, . \tag{4.4}$$

For a wavelength of 780 nm and a finesse of 5×10^4, the change in length is 6×10^{-13} meters. Thus, to keep a cavity locked to a mode, the length must be stabilized to a fraction of a picometer. Active locking is needed due to the this strict length stability requirement.

4.5.4.1 Transfer cavity

The transfer cavity is locked in a similar method as the lasers, but instead of an atomic spectrum, the cavity is locked to a TEM mode. The 780 nm and 784 nm lights are frequency modulated via AOMs and the cavity output signal is demodulated in a mixer to produce dispersion signals as is done for the master MOT laser. The transfer cavity locks to the 780 nm light with PI feedback to the PZT between the cavity mirrors. The 784 nm light is locked to the cavity by sending the integral feedback to the PZT on the diffraction grating while the proportional circuit servos

the current of the 784 nm laser diode.

4.5.4.2   Science cavity

Using a dispersion signal for locking puts the light at maximum intensity (the top of the mode peak). However, to minimize off-resonant scattering in the science cavity, we would like to be as far from the peak as possible. Thus, a different method is used to lock the cavity. The 784 nm light from the cavity output is delivered to a heterodyne system [50] that mixes the weak cavity signal with a strong local oscillator taken from the 784 nm laser before the EOM. The intensity of the mixed signal is

$$
\begin{aligned}
I = \frac{1}{2}(E_{sig}^2 + E_{LO}^2) + \frac{E_{sig}^2}{2}cos(2\omega_{sig}t) + \frac{E_{LO}^2}{2}cos(2\omega_{LO}t) + \\
E_{sig}E_{LO}cos(\omega_{sig} + \omega_{LO})t + E_{sig}E_{LO}cos(\omega_{sig} - \omega_{LO})t
\end{aligned}
\tag{4.5}
$$

where the electric field of the signal is $E = E_{sig}cos(\omega_{sig}t)$ and the electric field of the local oscillator is $E = E_{LO}cos(\omega_{LO}t)$. A bias-T filters out the large dc component of the signal from the detectors (EOT-2030). The fast oscillating components are filtered out as well, leaving the intermediate beat frequency $(\omega_{sig} - \omega_{LO})$ component.

Before the 784 nm light is sent to the science cavity, it is split into two beams, a local oscillator and the cavity locking light. The local oscillator is sent directly to the heterodyne system. The cavity locking light is first modulated with an electro-optic modulator (EOM) before sent to the science cavity. The EOM is modulated with two frequencies, with a separation on the order of the science cavity linewidth, κ. After the light passes through the cavity and into the heterodyne detection system, there are two beat frequencies on the heterodyne signal. The signal is sent to two spectrum analyzers (HP 8590L) centered on the two beat frequencies. The two signals from the analyzers are subtracted on a SRS 560 preamplifier to produce a dispersion signal, shown in Fig. 28. This dispersion signal is then used in a PI feedback lock system via the error signal input. The feedback controls the cavity PZT to keep the mirrors locked onto the correct frequency. The voltage to the science cavity PZT is controlled

through the BNC connectors on the vacuum chamber.
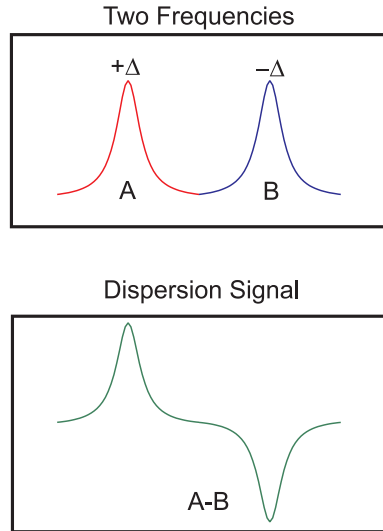
Figure 28: Dispersion signal used to lock the science cavity. The second frequency is subtracted from the first one on a preamplifier to create the signal.

4.6   Detection Systems

In our experiments, measurements and detection of the atoms are done via photon collection. Primarily, two different imaging devices are used, an EMCCD camera and an avalanche photodiode (APD).

4.6.1   EMCCD camera

An Andor IXon EMCCD camera is used to image atoms in the MOT and lattices. This camera is useful in that we can obtain a user-friendly picture in real-time for aide in applications such as alignment. Light is collected with either a high aperture laser objective, or HALO, (Linos Photonics 03-8903) or a microscope objective (Mitutoyo Corp. M Plan Apo NIR 5x). While a HALO has a larger numerical aperture (HALO: 0.38, objective: 0.14), the working distance is shorter than the microscope objective (HALO: 16.55 mm, objective: 37.5 mm). The HALO was used in the experiment

described in Chapter 5, but due to the location of the cavity in the glass cell, the microscope objective was used in the other experiments.

The light collected from the objective is focused onto the EMCCD camera by an achromatic lens with a focal length of 75 mm. To decrease the amount of noise in the signal due to stray light from the FORT beams and background from the lab, the path of the light is enclosed in 1" Thorlabs aluminum anodized lens tubes and a Semrock narrowband laserline filter at 780 nm is placed in the light path, shown in Fig. 29. For the HALO lens and microscope objective, the effective magnification of the lens system is 1.9, which leads to an effective pixel size of 8 μm for the camera imaging system.
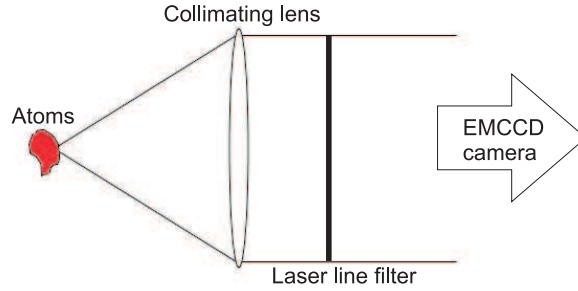
Figure 29: A schematic for light collection of the EMCCD camera.

The Andor camera can be used to count the number of atoms in the MOT and determine their temperature. When a probe beam is set to be at saturation intensity (1.64 mW/cm^2 for Rb) and on resonance, the scatter rate of one atom is $\gamma/4$, given from Eqn. 2.3. It is straightforward to see that the number of photons scattered from an atom is

$$n = \xi \frac{\gamma}{2} t \qquad (4.6)$$

where ξ is the measured detection efficiency and t is the exposure time. The imaging objective cannot collect all the light emitted by the atoms, so the fractional solid angle Ω_{sa} is multiplied with Eqn. 4.6. The number of atoms N can be determined

from the total detected photons on the camera with

$$N = \frac{\text{counts}}{\Omega_{sa}n}.$$ (4.7)

The temperature of the atoms can be determined by releasing the ensemble and measuring the expansion of the cloud after a known time. The width of the Gaussian expansion of the atoms is related to the temperature as shown in Ref. [62],

$$\sigma_t^2 = \sigma_0^2 + \frac{k_B T}{m}t,$$ (4.8)

where σ_0 is the initial width of the cloud at $t = 0$, k_B is the Boltzmann constant, T is the temperature of the cloud, m is the mass of an atom, and t is the expansion time. As the expansion time increases, the atoms drop further out of the focus of the imaging lens due to gravity and the temperature measurement is skewed. Therefore, short advance times on the order of milliseconds is used to minimize the error.

For most of our experiments, we are interested in trapping single atoms. For single atoms in a MOT, the number can be measured directly but the temperature cannot. We can see from Eqn. 4.6 that in order to see a strong signal from a single atom, the exposure time must be increased. Typically, we can continuously cool and observe a single atom in a MOT with exposure times on the order of a few hundred ms.

4.6.2 Single Photon Detector

Inside the science cavity, the atoms cannot be measured using the camera due to scatter of the cooling lights from the cavity mirrors. Taking advantage of the atoms being in a cavity, we can detect the atoms through the output of the cavity. The cavity field is directed on a single photon detector, a Perkin Elmer avalanche photodiode (APD). The APD can count single photons with 50% efficiency. Because it is so sensitive, high power signals can damage the detector and care must be taken to not overexpose the photodiode over 40×10^6 photons/s. For high signals used for coupling and to align the locking and probe beams, a Thorlabs PDA36A detector is used in

place of the APD. After the system is adjusted and set, the lights are all attenuated heavily so that they are within a safe level for the photodiode.

The gate on the APD is triggered by a LabVIEW sequence that is programmed to run the experimental procedure. When triggered, the TTL pulse output of the APD are counted and binned by a photon counter from National Instruments (PCI-MIO-16E-1) that has a timing resolution of 1.5 μs at no gain. For fast detection, a photon counter card from FAST ComTec (P7888) is used to bin the data with a timing resolution of 1 ns. The information is then processed through LabVIEW to produce the data in user indicated bin sizes. The data can also be post-processed and integrated for longer bin times as will be seen in the data plots of the next sections.

CHAPTER V

DETERMINISTIC DELIVERY OF SINGLE ATOMS INTO A CAVITY

The unique capabilities of optical cavity QED systems require controllably localizing individual atoms inside high-finesse, sub-mm length optical cavities. In the last decade, there has been considerable progress in integrating laser cooled and trapped atoms with optical cavity QED systems in the strong coupling regime [8, 63, 64, 65, 66]. Individual atoms have been cooled and stored in optical cavities for time spans exceeding a second [67, 68], and these advances have allowed demonstration of single photon sources and studies of the cavity QED system [69, 70].

Previous experimental efforts have relied on probabilistic loading of laser-cooled atoms into the cavity from free-falling atoms or from an unknown number of atoms transferred from optical dipole traps [67, 66]. Eventually, practical applications will require deterministic loading methods of single atoms into the cavity. In this experiment, we realize this goal by incorporating a deterministically loaded atom conveyor [71] that is used to deliver a precise number of atoms into a high finesse resonator. We achieve storage times exceeding 15 s for atoms in the cavity with continuous cooling and observation using cavity assisted cooling [67, 72]. The atom-cavity interaction is studied as a function of probe-cavity detuning and probe Rabi frequency, and the experimental results are in good agreement with theoretical predictions. We demonstrate the ability to manipulate the position of a single atom relative to the cavity mode with excellent control and reproducibility. The use of an atom conveyor was suggested in [73] as a means to scale cavity QED interactions to many atomic qubits, and the results of this work represent an important step towards this goal. In this

chapter, the work presented in Physical Review Letters [9] is explained in more detail.

5.1   *Trapping Atoms*

Delivering atoms to the cavity requires a multi-step process. First, they are captured from the background gas by a magneto-optical trap. Then they are transferred into an optical trap, which can deliver the atoms to the optical cavity. In this section, the complicated procedure is described in detail.

5.1.1   Capturing a Single Atom
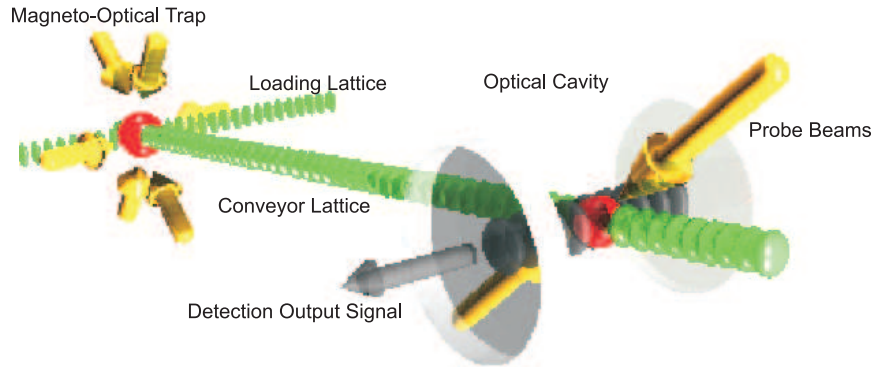
Figure 30: A single atom MOT is formed 8.5 mm away from the optical cavity. The atom is transported to the cavity mode by a conveyor lattice. Inside the cavity, the atom is cooled via cavity-assisted cooling driven by counter-propagating probe beams.

A magneto-optical trap (MOT) of ^{87}Rb atoms is formed 8.5 mm away from a high finesse optical cavity. A schematic of the experiment is illustrated in Fig. 30. To load single or small numbers of atoms, the MOT is operated with magnetic field gradients at 250 G/cm to decrease the loading volume. This also provides tight confinement of the atoms, localizing the trapped atoms to an area of approximately 25×25 μm^2.

Typical MOT gradients are run at around 15-30 G/cm and typically traps $10^5 - 10^7$ atoms. Because background collisions can easily knock the atom out of the MOT or introduce many more into the trap, the vacuum pressure must be in the very low 10^{-11} Torr. In our experiment, turning on a getter raises the pressure beyond workable conditions. However, low background pressure also means that it will take some time before atoms cross the MOT trapping regime. One can inefficiently wait up to a few minutes to eventually trap atoms, but this is not ideal. A solution is provided by introducing OptoTechnology broadband blue LEDs to the system. The light from the LEDs induce deabsorption of Rb atoms from the quartz cell walls via light-induced atom desorption (LIAD), essentially acting as an additional source of atoms [74]. By pulsing on the LEDs for a few ms during MOT loading, the flux of atoms is increased momentarily without affecting the background pressure significantly. Merely flashing the LEDs for a fraction of a millisecond is sufficient to drive an atom into the MOT within a couple seconds.

Once trapped in the MOT, the atoms are detected and counted by the EMCCD (Andor IXon) camera. In Fig. 31, a typical time sequence of the MOT fluorescence is shown. The discrete jumps of the observed fluorescence signal correspond to individual atoms loading into or leaving the MOT. In this figure, the observed scatter rate from a single atom is 500 counts for an exposure time of 500 ms.

5.1.2 Loading Lattice

After the atoms are counted in the MOT, they are transported to the cavity using the conveyor lattice. The lattice is created by two counterpropagating 1064 nm laser beams focused at the cavity with a waist, $w_0 = 34$ μm, which provides a trapping potential at the cavity of $U/k_B = 1$ mK with 4 W optical power per beam. However, the potential depth at the MOT location (8.5 mm away) is only 100 μK due to Gaussian beam divergence. This shallow trap depth cannot capture single atoms
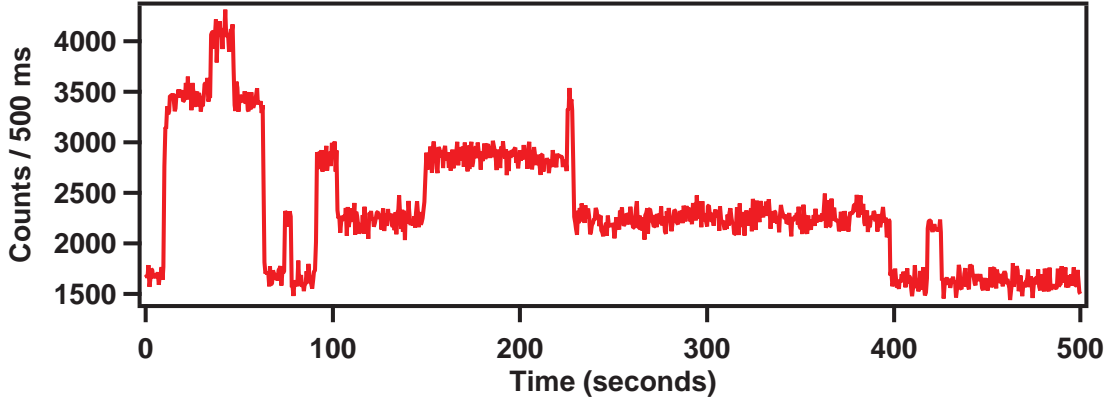
Figure 31: The fluorescence signal collected from the high-gradient MOT with an exposure time of 500 ms per data point. Discrete steps indicate individual atoms captured or lost from the MOT. The inset shows a histogram of the integrated fluorescence signal of 0 - 5 trapped atoms.

from the high gradient MOT with high efficiency, so a separate loading lattice is employed.

The loading lattice is set orthogonal to the conveyor axis and formed by a retro-reflecting a 1 W beam. The 1064 nm beam is focused to a 17 μm waist at the MOT, which corresponds to a trap depth of 1 mK. This loading lattice is 90% efficient in transferring atoms from the MOT to the conveyor lattice. Due to the complexity of the system, the alignment process for the lattices must be completed in a sequential order.

First, the conveyor lattice is set by aligning it to the cavity mode. This is done by blocking one of the lattice beams so that it is a single focus trap. After a shallow MOT is turned off, the atoms fall into the single focus trap and funnel to the focus of the trap located at the cavity. The cavity mode is locked and is probed along the cavity axis by a 780 nm beam on the $F = 2 \rightarrow F' = 3$ transition. When the lattice is aligned to the cavity mode, the transmission of the probe through the cavity drops as the atoms run into the cavity mode due to the vacuum Rabi splitting effect, shown in Fig. 32. To maximize the overlap of the lattice and the cavity mode, the

63

lattice is scanned along a transverse axis of the cavity to find the maximal drop in transmission.
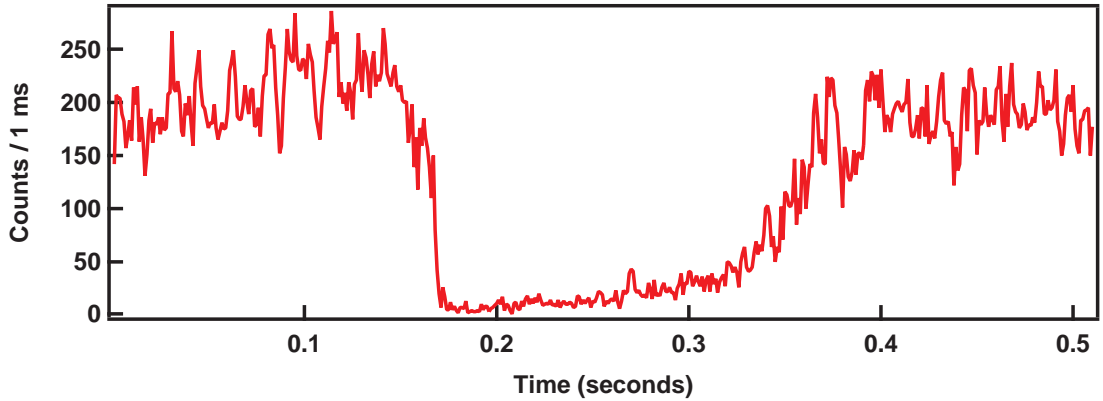
Figure 32: When atoms are brought into the cavity mode, the transmission of the cavity probe drops due to the vacuum Rabi splitting.

Next, the loading lattice is set to intersect the conveyor lattice. When the two lattices are overlapped, they form a cross trap at the point of intersection. The polarizations of the two lattices are set to be orthogonal so that they do not interfere with each other. Because it is impossible to directly see where the lattices cross, atoms are used to determine when they are aligned. With a shallow MOT gradient of 15 G/cm, millions of atoms are initially trapped in the MOT. Although the efficiency of atoms being transferred directly to the conveyor lattice may be small, there are enough atoms to see fluorescence signals on the EMCCD camera. When the lattices overlap, more atoms tend to gather into the cross trap due to the increased potential. By maximizing the number of atoms in the cross trap, i.e. maximizing the fluorescence signal, the alignment of the two lattices is optimized and the position of the intersection is recorded on the CCD camera, as can be seen in Fig. 33.

Finally, the gradient of the MOT is increased to trap only a few atoms. The single atom MOT is physically moved by adjusting the position of the gradient coil on the translation stage (see Fig. 19) until the atoms are placed at the location of
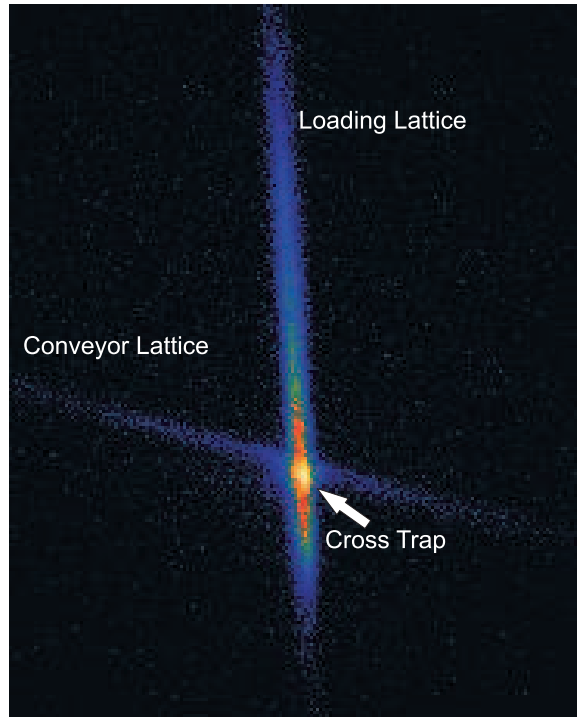
Figure 33: The crosstrap formed when the loading lattice intersects the conveyor lattice. Optimizing the signal in the crosstrap shows that many more atoms are trapped at that position and ensures the two lattices are overlapped well.

the cross trap on the camera. However, the camera can only provide two-dimensional information on the location of the cross trap for the MOT. The MOT position is then scanned in the third dimension by manually moving the gradient coil until the atomic fluorescence signal suddenly decreases due to Stark shift effects [75] from the deep cross trap. These steps ensures that the loading lattice, conveyor lattice, and high gradient MOT are optimally overlapped and aligned to the cavity.

5.1.3 Conveyor Lattice

Once the alignments are all optimized, the overall efficiency of single atoms taken from the MOT and translated to and from the cavity is $\sim$70-80%. In Figure 34, atoms are first observed in the MOT by the CCD camera with an exposure time of 100 ms. Then the MOT lights are turned off while the atoms are loaded into the conveyor lattice and transported 8 mm to the cavity and back to the MOT position. The high

gradient MOT is turned back on to recapture the atoms from the conveyor lattice and observed again on the CCD camera. In this figure, the efficiency of retaining a single atom through the process is 73%.
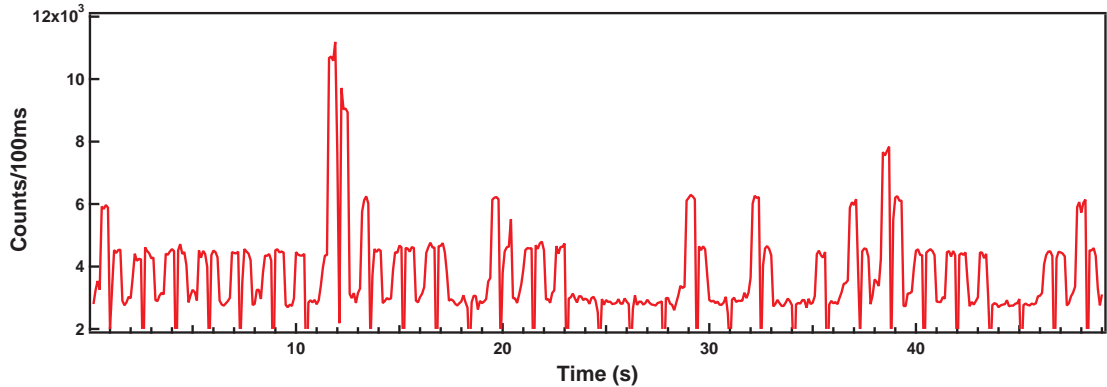
Figure 34: One atom corresponds to 1500 cts/100ms. Each pair represents an efficiency run. The first step represents how many atoms are initially trapped in the MOT for half a second. The signal drops sharply when the MOT lights and gradient are turned off while the atom(s) are transferred into the loading and conveyor lattices and transported to and back from the cavity. The MOT lights and gradient are turned back to recapture the remaining atom(s) from the lattice for observed for another half of a second before the gradient is turned off and the atom is let go. If only single atom runs are considered, the total efficiency is near 73 %.

5.2 *Deterministically Delivering Atoms to a Cavity*

In this experiment, the 222 μm cavity is used. The cavity parameters are $g = 17.1$ MHz, $\kappa = 7$ MHz, and $\gamma = 6$ MHz, making the single atom cooperativity 2 and putting the cavity in the strong coupling regime. The cavity is actively stabilized to the $F = 2 \rightarrow F' = 3$ transition of the ^{87}Rb D2 line.

The atoms are loaded into the MOT and counted before the loading lattice is turned on. The atoms are transferred to the conveyor lattice by ramping the loading lattice off in 75 ms. By inducing a frequency difference of 50 kHz between the two counter-propagating beams of the conveyor lattice, the atoms are transported to the cavity at a velocity of 2.6 cm/s for 320 ms. Once inside the cavity, different characteristics of the atom-cavity system are investigated.

5.2.1 Long Observation Times

Once the atom is inside the mode of the high finesse optical cavity, it is continuously detected and cooled using cavity-assisted cooling [67, 76]. The atoms are excited by two counter-propagating probe beams, and radiation scattered from the atoms is re-emitted into the cavity mode and subsequently detected by a photon counter as it leaks out the cavity. For positive cavity detunings with respect to the probe beams (*i.e*, $\triangle_{\mathrm{C}} = \omega_{\mathrm{c}} - \omega_{\mathrm{p}} > 0$, where $\omega_{\mathrm{c,p}}$ are the frequencies of the cavity and the probe, respectively) the photon absorbed by the atom from the probe has lower energy than that emitted into the cavity mode, resulting in net cooling of the atom.

The probe beams are oriented 45° from the conveyor axis and have a lin $\perp$ lin polarization configuration to provide cooling. They are tuned 21.5 MHz below the $F = 2 \rightarrow F' = 3$ transition with a Rabi frequency of $\Omega = (2\pi)$ 12 MHz per beam and hence also provide conventional Doppler cooling along the probe beam direction. A hyperfine repumping laser beam co-propagates with these beams to drive the $F = 1 \rightarrow F' = 2$ transition. The emitted photons from the cavity are detected with a single photon avalanche photodiode (APD).

Typical cavity emission signals corresponding to deterministically loaded atoms are shown in Fig. 35 for different numbers of atoms initially loaded in the MOT ($N_{\mathrm{atoms}} = 1 - 4$, respectively). In each case, the probe is turned on 250 ms after the atom(s) are brought to rest inside the cavity. The cavity emission signal is proportional to the number of atoms and corresponds to a detected count rate of 7 counts/ms for one atom. The particular data shown in Fig. 35(a-d) show atom storage exceeding 6 s, however the lifetime of the continuously cooled atoms in the cavity varies significantly depending on the exact experimental conditions and the number of atoms in the cavity. In general, for $N_{\mathrm{atoms}} > 3$, the storage time is < 1 s for the experimental regime explored to date, while for $N_{\mathrm{atoms}} = 1 - 3$, storage times of >15 s have been observed.
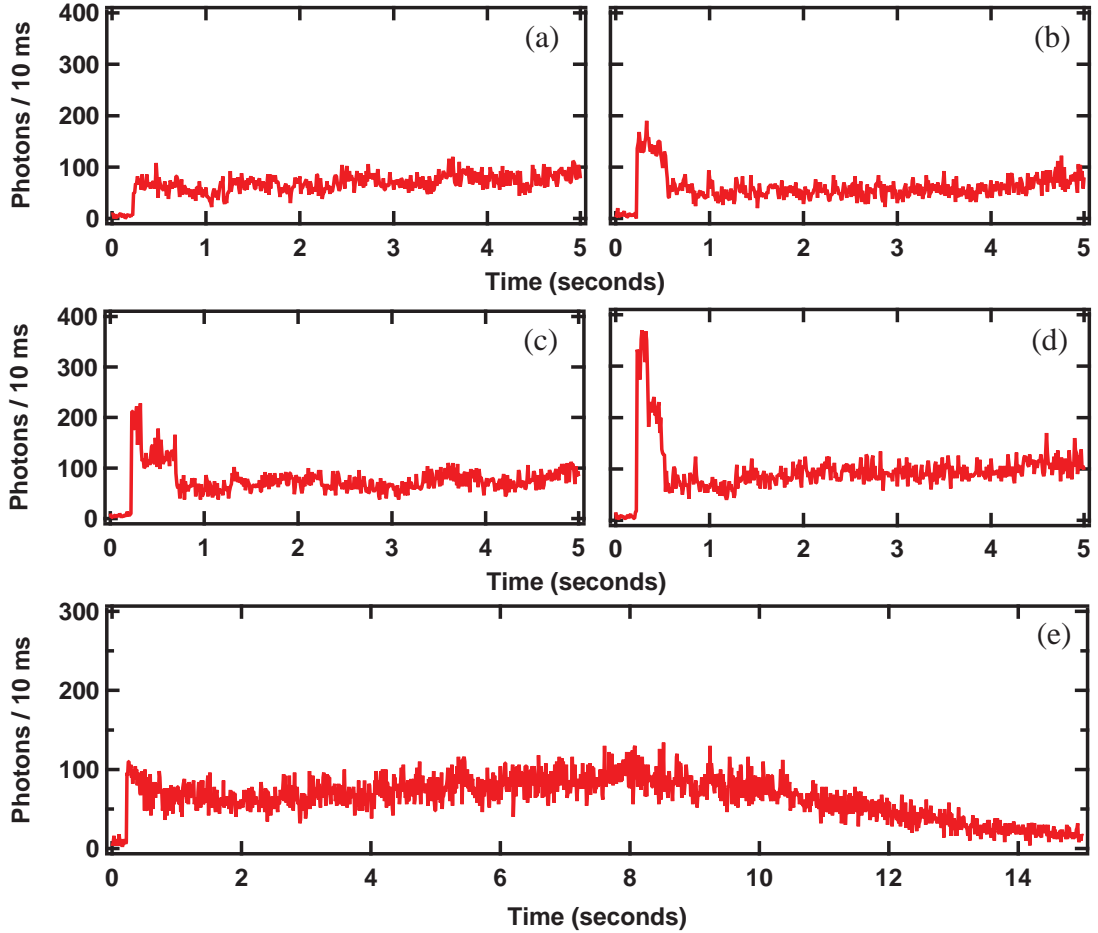
Figure 35: Detected cavity emission signal vs. time. In (a)-(d), the cavity emission signal corresponds to 1-4 atoms, respectively, initially loaded into the MOT and subsequently stored and detected in the cavity. In (e), storage of a single atom in the cavity for 15 s is shown.

For optimal experimental conditions, single atom storage times exceeding 15 s have been observed with good reproducibility. A typical example of such a signal is shown in Fig. 35(e). The drift in the single atom count rate in this trace is due to a drifting frequency offset between the rf synthesizers that drive the conveyor AOMs. This results in a drift speed of $v \sim 0.5$ μm/s, which can move the atom out of the cavity mode within the observation time.

5.2.2 Atom-Cavity Interactions

According to the theoretical model of cavity-assisted cooling developed in [67, 72], the rate at which a single atom scatters a photon into the cavity mode is given by:

$$R = 2\kappa \frac{g^2}{\triangle_c^2 + \kappa^2} \frac{\Omega^2}{\triangle_a^2 + \gamma^2},$$

(5.1)

where $\triangle_a = \omega_0 - \omega_p + \triangle_S$ is the detuning of probe beam with respect to the atom resonance, ω_0, including the Stark shift, $\triangle_S \sim (2\pi)83$ MHz due to the conveyor optical lattice. For the experimental parameters of the system, Eq. (5.1) predicts an emission rate of $R = 2400$ photons/ms. The detection efficiency is estimated to be 12.5%, including the 50% quantum efficiency of the APD, 50% in propagation losses from the cavity to the APD and 50% loss due to a polarizing beamsplitter in the detection optics. Accounting for these efficiencies, the predicted signal is 300 counts/ms, which is a factor of ~ 30 larger than measured in Fig. 35. This discrepancy varies from day-to-day as the alignment of the lattice and cavity changes. Single atom signals as high as 40 counts/ms (7.5 times smaller than predicted) have been observed. Possible sources of signal discrepancy are non-transmission losses in the cavity mirrors and a reduced effective coupling due to the Zeeman structure of the atoms, and/or varying Stark shifts that depends on the alignment of the conveyor lattice.

One of the advantages of the use of external fields to trap the atom inside the cavity is that it allows control of the atom coupling via the position dependence of the atom-cavity interaction strength. In Fig. 36, this control is exploited both to investigate the position dependence of the coupling strength as well as to repeatably move an atom in and out of the cavity mode. For a Fabry-Perot cavity, the coherent coupling rate of the TEM$_{00}$ Gaussian mode is given by $g(\mathbf{r}) = g_0 \cos(kz) \exp[-\rho^2/w^2]$ [16], written in a cylindrical coordinate system with z along the cavity axis and where w is the waist of the cavity mode. To study the dependence of the coupling on the transverse coordinate, ρ, single atoms are slowly moved through the cavity mode
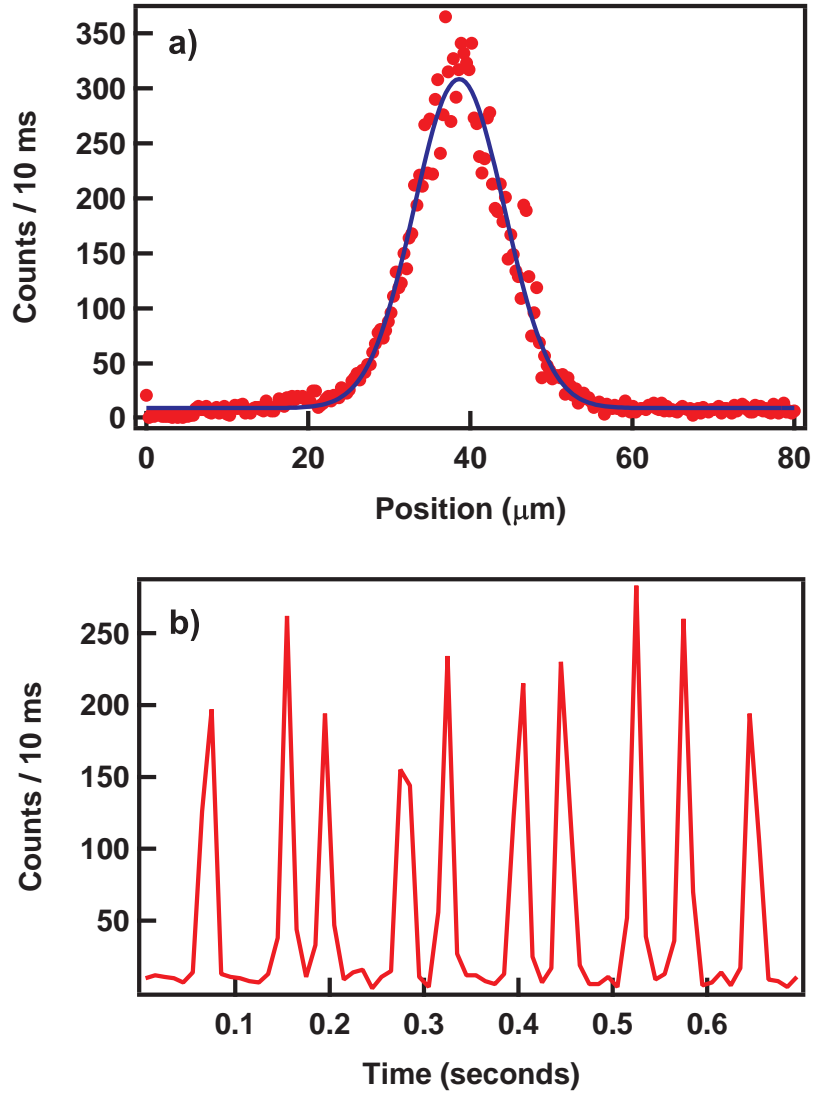
Figure 36: In (a), an atom is swept across the cavity mode at a slow speed of $v = 55$ μm/s, to achieve the high resolution scan shown. The solid line is the Gaussian fit to the data. In (b), an atom is swept across the cavity mode 10 times with a speed of 440 μm/s.
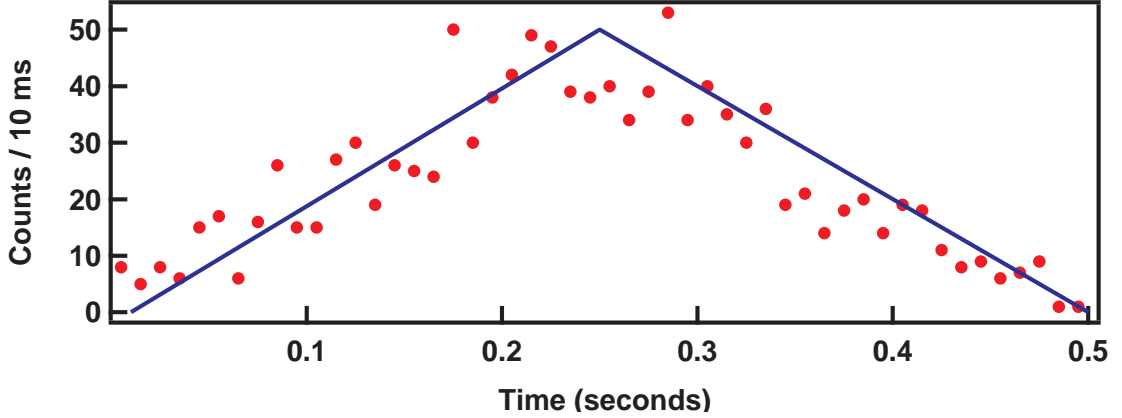
Figure 37: Single atom scattering rate versus probe beam power. The solid line is a linear fit to the data as expected from the dependence of the scattering rate to the probe beam power.

(with a speed of 55 μm/s) while being continuously cooled and detected. The single atom signal vs. position are shown in Fig. 36(a). The data, which are an average of 17 single atom runs, are fit well by a Gaussian function as expected from Eq. (5.1), however, the measured waist ($w_0 = 16$ μm), is 20% smaller than the waist calculated from the cavity geometry (20 μm). The atom conveyor allows for controllable and reversible introduction of the atom into the cavity mode. This is demonstrated in Fig. 36(b), which shows a single atom being moved in and out of the cavity 10 times. For this scan, the atomic speed was 440 μm/s.

The single atom signal as a function of the power of the probe beams is shown in Fig. 37. The power in the probe beams is linearly ramped from 24 nW to 24 μW in 250 ms after a single atom has been loaded into the cavity and linearly ramped back down to 24 nW in 250 ms. This corresponds to a variation in the Rabi frequency of $\Omega = (2\pi)0.8 - 25$ MHz. For this data the cavity detuning was -12 MHz and as expected from Eq. (5.1), the single atom signal is proportional to the power of the cooling beams ($\propto \Omega^2$). The solid line is the linear fit of the data as it corresponds to the linear ramping of the probe power.

For the data in Fig. 38, a single atom is loaded in the cavity, and the probe-cavity detuning, $\triangle_C = \omega_c - \omega_p$, is varied by detuning the cavity while holding the frequency of the probe beam constant at $\omega_p = \omega_0 - 21.5$ MHz. Over the range of $\triangle_C$ that is investigated, the scattering rate shows a Lorentzian dependence on $\triangle_C$ with a linewidth of 7.7 MHz (HWHM), close to the measured linewidth. This technique can only be used for investigating positive values of $\triangle_C$ because the negative values of $\triangle_C$ result in heating rather than cooling of the atoms [72] and lead to rapid loss of the trapped atoms.
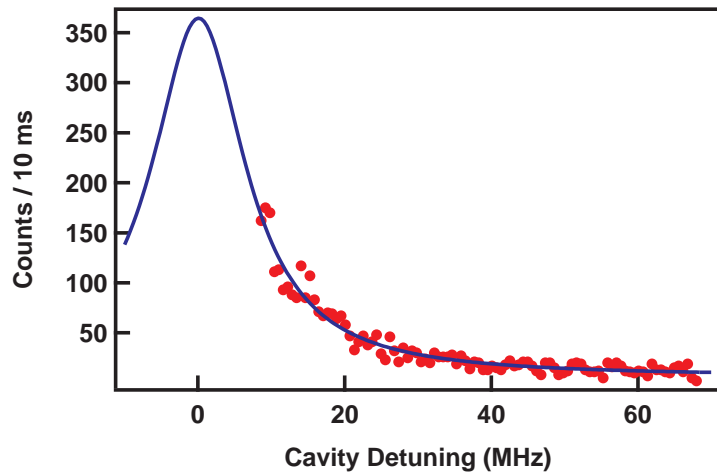
Figure 38: The dependence of the single atom scattering rate with respect to the cavity detuning. The solid line is a Lorentzian fit to the data.

5.3 State Preparation

With the ability to deterministically deliver an atom to the cavity, the next step is to coherently prepare the state of the atom for quantum information processing. While optical Raman beams are typically used to create a superposition of the atomic ground hyperfine states, microwave pulses can accomplish the same. In our experiment, we use short microwave pulses to drive an atom from one ground state to the other.

A microwave source (HP E4430B) is set to 3.417 GHz, which is the half the separation between the $F = 1$ and $F = 2$ ground states of ^{87}Rb. To ensure that the

frequency is accurate, the source is phase-locked to a GPS signal (EndRun Technologies) via the 10 MHz reference input on the device. The signal frequency is doubled and amplified before sent to a cylindrical copper horn [77]. The horn is positioned to excite the atoms at the MOT and at the cavity.

Because the microwave transition is sensitive to the magnetic Zeeman levels, the background magnetic field is set to be as low as possible using bias magnetic coils in all three directions. This is done by scanning the microwave pulse frequency to excite the different magnetic levels separately. A probe then measures the population of the atoms that were transferred to the $F = 2$ state from the $F = 1$ ground state. In the presence of no magnetic field, the transitions are degenerate and no splitting occurs. Therefore, to minimize the background magnetic field, the splitting is reduced as much as possible. In our experiment, we can only reduce the background field to 28 mG, shown in Fig. 39(a). In this figure, the $+2\Delta$ peak is slightly shifted from its predicted position by $\sim$10 MHz. This is due to random background fluctuations in the system while the time-consuming data is being taken.

Once the background field is minimized, the strength of the microwave signal is determined by measuring the state populations for different pulse lengths. A 1 G bias field is applied so that only the clock transition ($\Delta = 0$) is probed. The atoms are initially put into the dark ($F = 1$) state by turning off the repump MOT light before the trapping MOT lights. A microwave pulse transfers the atoms to the $F = 2$ state with a specific probability. The atomic population in the $F = 2$ state is then measured by a probe beam along the FORT axis, tuned to the $F = 2 \rightarrow F' = 3$ transition. Figure 39 (b) is a plot of the population of atoms in the $F = 2$ state for varying microwave pulses. For this data set, pulsing the microwaves 0.35 ms transfers all the atoms to the $F = 2$ state. This pulse is referred to as a π pulse. A 2π pulse of 0.7 ms brings the atoms back to the original $F = 1$ ground state. As the pulses get longer, it continues to oscillate and is referred to as Rabi oscillations [39].
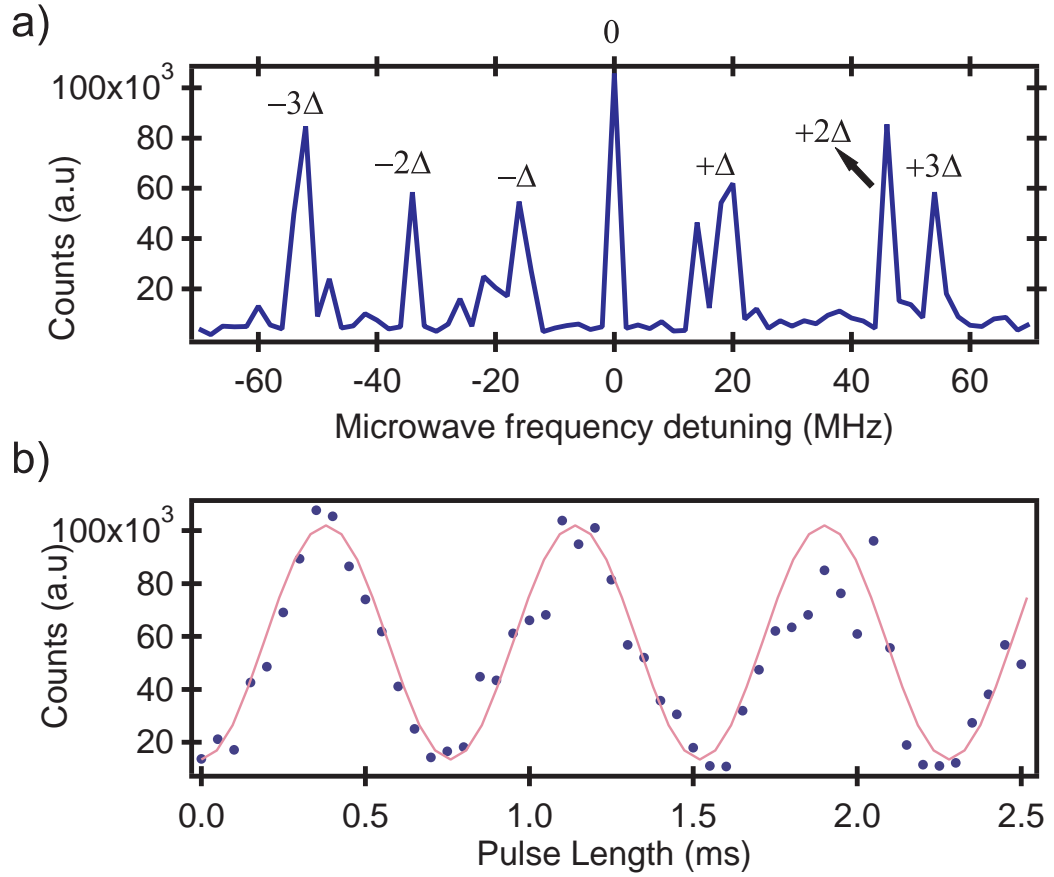
Figure 39: (a) Scanning the microwave frequency stimulates different microwave transitions. The splitting between the transitions corresponds to the existing magnetic field. In this case, there is a 28 mG background field. (b) A 1 G bias magnetic field is applied. By changing the pulse length of the microwave pulse, the atoms are cycled through the clock transition. The solid line represents a theoretical fit of the Rabi oscillations.

Because there are many atoms, it is easy to see the population oscillating in single measurements. When a single atom is measured, quantum mechanics dictates that the wavefunction collapses and it is found to be in either in one ground state or the other. Thus, many measurements must be taken and averaged to obtain the statistical mixture of the two states. After delivering an atom to the cavity, the atom is probed by a microwave π pulse and measured multiple times before the atom is lost. When the atom is probed by microwaves just outside the cavity mirrors and transported into the cavity for measurement, Rabi flopping can be seen. In Fig. 40, a 1 G bias fied is applied and only the clock transition is probed. The atom is first pulsed with a microwave field at the MOT and then transported into the cavity where it is probed. This sequence is repeated many time and averaged to show Rabi flopping.
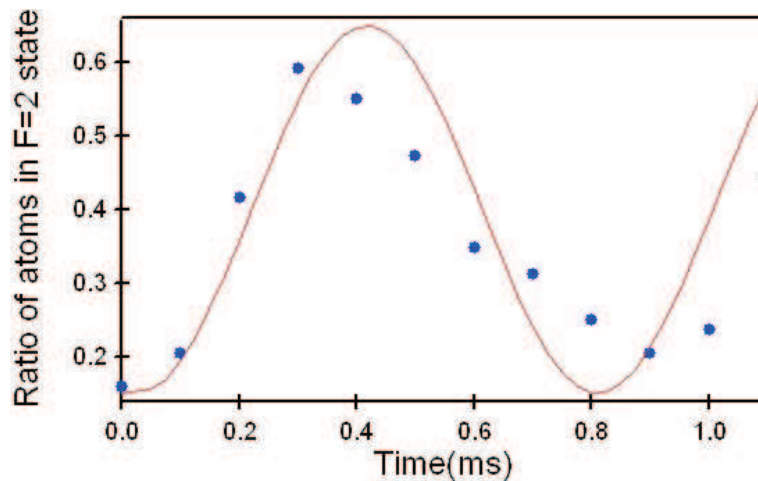
Figure 40: Single atoms are probed with microwave pulses at the MOT and transported to the cavity. The state of the atom is measured at the cavity. Each point on the plot is an average of 100 single atom runs. The solid line represents a theoretical fit of the Rabi oscillations.

The next step would be to probe the atoms when in the cavity mode. Unfortunately for our system, we have seen that the atom decoheres too quickly and no Rabi flopping is observed. This could possibly be due to the dielectric coatings on the mirrors interacting with the microwave pulses. An alternative option is to use

stimulated Raman adiabatic passage (STIRAP) [78] to prepare the atomic states in the cavity and observe Rabi oscillations.

CHAPTER VI

SINGLE PHOTON PAIRS

Producing entangled photon pairs is an important tool for quantum communication [79], quantum computing [80] and quantum networking [81]. Electromagnetically induced transparency (EIT) has been demonstrated in ensembles to generate single photons on demand and to show nonclassical correlations of paired photons [82, 83]. Although single photon pairs have been generated in cavity QED experiments [84, 11], the lifetime of the quantum state lasts on the order of microseconds. By placing the ensemble in an optical lattice, the storage of the quantum memories is predicted to extend to seconds [85].

In this chapter, an ensemble of $\sim 10^3$ atoms is delivered to a high finesse optical cavity via a conveyor lattice. Adapting the probing scheme by S. E. Harris [86], we present work towards producing entangled single photon pairs in the cavity. The first section will describe the preparation and entanglement scheme towards producing single photon pairs. In the latter section, the preliminary studies performed on the effect of the entangling pump lasers on the ensemble will be presented.

6.1 Entangled Photon Pairs

A scheme adapted from Ref. [86] lays the foundation of the entangling process. The atoms are first prepared in the $F = 2$ ground state by using a repump probe along the optical lattice axis. A write pulse is then applied on the ensemble. Because the write pulse is set to be 6.8 GHz off-resonant from the $F = 2 \rightarrow F' = 2$ transition, the probability of exciting more than one atom is low. After an atom is excited, it decays via the cavity mode to the $F = 1$ ground state, emitting a photon with a frequency 6.8 GHz below the $F = 1 \rightarrow F' = 2$ transition.

In order to detect the photon pairs in the cavity output, they must both be resonant with the cavity mode. By inverting the probe pulses with the detected pulses in the scheme in Ref. [86], it should be possible to produce a pair of single photons that are the same frequency. A schematic of the probing sequence is shown in Fig, 41.

To read out state of the ensemble, a read pulse on resonant with the $F = 1 \rightarrow F' = 2$ is applied to the atoms. Because only one atom has been pumped to the $F = 1$ ground state, only that atom will interaction with the read beam. As the atoms falls back to the $F = 2$ ground state, it emits a second photon that is on resonant with the cavity frequency. This frequency is the same as the $F = 2 \rightarrow F' = 2$ because the splitting between the two ground states is also 6.8 GHz.
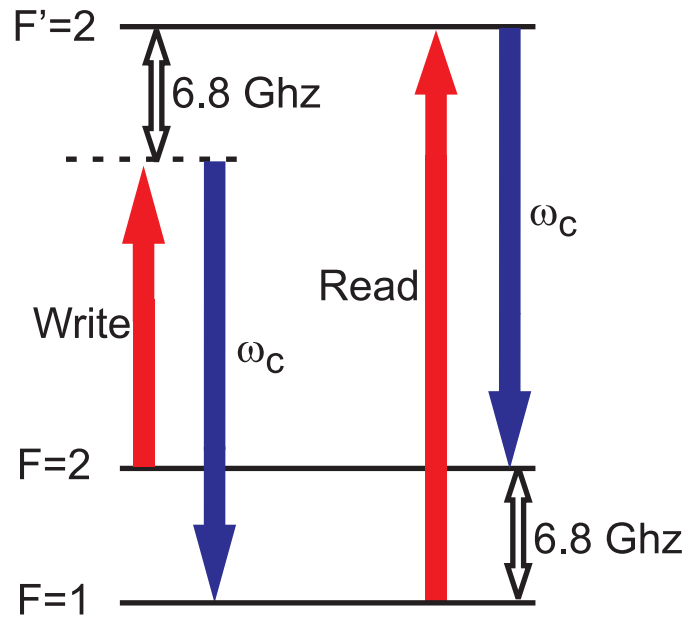
Figure 41: A diagram of the read and write pulses for producing single photon pairs.

6.1.1 Implementation

Three laser frequencies are needed for this experiment: write pulse, read pulse and a cavity locking reference. The read pulse is the same as the repump light used for atom

trapping in the MOT, so no extra effort is needed to obtain this light. The cavity locking reference is 266 MHz detuned from the $F = 2 \rightarrow F' = 3$ MOT trapping transition, which can be easily accomplished by using an AOM. Another option is to set up another laser locked directly to the $F = 2 \rightarrow F' = 2$ transition, which is what we have chosen to do.

The write pulse, however, is not easily attained since there is no convenient atomic transition at that frequency. While an EOM can easily shift the frequency 6.8 GHz, the carrier is also present on the light, which is directly on resonant with the atoms. The atoms will interact with the carrier before the write pulse can pump the ensemble, so an EOM is not an effective solution. Instead, we use two double-passed Brimrose AOMs driven at 1.709 GHz.

A separate laser is locked to the $F = 2 \rightarrow F' = 2$ transition for the write pulse and cavity locking reference. To prevent from having to realign the two double-passed AOMs, light is fibercoupled from the laser to the AOM setup. We couple around 50 mW from the laser into a fiber. Because the 1.7 GHz AOMs are quite inefficient ($\sim 25\%$), we use the zeroth order of the first AOM for the cavity reference laser instead of splitting it from the initial laser output. After the light is double-passed twice, the remaining light is a few hundred microwatts. While this is not enough power for the write pulse in the experiment, it is enough to seed a slave.

A slave laser is set in the same method as the MOT slave laser. About 100 μW is used to inject the slave. However, unlike the MOT trapping lasers, there is no spectrum to be seen on the slave output to ensure that the slave laser is following correctly. One could change the master laser to the repump $F = 1 \rightarrow F'$ spectrum and see the trapping $F = 2 \rightarrow F'$ spectrum to know that the slave laser is following the master. However, there is no guarantee that the slave will follow the master laser mode-hop free while it is shifted 6.8 GHz to the correct transition. Thus, a cavity is used to verify that the slave is following.

An small locking cavity is used to monitor the status of the slave laser. It is constructed to be 1 mm long, giving it a free spectral range of about 150 GHz and a linewidth of $\kappa = 2.4$ MHz. While it would be best to compare the slave output with the seeding light, the low availability of power due to the bad efficiencies does not allow any light to be taken from the seed. Therefore, part of the strong zeroth order beam used for the science cavity reference is used in the small invar cavity. A schematic of the whole setup is presented in Fig. 42.
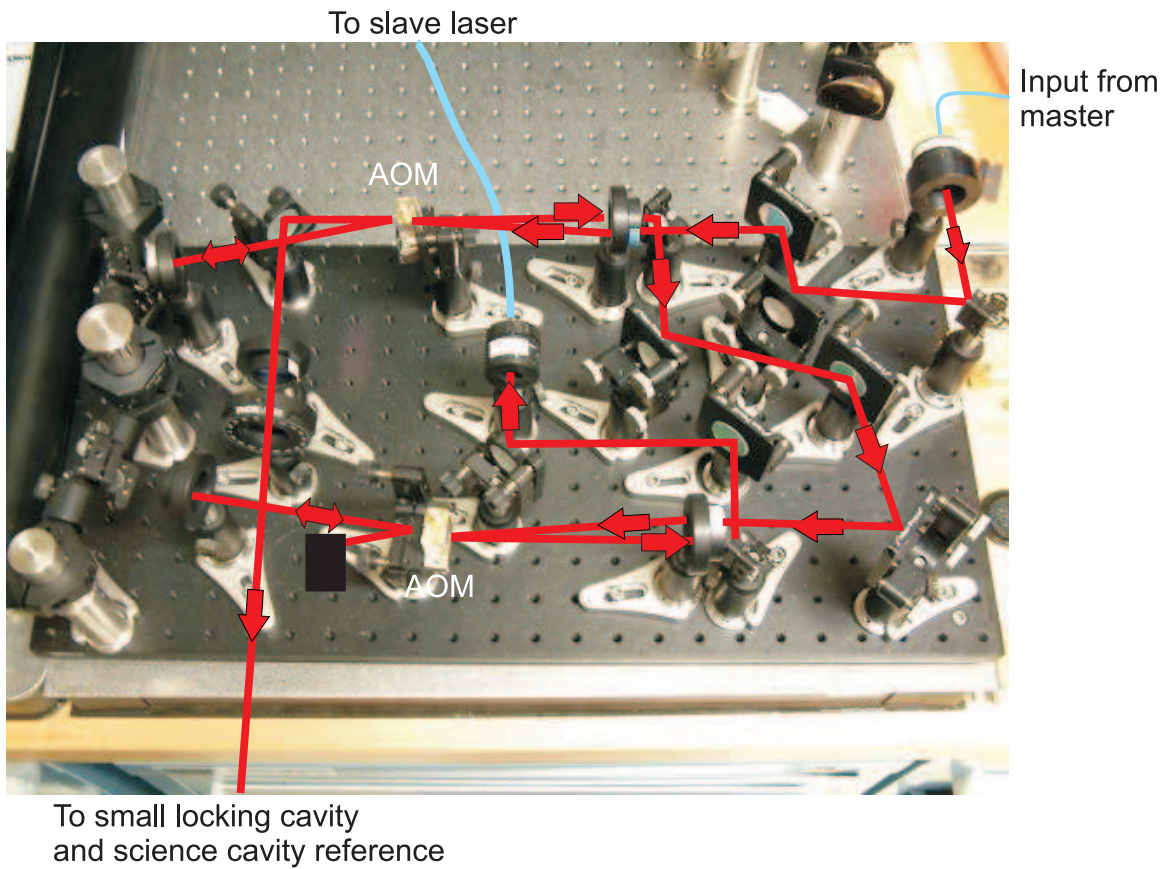
Figure 42: A diagram of the two double-passed AOMs to provide the science cavity locking reference light, the light for the small locking cavity, and the seed for the write pulse slave laser. In this figure, the seed to the write pulse slave laser is coupled into a fiber.

The radius of curvature for each of the two cavity mirrors is 10 cm, which translates to a transverse mode spacing of ~6.8 GHz. Thus, the two TEM$_{00}$ modes from the

master and the slave are separated by one mode spacing. In other words, the TEM_{00} mode of one laser aligns with the TEM_{01} mode of the other. Mode-hops on the slave laser can also be monitored by judging the shape of the mode. If the cavity mode is not a Gaussian TEM_{00} mode, then the slave is at an unstable point.

Finally, AOMs are added to the paths of the read and write pulses before they are coupled into fibers. This allows us to have the ability to switch the beams on and off in a few nanoseconds by placing voltage controlled switches on the rF signals to the AOMs. Because the lights are already at the correct frequencies, two AOMs are used to counteract the shifts in frequencies. This also prevents leakage of the light in the first order when the AOM is turned "off". The fibers are set up to combine with the FORT light through a 780 nm/1064 nm dichroic mirror so that the light propagates along the FORT axis, as seen in Fig. 43.

6.1.2 Detection

In order to detect single photon pairs, we must first be able to detect single photons. The output of the avalanche photodiode is taken to the input of the fast photon counting card. This digitizer has two inputs with 1 ns resolution, ideal for future two photon pair detection and correlation measurements. The FAST ComTec card is run by a program called MCDWIN, which plots the detected counts for the separate channels and save the data as ascii files. The data files are then analyzed in IGOR Pro.

With nanosecond resolution detection, it is essential that all components of the experiment are synced to run on the same clock. Therefore, a 5 ns resolution pulse generator from SpinCore is used to run the single photon detection part of the lab. Although it has 24 channels, only three are used in this experiment: the write AOM switch, the read AOM switch and the photon counting card gate trigger. After atoms are delivered to the cavity, a pulse from LabVIEW triggers the SpinCore pulse
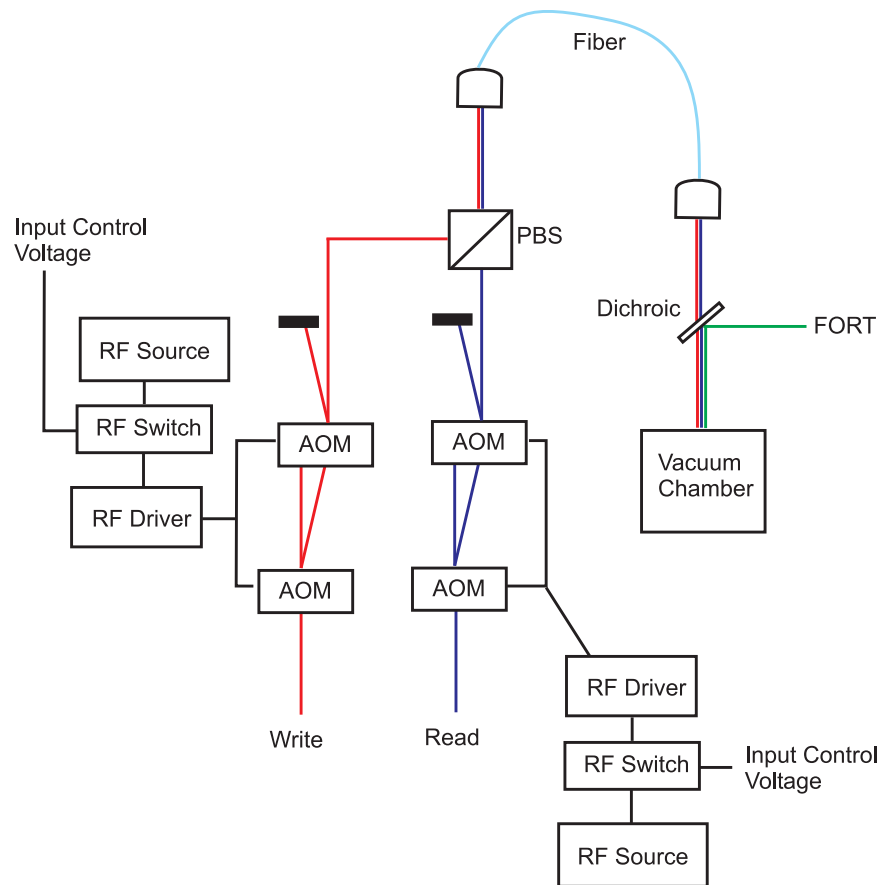
Figure 43: A schematic of the AOM switching system for the read and write pulses. The light is combined with the FORT by a dichroic.

generator to run a sequence written in C. When at the nanosecond level, small delays due to a finite drift velocity of signals are no longer negligible. When pulses are sent via BNC cables over several meters, delays of many nanoseconds are experienced. Also, the AOMs require a few nanoseconds to turn on and off. All these delays are measured on a Textronix digital oscilloscope with a bandwidth of 500 MHz. Each delay is taken into account and corrected in the SpinCore timing sequence to warrant that all components of the experiment run at the correct times.

6.2   Effects Due to Probe

Because our write pulse is greatly detuned, extra power is needed to obtain a reasonable scatter rate as can be determined from Eqn. 2.3. Therefore, our write beam power is 155 mW with a waist of 164 μm. Before moving to the cavity, the effects of the write probe is tested in the lattice in free space. A repump pulse is applied to the ensemble first to ensure that all the atoms are in the $F = 2$ ground state. Then the write probe is pulsed onto the atoms. Next, a $F = 2 \rightarrow F' = 3$ probe fluoresces the atoms and the signal is detected on the EMCCD camera. The total population of atoms in the trap is measured by probing the atoms again the probe along with a $F = 1 \rightarrow F' = 2$ repump probe.

To align the center of the read and write probe to the center of the FORT axis, a 0.2 ms write probe pulse is scanned across the FORT. In Fig. 44, the red circles represent the population of the atoms in the $F = 2$ ground state. Because the probe beam is a Gaussian beam, most of the atoms are pumped to the $F = 1$ state when the intense center of the probe addresses the atoms in the trap. To check that atoms have not been kicked out the lattice, both ground states are probed and the blue square data show that the total population in the trap does not change.

However, as the pulse length of the probe increases, we see that atoms are eventually heated and leave the trap. As in the figure above, the blue square data represents
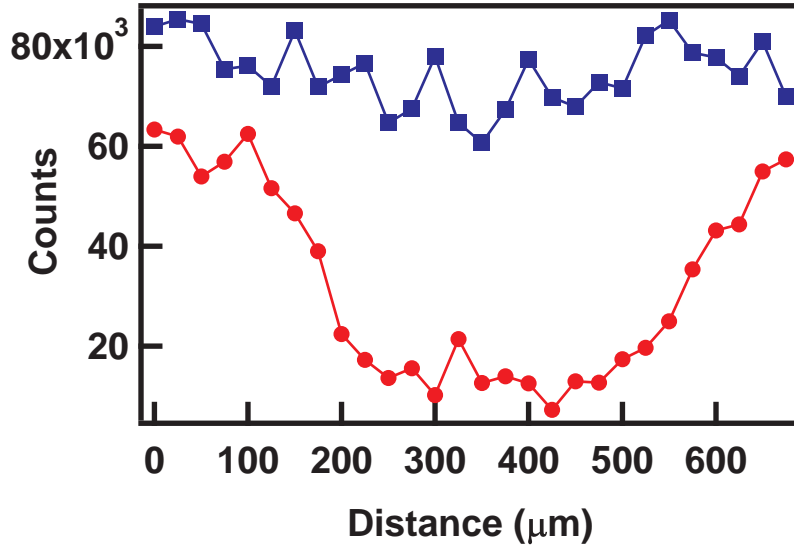
Figure 44: The position of a 0.2 ms probe pulse is scanned along the transverse axis of the FORT. The blue squares represent the entire atomic population in the lattice, and the red circles represent the population of atoms in the $F = 2$ state only. The probe has a waist of 164 μm and an intensity of 155 mW.

the total atomic population in the trap for a 0.2 ms pulse in Fig. 45. When the pulse length is increased to 1 ms, represented in the pink bowtie data, mechanical effects due to the probe is seen. The varying edges of the probe beam force atoms out of the trap, but the flatter center does not. Then as the probe length is increased to 5, 10, and 20 ms, all positions of the probe push atoms out of the optical trap. This shows that while the off-resonant probe provides a low scatter rate, it still experiences radiation pressure from the intense beam. Therefore, pulse lengths must be kept low and cannot exceed 200 μs.

6.3 Generating Photon Pairs

In order to generate photon pairs, first a write pulse is applied to the ensemble of atoms in the cavity. After a delay, a read pulse is applied to the atoms. This process is repeated many times until the atoms are no longer in the trap and the cavity mode. Data is continuously taken by the photon counter, so the information is cut
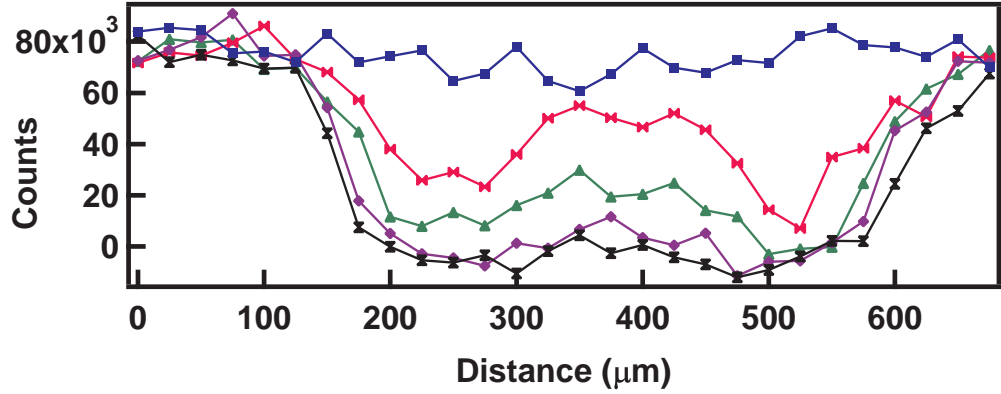
Figure 45: The position of the probe is scanned along the FORT axis and the atomic population in the lattice is monitored for varying pulse lengths. In the blue square data, the pulse length is 0.2 ms. In the pink bowtie data, the pulse length is 1 ms. In the green triangle data, the pulse length is 5 ms. In the purple diamond data, the pulse length is 10 ms. Finally, in the black hourglass data, the pulse length is 20 ms. The probe has a waist of 164 μm and an intensity of 155 mW.

into write/read cycles and summed in IGOR. In Fig. 46, the delay between the write and read pulse is varied. As can be seen, for a longer delay of 14.75 μs, the number of read photons drops to almost half of the case of a 7.25 μs delay. This is similar to the effect seen in Ref. [85].

The pulse length of the write can be varied. In Fig. 47(a), the length of the write pulse is 750 ns. When the write pulse length is increased to 7.5 μs, the number of read photons increases. This is expected because more atoms are pumped into the $F = 1$ ground state the longer the write pulse is turned on. One would assume that if the write pulse is applied long enough, all the atoms should be transferred out of the $F = 2$ ground state if the pulse beam does not push the atoms out of the trap.

It is interesting to note that the signal shape of the write pulse is flat as if it has reached an equilibrium. One would assume to see a decay as like is seen for the read data as atoms are slowly pumped out of the $F = 2$ state. Longer pulses of up to a second have been observed to retain the flat shape. The next study was to change the intensity of the write pulse and see what effect ensued.

85
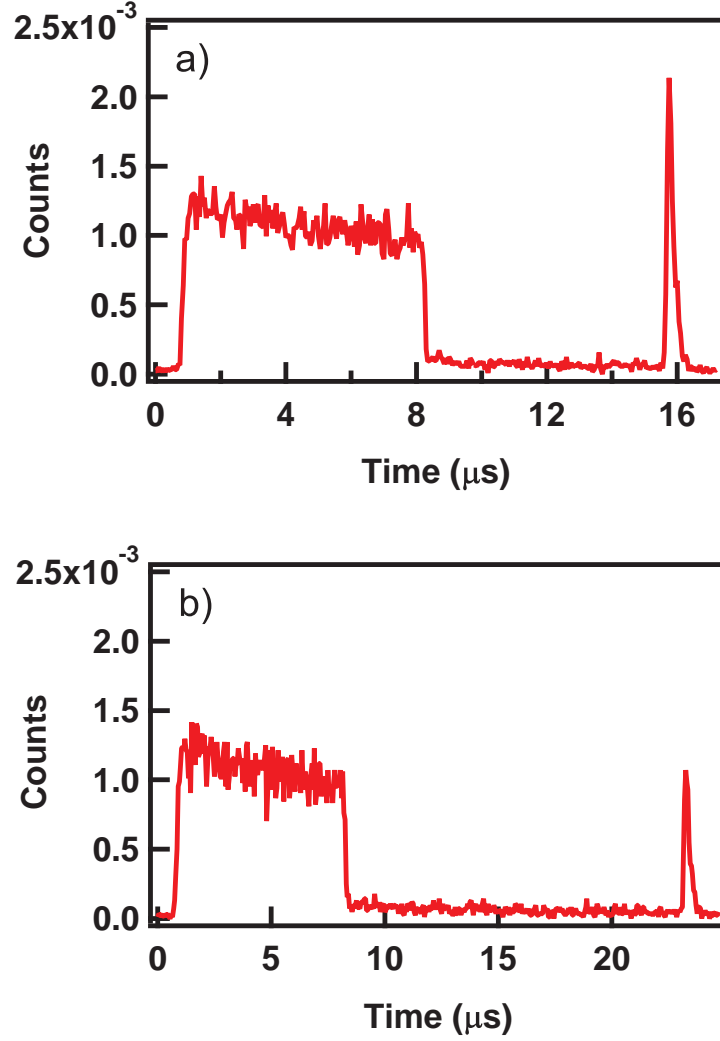
Figure 46: The delay between the write and read pulse is varied. In part (a), the delay is 7.25 μs. In part (b), the delay is 14.75 μs.

In Fig. 48, the pulse intensity is varied from 25 mW to 2.5 mW. While the overall number of counts drop, it seems that the flat shape still remains. Since we see less atoms pumped into the $F = 1$ state for lower pulse intensities, there should be a drop in read photons as is seen in the figure. If we look back at the read/write driving pulses, we see that the write beam frequency is 13.6 GHz detuned from the $F = 1 \rightarrow F' = 2$ transition. This causes the write pulse to have a small but non-negligible probability of pumping the atoms back into the $F = 2$ state. The write
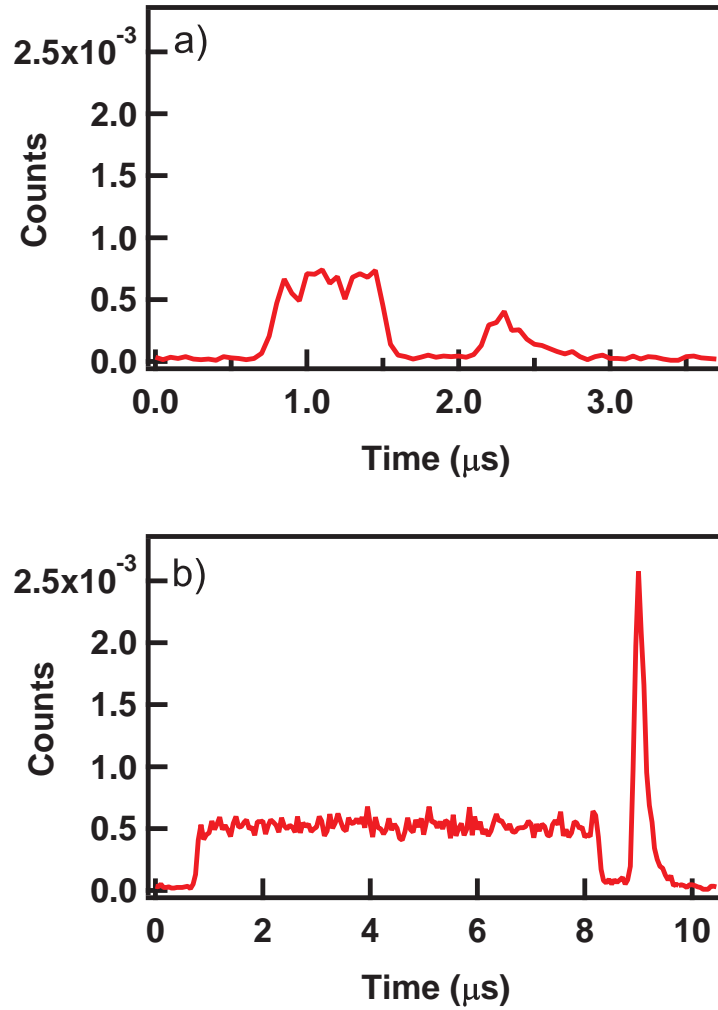
Figure 47: The pulse length of the write pulse is varied. In part (a), the pulse length is 750 ns, while in the part (b), the pulse length is 7.5 μs.

pulse must then be decreased so that the atom does not have a chance to be pumped back into its original state. However, we have seen that we either do not see a signal for very short pulses. Therefore, either the detection method must be improved or a different pumping scheme needs to be implemented to further these studies.
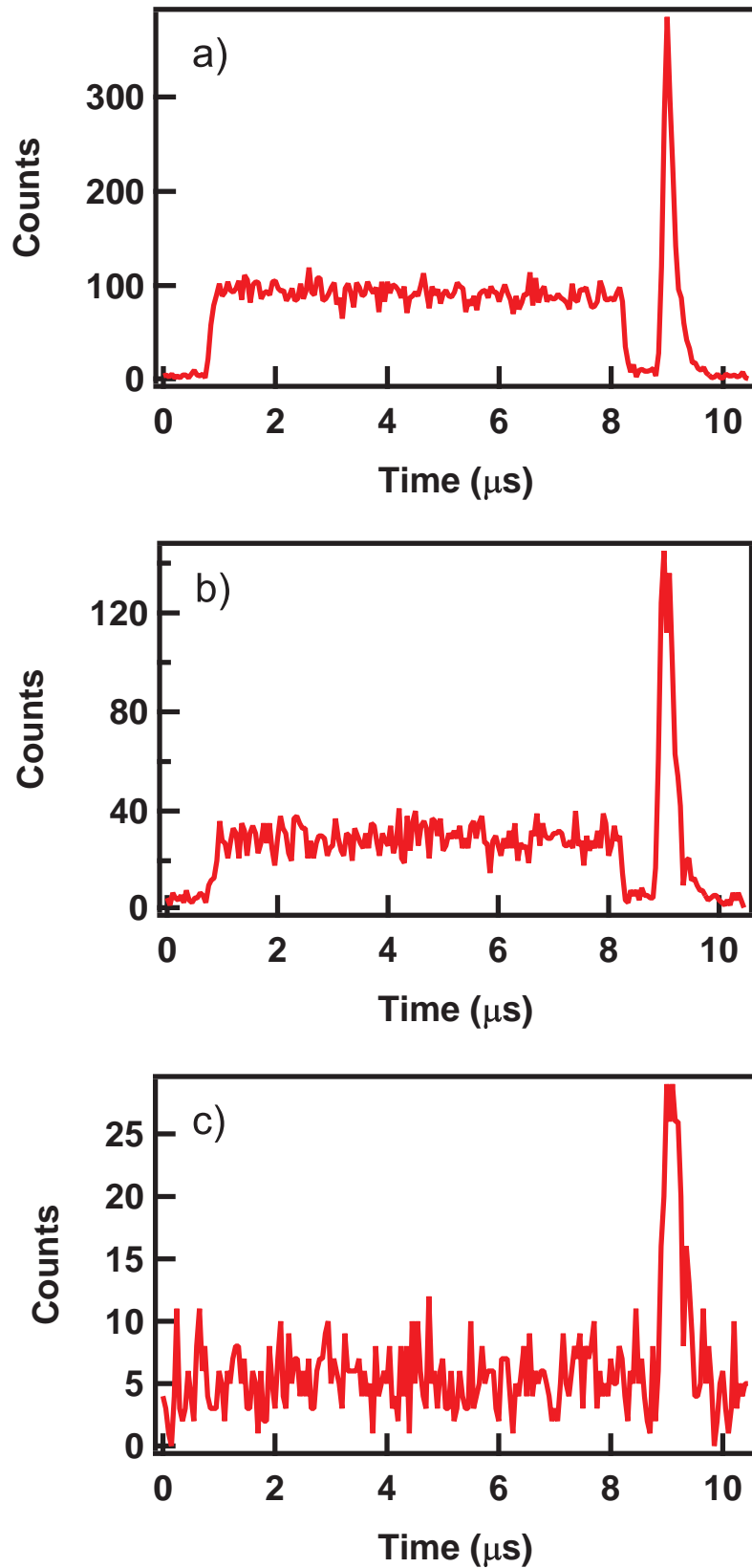
Figure 48: The intensity of the write pulse is varied. In part (a), the pulse intensity is 25 mW. In part (b), the pulse pulse intensity is 10 mW. In part (c), the pulse intensity is 2.5 mW.

88

CHAPTER VII

SINGLE ATOMS IN DUAL LATTICES

Despite their complexity, modern cavity QED experiments have been successful in trapping and cooling single atoms in a cavity [87, 67], creating [7, 88] and manipulating [89, 90] single photons, and studying cavity QED systems [9, 88]. A necessary step towards expanding the frontiers of current experiments towards quantum communication and computation is to demonstrate the scalability of these experiments. One way to accomplish this task is to establish a network of stationary quantum systems and to interconnect them by flying qubits [81]. Another approach to scale current experiments is to entangle nearby qubits. In principle, both of these methods can be realized with either different optical cavities separated by a macroscopic distance [91, 92, 93] or with many single atoms coupled to an optical cavity [94, 95, 96].

To implement quantum processes such as atom-atom entanglement schemes and 2-qubit gates, e.g. a CNOT gate, we must demonstrate the ability to deliver two atoms to the optical cavity. In this chapter, we begin with using a single lattice as a controllable neutral atom register. Then by adding a second lattice, we advance towards creating two coherently manipulatable qubit registers.

7.1 Neutral Atom Register

We begin with a single optical dipole trap to store multiple qubits as a neutral atom register [97]. Figure 49 shows an overall illustration of the experiment. ^{87}Rb atoms are initially captured in a magneto-optical trap (MOT) 3.5 mm from the optical cavity. The atoms are then loaded into a 1D far-off resonant optical dipole trap (FORT). By reducing the magnetic field gradient of the MOT from 12 G/cm to ~5 G/cm, atoms can be loaded sparsely over half a millimeter in the optical dipole trap.

89
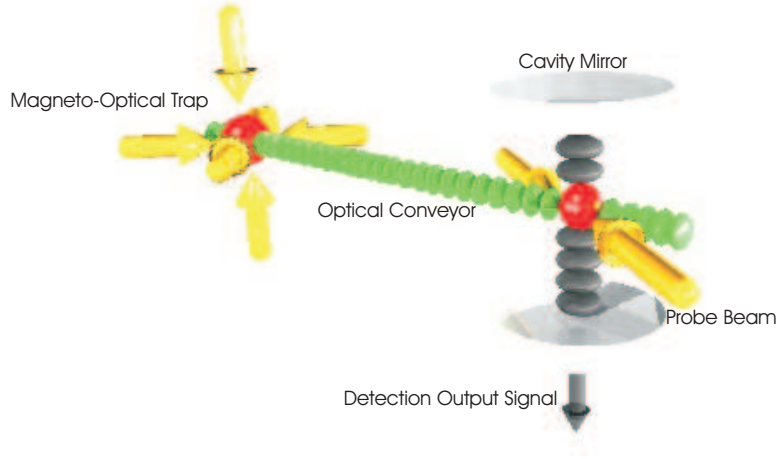
Figure 49: An illustration of the experimental setup. In the dual lattices experiment, an identical lattice is formed below the existing lattice so that both overlap with the MOT and the cavity mode.

The FORT consists of two counter-propagating beams from a fiber laser operating at $\lambda = 1064$ nm. The foci of the lattice beams are situated at the cavity with a waist of 25 μm and optical powers of 5.5 W each, providing a trap depth of $U/k_B = 2.7$ mK at the cavity and 600 μK at the MOT. For the atom register, we induce a frequency difference of 50 kHz between the two AOMS for the lattice beams so that the atoms travel to the cavity with a velocity of 2.6 cm/s. The atoms are transported 2.6 mm from the MOT and stopped about a millimeter from the center of the cavity. Then the atoms are brought in slowly, at a velocity of 5 mm/s through the cavity mode.

The 500 μm cavity is used for this experiment. The cavity is situated in a quartz vacuum cell pumped down to $10^{-10} - 10^{-11}$ Torr. For this system, the cavity QED parameters are $(g_0, \kappa, \gamma) = 2\pi \times (9.3, 6.1, 3)$ MHz, respectively. This corresponds to a single atom cooperativity of 4.7, which puts the system in the strong coupling regime. The cavity is locked on resonant to the $F = 2 \rightarrow F' = 3$ transition via an off-resonant beam ($\lambda = 784$ nm) that is locked on a different longitudinal mode.

In order to separate the different lights in the output of the cavity, a narrowband laserline filter is used such that the 784 nm locking light is reflected and the 780 nm

atomic signal passes with 99% efficiency. The 784 nm light is fibercoupled into an optical heterodyne system to produce a locking signal. Then, the 780 nm is filtered once more with another narrowband laserline filter before it is fibercoupled into an avalanche photodiode (APD) for photon counting. As the atoms enter into the cavity mode and are excited by the probe beam, the APD detects the scatter from the passing atoms with a total efficiency of 20%. This efficiency accounts for a 50% quantum efficiency of the APD and 40% efficiency from fiber coupling losses.
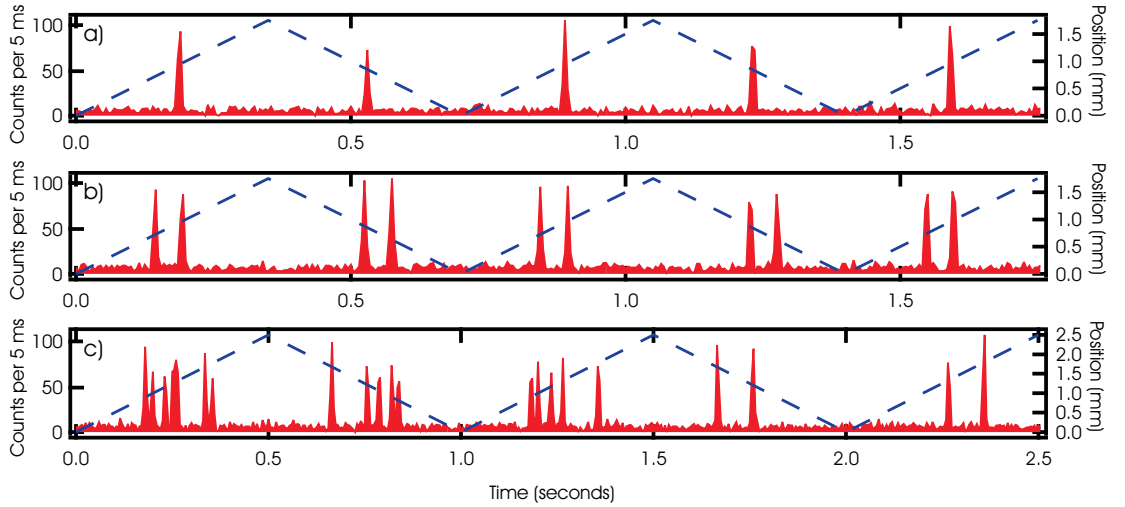
Figure 50: Neutral atom registers. The dashed blue line represents the position of the atoms as they are ramped back and forth. In part (a), one atom is loaded into the atom register and scanned back and forth through the cavity mode. In part (b), two atoms are loaded. In part (c), we start with 7 atoms in the cavity mode. Two atoms are lost after the initial pass through the cavity, leaving 5 atoms. In the last two movements through the cavity mode, only two atoms remain the trap.

After the atoms are scanned through the cavity, the atoms are stopped and pulled back through the cavity mode again. This can be repeated several times before the atoms are lost from the FORT. In Fig. 50, atoms are scanned through the cavity mode 5 times. In Fig. 50(a), one atom is moved 1.75 mm across the cavity mode. In Fig. 50(b), two atoms are also moved 1.75 mm across the cavity mode. The atoms are distinctively separated by 250 μm, or 470 lattice sites. It should be noted that the distance between the two atoms remains constant throughout the ramping process.

We have occasionally seen atoms to jump to different lattice sites, but they mostly remain in their original position. We also show that we can have a register of many atoms, as can be seen in Fig. 51(c). Initially, 7 atoms are delivered and carried 2.5 mm through the cavity mode. While 5 of the atoms can be seen clearly, 2 atoms are in different lattice sites, but are indistinguishable because they are close enough to simultaneously interact with the cavity mode. For the atoms to not overlap in the cavity mode, they must be at least 100 μm apart. In the second and third passes, 2 atoms are lost and 5 individual atoms are seen. Only 2 atoms separated by 475 μm survive the entire process in the final two passes of the run. The dashed line in each graph displays the position of the trapped atoms as they are ramped back and forth through the cavity mode, starting from where the atoms were initially stopped, 2.6 mm from the MOT. This data demonstrates our ability to control individual qubits in a neutral atom register and to repeatedly address each qubit separately in the cavity.
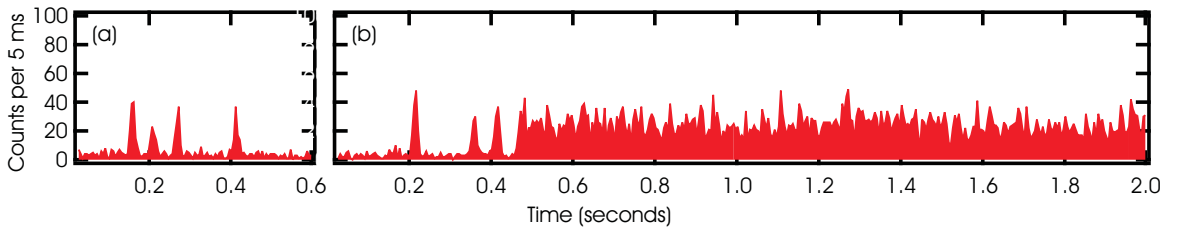
Figure 51: In part (a), four atoms are swept through the cavity mode. After the location of each atom is identified, the first atom is brought back into the cavity in part (b). The other three atoms are seen as they fly through the cavity mode, ensuring that it is the first atom that is being delivered to the cavity.

Next, we demonstrate our ability to deterministically choose an atom from the neutral atom register. Atoms are first scanned through the cavity mode, so that the number of atoms in the register can be counted and their locations in the trap can be determined. Figure 51 (a) shows that there are four atoms loaded into the trap. We decide that we want to bring the first atom back into the cavity mode. As the first atom is being delivered in part (b), the other three atoms can be seen flying by,

ensuring that it is indeed the desired atom that is being returned.

While the loading of that register may be probabilistic, we have shown that we can deterministically deliver atoms into the cavity mode. The next step is to add a second lattice with the same capabilities. The next section shows how we accomplished this task.

7.2 Dual Lattices
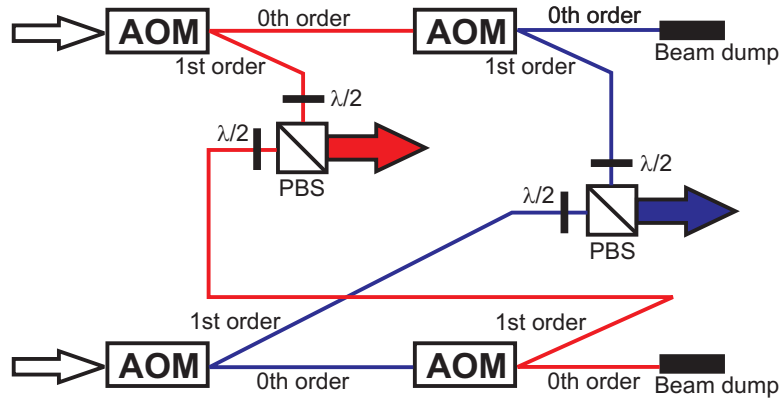
Figure 52: The configuration of the beams to create dual lattices. The red lines represent the beams that are modulated for the moving lattices. The blue lines represent the counterpropagating beams to create lattices with the corresponding red beams of like polarization.

In order to change the system from a single atom register conveyor to a two register system, the FORT AOM configuration was altered to utilize the maximum possible of the trapping light. As can be seen in Fig. 52, the zeroth order beams of the first AOMs are recycled to produce the other two beams necessary. The red lines in the figure represent the two beams of each lattice that are modulated to produce the traveling waves. Likewise, the blue lines represent the unmodulated beams that counterpropagate with the corresponding red beam of the same polarization to form the two lattices in the cavity. Using a polarizing beamsplitter to bring in both lattices, the two traps do not interfere due to their opposite polarizations.

The two lattices are set so that they are separated vertically by 150 μm at the
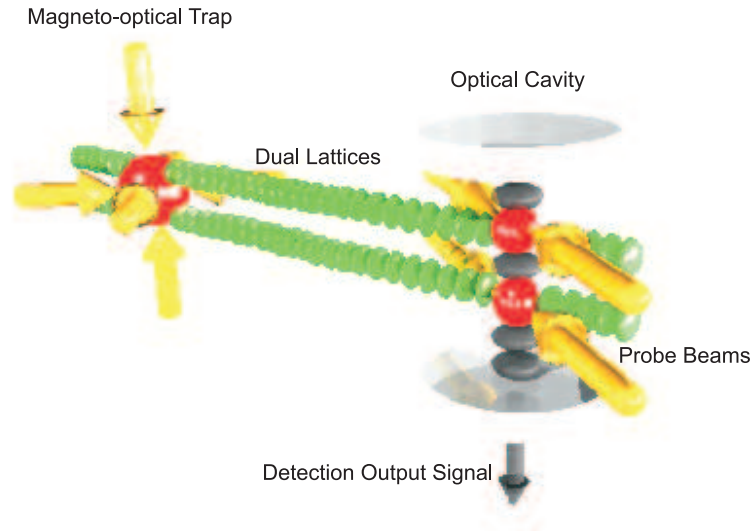
Figure 53: The conveyor lattices are separated so that they are distinguishable at the cavity but still overlap with the MOT.

cavity, sufficiently apart so that atoms do not jump from one lattice to the other. An illustration of the experimental apparatus is shown in Fig. 53. The atoms are loaded simultaneously from the MOT, but each lattice has individual control in translation, as is shown in Fig. 54. In Fig. 54(a), only the top lattice is brought into the cavity from the MOT while the bottom lattice is left to remain at the position of the MOT. In Fig. 54(b), the bottom lattice is moved while the top lattice is left to remain at the MOT. And finally in Fig. 54(c), both lattices are delivered together to the cavity. These figures are taken by illuminating the trapped atoms with an on-resonant probe beam along the FORT axis. The atomic fluorescence is then collected by a microscopic objective with numerical aperture of 0.4 and focused onto an EMCCD (Andor IXon) camera. The image is taken with probe time of 1 ms.

While many atoms can be detected easily, single atoms are not detectable in this configuration by the EMCCD camera. Thus, the fluorescence of the single atoms are collected through the leakage of the high finesse cavity and counted on the single photon counter in Fig. 55. Atoms are cooled and observed for a quarter of a second before both the lattices are pulled out of the cavity mode. The atoms in the top lattice
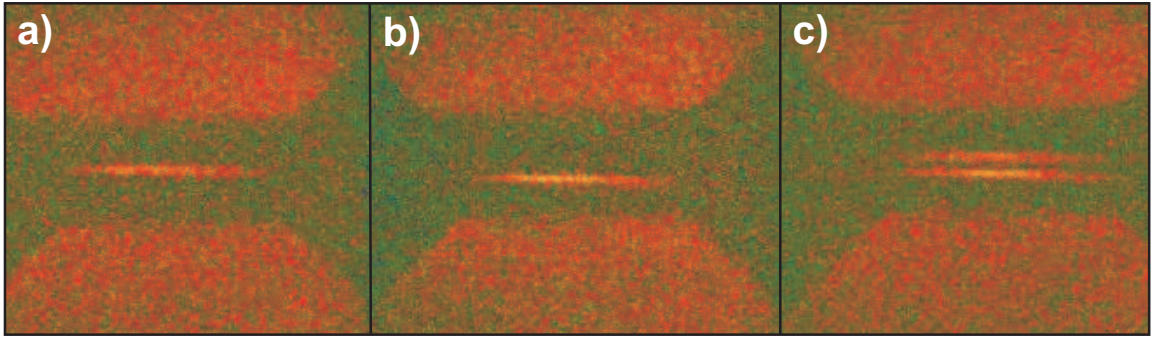
Figure 54: (a) The top lattice is translated to the cavity while the bottom lattice remains at the MOT. (b) The bottom lattice is translated to the cavity while the top lattice remains at the MOT. (c) Both lattices are translated to the cavity.

are first moved into the cavity and observed for 225 ms before the atoms in the bottom lattice are moved into the cavity mode. After 225 ms of observation, the top lattice is moved out of the cavity mode and the bottom lattice atoms are observed for another 225 ms before they are also moved out of the cavity. This process is repeated once more before they are lost from the optical trap. As atoms are brought into the cavity mode, one can see quantized steps in the detected counts. In the latter half of Fig. 55, one atom enters the cavity from the top lattice at 1.02 seconds from when the data begins, increasing the scatter rate by 3 cts/ms. The bottom lattice delivers the second atom at 1.245 seconds, doubling the detected scatter rate from the atoms. Finally, the first atom is moved out of the cavity mode at 1.465 seconds, leaving the second atom to be observed alone.

Due to the limitations of available power for the optical lattices, the shallow trap depth does not allow the atoms to be observed with the same cooling probe as the neutral atom register. The Rabi frequency of the probe light was set to be $\Omega = (2\pi)15$ MHz but was red-detuned from atomic resonance by 36 MHz, and the cavity was red-detuned from atomic resonance by 26 MHz. This drops the scatter rate of the atoms to be ~3 cts/ms, whereas in the earlier data shown for the single lattice register, the scatter rate of the atoms reach up to 20 cts/ms. Changing the waists of the lattices at the cavity mode could provide a deeper trap depth for implementing probe beams
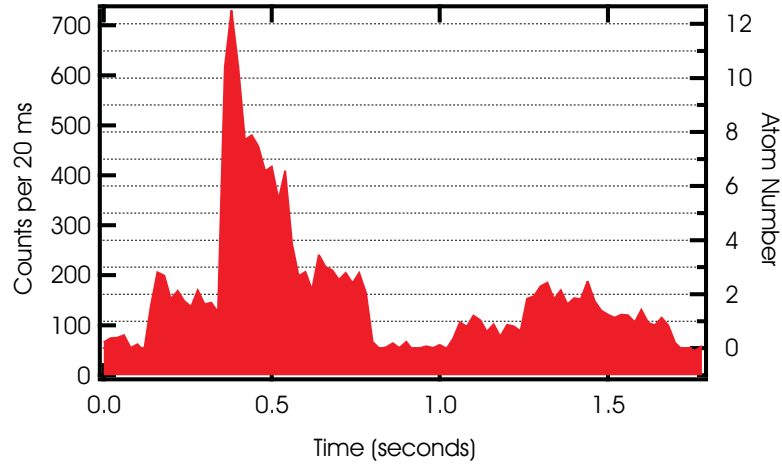
Figure 55: Atoms in two lattices are transported separately to the cavity mode. Two atoms are delivered from the top lattice and observed before more atoms are delivered to the cavity from the bottom lattice. The atoms in the top lattice is removed from the mode and the remaining three atoms in the bottom lattice are observed before being pulled out as well. The sequence is repeated and only one atom remains in each lattice.

that would produce higher scatter rates, but the trap depth at the MOT would be much shallower. Fortunately, that does not seem to have high potential of being a limiting factor in this experiment.

CHAPTER VIII

CONCLUSION AND OUTLOOK

Single atoms have been observed for long times in our experiments. Even after being transported to an optical cavity millimeters away, atoms have shown that they can be cooled and continuously observed via the cavity output for many seconds. Noise was seen on the function generator for the AOMs that caused the atoms to drift in the optical lattice, but the long storage time in the cavity mode is sufficient for any experimental protocol that would be implemented in the system.

Deterministic delivery of single atoms to a high-finesse optical cavity from a MOT located 8 mm away has been demonstrated with 70-80% efficiency. After being transported into the cavity mode, the atoms were scanned across the cavity mode with varying velocities, exhibiting our ability to exert precise control. The atom-cavity scatter rate was studied for its dependence on various parameters of the system. The scatter rate dependence on the Rabi frequency of the probe was quadratic (linear to the intensity of the probe) and was shown to have a Lorentzian dependence on the cavity detuning, verifying Eqn. 5.1. Initial steps were made to perform single qubit rotations in the cavity mode.

An atomic ensemble was delivered to an optical cavity for creating entangled single photon pairs. Although single photon pairs were not produced, various studies of the interactions between the atoms and light pulses were performed. As it was determined, the entangling light scheme utilized was not optimal for observing photon pairs.

Atoms were also probabilistically loaded into the lattice as a neutral atom register. Although the loading was not, the controllability was shown to be deterministic as

targeted atoms were brought back into the cavity mode. Another lattice was added to the system to provide dual atom registers in the optical cavity. Two single atoms in two separate lattices have been shown to move independently in and out of the cavity mode. These accomplishments have met the goals proposed in Ref. [98].

8.1 Future Direction

As my predecessor left with suggestions of future direction of the experiment, I shall do the same. For my successor, Chung-Yu Shih, I leave the following suggestions for pursuing this experiment. First, I shall point out the current ongoing observations of the nonlinearity effects in the dual lattices cavity system. Then, I will comment on the possibility of producing two qubit operations in the cavity.

8.1.1 Nonlinearity Observations

The dual lattices assembly allows for two atoms to interact in the cavity mode but retain spatial independence. This allows the atoms to be probed separately. To observe the work described in Section 3.2, the probes of the two lattices must be different. The first lattice is probed by light tuned to the $F = 2 \rightarrow F' = 3$ transition and a repump to keep the atoms out of the dark state. The second lattice is only probed by a repumping beam because the atoms do not interact with the cavity mode when in the dark state. The atoms in the second lattice are probed only by the resonant photons in the cavity mode emitted by the probed atoms in the first lattice.

In Fig. 56, atoms in the first lattice are delivered and stopped in the empty cavity. The atoms in the second lattice are stopped a couple millimeters before the cavity mode. 100 ms later, the atoms in the first lattice are probed. After another 100 ms, the second lattice brings an atom into cavity mode. As can be seen, the signal decreases when the atom in the second lattice are delivered. When the atom in the second lattice heats due to no cooling and leaves the cavity mode, the signal rises back to the original level before the second atom was brought into the cavity. Looking
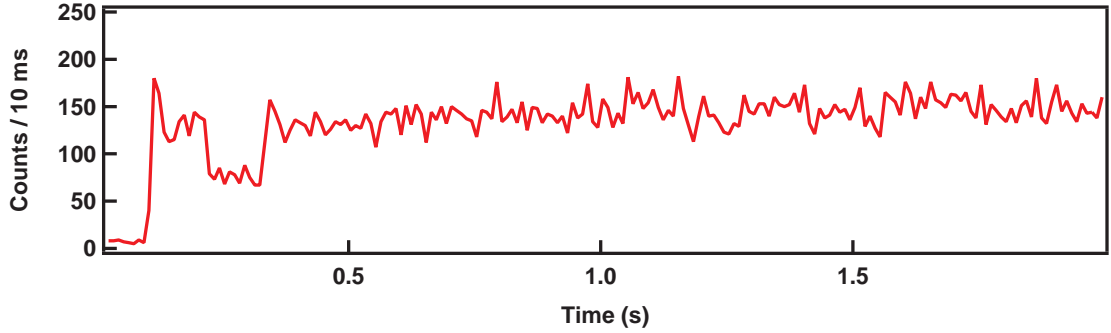
Figure 56: Dual lattices in cavity mode. Atoms in the first lattice are probed at 100 ms. After continuous observation and cooling for 100 ms, the second lattice brings in an atom and a dip is observed.

back to what was expected from the theory, the observed dip in signal seems to agree.

Interestingly, we have also observed a different behavior when many atoms are in the second lattice. Figure 57 shows that when the second lattice delivers many atoms to the cavity at $t = 450$ ms, the signal decreases as seen before. However, as the atoms slowly decay out of the cavity mode, the signal increases above the level of florescence from the atoms in the first lattice. Perhaps the atoms are jumping to the first lattice, but the two traps have been separated sufficiently to ensure that lattice hopping is prevented. Unfortunately, due to technical limitations of the trap, we currently cannot probe the two lattices separately.

The next step for this experiment is to tune the lattices so that they can be probed separately. Only after this hurdle is overcome, the experiment can be understood fully. Once two identically probed lattices are situated, two qubit entanglement can be explored.

8.1.2 Two Qubit Entanglement

Quantum information is based on logic gates. As mentioned in Section 1.2.2, the CNOT gate is needed for most operations. This operation requires two qubits: a control qubit, and a target qubit. Although a CNOT gate has been demonstrated
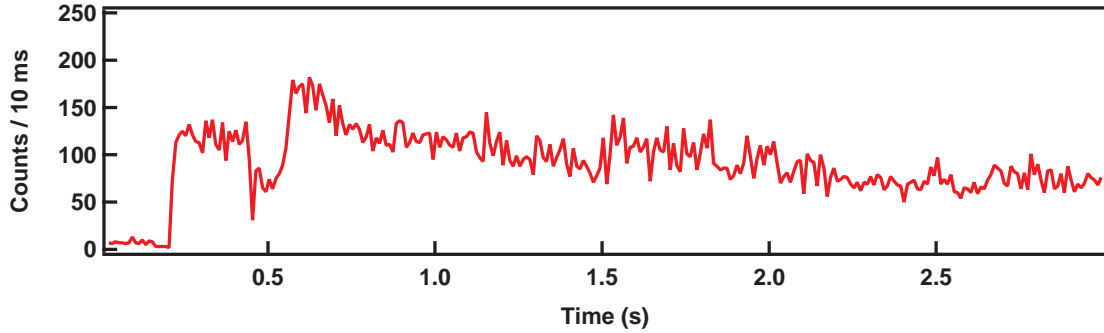
Figure 57: Dual lattices in cavity mode. Atoms in the first lattice are probed at 200 ms. After continuous observation and cooling for 250 ms, the second lattice brings in atoms. Initially, a dip is observed, but as the atoms escape the cavity mode, the signal goes above the initial level of florescence from the atoms in the first lattice.

using different degrees of freedom of a single ion, it has not yet been demonstrated with two neutral atoms.

In order to measure the entanglement, a few extra steps are needed. First, optical pumping is needed to initialize the atoms in a specified hyperfine ground state. Lasers for the different light frequencies have been constructed but not yet used in the system. Fortunately, single atoms and the cavity are not needed for verification of optical pumping. Many atoms can be pumped to the ground state in an optical lattice and probed at the MOT. Using microwaves can show the efficiency of the atoms being initialized to a selective magnetic ground state.

After optical pumping is optimized, the next step is to detect single photons. Again, most of the setup had been set up before and only needs to be optimized. The only change will be to add another photon counter. Two photon counters are needed to show anti-bunching and ensure that single photons are being detected. The work performed in Ref. [7] can be used as a guide to complete this task.

Once these requirements are fulfilled, gate operations can be performed. In Ref. [99], explanations of how to carry out gate operations are presented. A CZ, Hadamard and CNOT gate operations are outlined in detail for a strong coupling cavity. The

work proposed in this paper can only be executed with dual lattices, which only we have demonstrated.

Over the years, the cavity QED experiment has shown growth in complexity but increased usability and practicality. As the experiment matures, it shows great potential for exploring deeper into the realm of nonlinear quantum physics and advancing the field of quantum computing. It is exciting to see what more this cavity QED project will have to offer in the near future.

REFERENCES

[1] A. Einstein. Zur Quantentheorie der Strahlung. *Physikalische Zeitschrift*, 18:121–128, 1917.

[2] A. L. Schawlow and C. H. Townes. Infrared and optical masers. *Phys. Rev*, 112:1940, 1958.

[3] D. J. Wineland and H. Dehmelt. *Bull. Am. Phys. Soc.*, 20:637, 1975.

[4] T. W. Hänsch and A. L. Schawlow. Cooling of gases by laser radiation. *Opt. Commun.*, 13:68, 1975.

[5] E. M. Purcell. Spontaneous emission probabilities at radio frequencies. *Phys. Rev.*, 69:681, 1946.

[6] R. J. Thompson, G. Rempe, and H. J. Kimble. Observation of normal-mode splitting for an atom in an optical cavity. *Phys. Rev. Lett.*, 68:1132, 1992.

[7] M. Hijlkema, B. Weber, H. P. Specht, S. C. Webster, A. Kuhn, and G. Rempe. A single-photon server with just one atom. *Nat. Phys.*, 3:253, 2007.

[8] S. Nußmann, M. Hijlkema, B. Weber, F. Rohde, G. Rempe, and A. Kuhn. Submicron positioning of single atoms in a microcavity. *Phys. Rev. Lett.*, 95:173602, 2005.

[9] K. Fortier, S. Kim, M. Gibbons, P. Ahmadi, and M. Chapman. Deterministic loading of individual atoms to a high-finesse optical cavity. *Phys. Rev. Lett.*, 98:233601, 2007.

[10] M. Khudaverdyan, W. Alt, I. Dotsenko, T. Kampschulte, K. Lenhard, A. Rauschenbeutel, S. Reick, K. Schörner, A. Widera, and D. Meschede. Controlled insertion and retrieval of atoms coupled to a high-finesse optical resonator. *New J. Phys.*, 10:073023, 2008.

[11] T. Wilk, S. C. Webster, A. Kuhn, and G. Rempe. Single-atom single-photon quantum interface. *Science*, 317:488, 2007.

[12] M. A. Armen and H. Mabuchi. Low -lying bifurcations in cavity quantum electrodynamics. *Phys. Rev. A*, 73:063801, 2006.

[13] S. Gupta, K. L. Moore, K. W. Murch, and D. M. Stamper-Kurn. Cavity nonlinear optics at low photon numbers from collective atomic motion. *Phys. Rev. Lett.*, 99:213601, 2007.

[14] S. V. Prants, M. Edelman, and G. M. Zaslavsky. Chaos and flights in the atom-photon interaction in cavity qed. *Phys. Rev. E*, 66:046222, 2002.

[15] D. Ellinas and I. Smyrnakis. Asymptotics of a quantum random walk driven by an optical cavity. *J. Opt. B: Quantum Semiclass. Opt*, 7, 2005.

[16] Paul R. Berman. *Cavity Quantum Electrodynamics.* Academic Press, Inc., Boston, 1994.

[17] H. Mabuchi and A. C. Doherty. Cavity quantum electrodynamics: Coherence in context. *Science*, 292:1372, 2002.

[18] B. B. Blinov, D. L. Moehring, L.-M. Duan, and C. Monroe. Observation of entanglement between a single trapped atom and a single photon. *Science*, 428:153, 2004.

[19] J. Volz, M. Weber, D. Schlenk, W. Rosenfeld, J. Vrana, K. Saucke, C. Kurtsiefer, and H. Weinfurter. Observation of entanglement of a single photon with a trapped atom. *Phys. Rev. Lett.*, 96:030404, 2006.

[20] B. Julsgaard, A. Kozhekin, and E. S. Polzik. Experimental long-lived entanglement of two macroscopic objects. *Nature*, 413:400, 2001.

[21] D. Matsukevich, T. Chaneliere, S. D. Jenkins, S.-Y. Lan, T.A.B. Kennedy, and A. Kuzmich. Entanglement of remote atomic qubits. *Phys. Rev. Lett.*, 96:030405, 2006.

[22] C. W. Chou, J. Laurat, H. Deng, K. S. Choi, H. de Riedmatten, D. Felinto, and H. J. Kimble. Functional quantum nodes for entanglement distribution over scalable quantum networks. *Science*, 316:1316, 2007.

[23] P. Maunz, D. L. Moehring, S. Olmschenk, K. C. Younge, D. N. Matsukevich, and C. Monroe. Quantum interference of photon pairs from two remote trapped atomic ions. *Nat. Phys.*, 3:538, 2007.

[24] D. L. Moehring, M. J. Madsen, K. C. Younge, Jr. R. N. Kohn, P. Maunz, L. M. Duan, C. Monroe, and B. Blinov. Quantum networking with photons and trapped atoms. *J. Opt. Soc. Am. B: Opt. Phys.*, 24:300, 2007.

[25] D. L. Moehring, P. Maunz, S. Olmschenk, K. C. Younge, D. N. Matsukevich, L. M. Duan, and C. Monroe. Entanglement of single-atom quantum bits at a distance. *Nature*, 449:68, 2007.

[26] G. Moore. Cramming more components onto integrated circuits. *Electronics*, 38, 1965.

[27] R. Feynman. Simulating physics with computers. *Int. J. Theor. Phys.*, 21:467, 1982.

[28] D. Deutsch. Quantum theory, the church-turing principle and the universal quantum computer. *Proc. R. Soc. Lond. A*, 400:97, 1985.

[29] P. Shor. Polynomial-time algorithms for prime factorization and discrete logarithms on a quantum computer. *SIAM J.Sci.Statist.Comput.*, 26:1484, 1997.

[30] L. Grover. Quantum mechanics helps in searching for a needle in a haystack. *Phys. Rev. Lett.*, 79:325, 1997.

[31] I. Cirac and P. Zoller. Quantum computations with cold trapped ions. *Phys. Rev. Lett.*, 74:4091, 1995.

[32] Michael Nielsen and Isaac Chuang. *Quantum Computation and Quantum Information.* Cambridge University Press, Cambridge, 2000.

[33] I. Cirac and P. Zoller. Demonstration of a fundamental quantum logic gate. *Phys. Rev. Lett.*, 75:4714, 1995.

[34] B. P. Lanyon, T. J. Weinhold, N. K. Langford, M. Barbieri, D. F. V. James, A. Gilchrist, and A. G. White. Experimental demonstration of shor's algorithm with quantum entanglement. *Phys. Rev. Lett.*, 99:250505, 2007.

[35] D. DiVincenzo. The physical implementation of quantum computation. *Fortschr. Phys.*, 48:771, 2000.

[36] Annenberg Media. Interactives: The periodic table. http://www.learner.org/-interactives/periodic/groups2.html, 1997-2008. [Online; last accessed October 2008].

[37] N. R. Claussen, S. L. Cornish, J. L. Roberts, and Cornell.

[38] D. A. Steck. Rubidium 87 d line data. http://steck.us.alkalidata, 2008.

[39] Harold Metcalf and Peter van der Straten. *Laser Cooling and Trapping.* Springer, New York, 1999.

[40] P. Lett, R. Watts, C. Westbrook, W. Phillips, P. Gould, and H. Metcalf. Observation of atoms laser cooled below the doppler limit. *Phys. Rev. Lett.*, 61:169, 1988.

[41] J. Dalibard and C. Cohen-Tannoudji. Laser cooling below the Doppler limit by polarization gradients: simple theoretical models. *J. Opt. Soc. Am. B*, 6:2023, 1989.

[42] S. Chu, J. E. Bjorkholm, A. Ashkin, and A. Cable. Experimental observation of optically trapped atoms. *Phys. Rev. Lett.*, 57:314, 1986.

[43] A. Ashkin, J. M. Dziedzic, J. E. Bjorkholm, and S. Chu. Observation of a single beam gradient force trap for dielectric particles. *Optics Lett.*, 11:288, 1986.

[44] S. A. Ashkin and J. M. Dziedzic. Optical trapping and manipulation of viruses and bacteria. *Science*, 235:1517, 19867.

[45] M. D. Barrett, J. A. Sauer, and M. S. Chapman. All-optical formation of an atomic bose-einstein condensate. *Phys. Rev. Lett.*, 87:010404, 2001.

[46] R. Higashi M. Takamoto, F. L. Hong and H. Katori. An optical lattice clock. *Nature*, 435:321, 2005.

[47] A. D. Ludlow S. M. Foreman S. Blatt T. Ido M. M. Boyd, T. Zelevinsky and J. Ye. Optical atomic coherence at one second time scale. *Science*, 314:1430, 2006.

[48] R. Grimm, M. Weidemüller, and Yu. B. Ovchinnikov. Optical dipole traps for neutral atoms. *Adv. At. Mol. Opt. Phys*, 42:95, 2000.

[49] John David Jackson. *Classical Electrodynamics.* John Wiley and Sons, Inc., New York, 1999.

[50] Bahaa E. A. Saleh and Malvin Carl Teich. *Fundamentals of Photonics.* John Wiley and Sons, Inc., New York, 1991.

[51] D. Schrader, S. Kuhr, W. Alt, M. Müller, V. Gomer, and D. Meschede. An optical conveyor belt for single neutral atoms. *Appl. Phys. B*, 73:819, 2001.

[52] Jacob A. Sauer. *Cold Atom Manipulation for Quantum Computing and Control.* PhD thesis, Georgia Institute of Technology, August 2004.

[53] Christina J. Hood. *Real-Time Measurement and Trapping of Single Atoms by Single Photons.* PhD thesis, California Institute of Technology, May 2000.

[54] E. T. Jaynes and F. W. Cummings. Comparison of quantum and semiclassical radiation theories with application to the beam maser. *Proc. of IEEE*, 51:89, 1963.

[55] Howard Carmichael. *An Open Systems Approach to Quantum Optics.* Springer, Berlin, 1993.

[56] Maximilian A. Schlosshauer and Maximilian Schlosshauer-Selbach. *Decoherence and the Quantum-to-classical Transition.* Springer, Berlin, 2007.

[57] S. M. Tan. A computational toolbox for quantum and atom optics. *J. Opt. B: Quant. Semiclass. Opt.*, 1:424, 1999.

[58] Wolfgang Demtroder. *Laser Spectroscopy.* Springer-Verlag, Berlin, 1981.

[59] R. W. P. Drever, J. L. Hall, F. V. Kowalski, J. Hough, G. M. Ford ad A. J. Munley, and H. Ward. Laser phase and frequency stabilization using an optical resonator. *Appl. Phys. B*, 31:97, 1983.

[60] C. C. Bradley, J. Chen, and R. G. Hulet. Instrumentation for the stable operation of laser diodes. *Rev. Sci. Instrum.*, 61:2097, 1990.

[61] K. G. Libbrecht and J. L. Hall. A low-noise high speed diode laser current controller. *Rev. Sci. Instrum.*, 64:2133, 1993.

[62] P. J. Ungar, D. S. Weiss, E. Riis, and S. Chu. Optical molasses and multilevel atoms: theory. *J. Opt. Soc. Am. B*, 6:2058, 1989.

[63] A. D. Boozer, A. Boca, R. Miller, T. E. Northup, and H. J. Kimble. Cooling to the ground state of axial motion for one atom strongly coupled to an optical cavity. *Phys. Rev. Lett.*, 97:83602, 2006.

[64] P. Maunz, T. Puppe, I. Schuster, N. Syassen, P. W. H. Pinkse, and G. Rempe. Cavity cooling of a single atom. *Nature*, 428:50, 2004.

[65] J. McKeever, J. R. Buck, A. D. Boozer, and H. J. Kimble. Determination of the number of atoms trapped in an optical cavity. *Phys. Rev. Lett.*, 93:143601, 2004.

[66] J. A. Sauer, K. M. Fortier, M. S. Chang, C. D. Hamley, and M. S. Chapman. Cavity QED with optically transported atoms. *Phys. Rev. A*, 69:051804, 2004.

[67] S. Nußmann, K. Murr, M. Hijlkema, B. Weber, A. Kuhn, and G. Rempe. Vacuum-stimulated cooling of single atoms in three dimension. *Nat. Phys.*, 1:122, 2005.

[68] J. Ye, D. W. Vernooy, and H. J. Kimble. Trapping of Single Atoms in Cavity QED. *Nat. Phys.*, 83:4987, 1999.

[69] J. McKeever, A. Boca, A. D. Boozer, R. Miller, J. R. Buck, A. Kuzmich, and H. J. Kimble. Deterministic generation of single photons from one atom trapped in a cavity. *Science*, 303:1992, 1999.

[70] T. Legero, T. Wilk, M. Hennrich, G. Rempe, and A. Kuhn. Quantum beat of two single photons. *Phys. Rev. Lett.*, 93:070503, 2004.

[71] S. Kuhr, W. Alt, D. Schrader, M. Müller, V. Gomer, and D. Meschede. Deterministic delivery of a single atom. *Science*, 293:278, 2001.

[72] K. Murr, S. Nußmann, T. Puppe, M. Hijlkema, B. Weber, S. C. Webster, A. Kuhn, and G. Rempe. Three-dimensional cavity cooling and trapping in an optical lattice. *Phys. Rev. A*, 73:063415, 2006.

[73] M. Barrett, A. Prasad, and M. Chapman. Translating atomic traps for scalable quantum logic in cavity QED. *Bull. Am. Phys. Soc.*, 1999.

[74] C. Klempt, T. van Zoest, T. Henninger, O. Topic, E. Rasel, W. Ertmer, and J. Arlt. Ultraviolet light-induced atom desorption for large rubidium and potassium magneto-optical traps. *Phys. Rev. A*, 73:013410, 2006.

[75] B. H. Bransden and C. J. Joachain. *Physics of Atoms and Molecules*. Pearson Education, New Jersey, 2003.

[76] H. W. Chan, A. T. Black, and V. Vuletić. Observation of collective-emission-induced cooling of atoms in an optical cavity. *Phys. Rev. Lett.*, 90:063003, 2003.

[77] Ming-Shien Chang. *Coherent Spin Dynamics of a Spin-1 Bose-Einstein Condensate*. PhD thesis, Georgia Institute of Technology, May 2006.

[78] F. Vewinger, M. Heinz, R. G. Fernandez, N. V. Vitanov, and K. Bergmann. Creation and measurement of a coherent superposition of quantum states. *Phys. Rev. Lett.*, 91:213001, 2003.

[79] D. Bouwmeester, J. W. Pan, K. Mattle, M. Eibl, H. Weinfurter, and A. Zeilinger. Experimental quantum teleportation. *Nature*, 390:575, 1997.

[80] E. Knill, R. Laflamme, and G. J. Milburn. A scheme for efficient quantum computation with linear optics. *Nature*, 409:46, 2001.

[81] J. I. Cirac, P. Zoller, H. J. Kimble, and H. Mabuchi. Quantum state transfer and entanglement distribution among distant nodes in a quantum network. *Phys. Rev. Lett.*, 78:3221, 1997.

[82] A. Kuzmich, W. P. Bowen, A. D. Boozer, A. Boca, C.W. Chou, L. M. Duan, and H. J. Kimble. Generation of nonclassical photon pairs for scalable quantum communication with atomic ensembles. *Nature*, 423:731, 2003.

[83] C. H. van der Wal, M. D. Eisaman, A. André, R.L. Walsworth, D. F. Phillips, A. S. Zibrov, and M. D. Lukin. Atomic memory for correlated photon states. *Science*, 301:196, 2003.

[84] J. K. Thompson, J. Simon, H. Loh, and V. Vuletić. A high-brightness source of narrowband, identical-photon pairs. *Science*, 313:74, 2006.

[85] A.T. Black, J. K. Thompson, and V. Vuletić. On-demand superradiant conversion of atomic spin gratings into single photons with high efficiency. *Phys. Rev. Lett.*, 95:133601, 2005.

[86] P. Kolchin, S. Du, C. Belthangady, G.Y. Yin, and S. E. Harris. Generation of narrow-bandwidth paired photons: use of a single driving laser. *Phys. Rev. Lett.*, 97:113602, 2006.

[87] T. Aoki, B. Dayan, E. Wilcut, W. P. Bowen, A. S. Parkins, T. J. Kippenberg, K. J. Vahala, and H. J. Kimble. Observation of strong coupling between one atom and a monolithic microresonator. *Nature*, 443:671, 2006.

[88] A. Kuhn, M. Hennrich, and G. Rempe. Deterministic single-photon source for distributed quantum networking. *Phys. Rev. Lett.*, 89:067901, 2002.

[89] T. Wilk, S. C. Webster, H. P. Specht, G. Rempe, and A. Kuhn. Polarization-controlled single photons. *Phys. Rev. Lett.*, 98:063601, 2007.

[90] A. D. Boozer, A. Boca, R. Miller, T. E. Northup, and H. J. Kimble. Reversible state transfer between light and a single trapped atom. *Phys. Rev. Lett.*, 98:193601, 2007.

[91] L. M. Duan and H. J. Kimble. Efficient engineering of multiatom entanglement through single-photon detections. *Phys. Rev. Lett.*, 90:253601, 2003.

[92] X. L. Feng, Z. M. Zhang, X. D. Li1, S. Q. Gong, and Z. Z. Xu. Entangling distant atoms by interference of polarized photons. *Phys. Rev. Lett.*, 90:217902, 2003.

[93] Y. L. Lim, S. D. Barrett, A. Beige, P. Kok, and L. C. Kwek. Repeat-until-success quantum computing using stationary and flying qubits. *Phys. Rev. A*, 73:012304, 2006.

[94] T. W. Chen, C. K. Law, and P. T. Leung. Generation of entangled states of two atoms inside a leaky cavity. *Phys. Rev. A*, 68:052312, 2003.

[95] P. Lougovski, E. Solano, and H. Walther. Generation and purification of maximally entangled atomic states in optical cavities. *Phys. Rev. A*, 71:013811, 2005.

[96] A. S. Sørenson and A. K. Mølmer. Measurement induced entanglement and quantum computation with atoms in optical cavities. *Phys. Rev. Lett.*, 91:097905, 2003.

[97] D. Schrader, I. Dotsenko, M. Khudaverdyan, Y. Miroshnychenko, A. Rauschenbeutel, and D. Meschede. Neutral atom quantum register. *Phys. Rev. Lett.*, 93:150501, 2004.

[98] Kevin Fortier. *Individual trapped atoms for cavity QED quantum information applications.* PhD thesis, Georgia Institute of Technology, 2007.

[99] P. Xue and Y. F. Xiao. Universal quantum computation in decoherence-free subspace with neutral atoms. *Phys. Rev. Lett.*, 97:140501, 2006.